Master Thesis

Preparation and characterization of polyimide-based composites

Technische Universität WIEN
Institute of Chemical Technologies and Analytics
Getreidemarkt 9/164-CT
A - 1060 Wien

Under supervision of:

Assistant Prof. Dipl.-Chem. Dipl.-Ing. Dr.rer.nat. Miriam Margarethe Unterlass, MSc

Assistant Prof. Dipl.-Ing. Dr.techn. Thomas Konegger

Johannes Eßmeister

Florianigasse 15/14a
1080 Vienna

Vienna, 27.11.2019 Signature

Acknowledgements

First of all, I would like to thank my supervisor Thomas Konegger for providing me with this work and foremost for his advice with the experiments and discussing results. Whenever I had troubles during my work he was open for my questions, which I am very thankful for.

I want to thank Miriam Unterlass for her supervision and the framework of this work. Her enthusiasm and scientific spirit encouraged me to work out the problems within my investigations.

I would also like to thank Michael Taubländer for his support during my work, especially in terms of planning experiments and trying different materials within my procedures.

Furthermore, I want to express my gratitude to Thomas Koch from the research group for structural polymers for his various measurements and also for the discussions we had. His experience helped me learn a lot about the materials I studied and to see things from different perspectives.

I am also grateful for the financial support received through the Austrian Science Fund FWF. (Project number PIR 10)

A special thanks remains to all the students at the second floor, especially the colleagues in my office who gave me an ear whenever I faced challenges and provided great advice. When working with such tremendous and fun people even the most tedious workdays feel enjoyable.

I want to say thank you to all my friends and family who all supported me during my whole studies.

Finally, I want to express my endless gratitude to my partner Eva, for her support and encouragement through the process of writing this work.

Abstract

The objective of this work was the preparation of different polyimide-particle-reinforced composites containing poly(p-phenylene pyromellitimide) (PPPI) as reinforcement, and their mechanical, thermal and microstructural characterization. PPPI was produced as highly crystalline particles by hydrothermal (HT) synthesis, under high pressure and temperature. Due to their strict crystalline structure, these novel polyimide particles (HT-PPPI) show unique properties, such as a high theoretical young's modulus and high thermal stability. Because of these properties, PPPI is a promising material for the use in lightweight polymer composites, with a high application potential in the electronic, automotive and aeronautic sector.

Three distinct matrix materials were investigated including two polyimide materials (P84 NT, P84) as well as an epoxy-based material.

P84 NT-polyimide powder was investigated as matrix compound in direct forming and hot compression moulding (HCM).

P84–polyimide powder was studied for its use in HCM processing. Three different particle sizes of the P84 powder, different powder mixing techniques and pressures during HCM were investigated. Furthermore, the influence of different amines (hexamethylenediamine, 1,2-diaminocyclohexane and polyetheramines) for interfacial surface-modification were analysed.

As a third matrix material, a Bisphenol A based hot curing epoxy resin with an amine hardener (based on 1,2-diaminocyclohexane and diethyltoluoldiamine) was used. To incorporate the PPPI-particles into the resin, ultra-sonication and high-speed stirring was applied.

The mechanical and thermal properties of the composite samples were characterized by three point bending tests, tensile tests, dynamic mechanical thermal analysis, Vickers hardness, nanoindentation and thermogravimetric analysis. The microstructure was analysed using SEM and light microscopy techniques.

The P84 NT composites exhibited problems in their structural integrity and density, and were therefore not investigated in detail.

In case of the P84 composites, the flexural strength and strain decreased while no difference in hardness or glass transition temperature was observed. A significant increase of flexural, storage, and indentation modulus could be observed. The addition of hexamethylenediamine as surface modification resulted in an increase in strength and strain relative to the unmodified samples. The thermal stability was unaffected by the addition of PPPI in the P84 matrix. In these samples an anisotropic but homogenous microstructure exhibiting the same mechanical properties in different testing directions could be observed.

In the epoxy composites, flexural, storage, indentation, and Youngs modulus increased significantly with increasing filler content. Flexural strength was consistent with an increasing PPPI content, while the flexural strain decreased. In case of tensile testing, the strength and strain until break decreased. The glass transition temperature of the composite decreased significantly with increasing PPPI content, while thermal stability was increased. In these samples an isotropic and homogenous microstructure could be observed.

This leads to the conclusion that an incorporation of the HT-PPPI particles into these matrix polymers is possible. In the case of the epoxy-based samples, preferable effects could be observed, which makes this combination an interesting material for future investigations.

Kurzfassung

Ziel dieser Arbeit war die Herstellung verschiedener Polyimidpartikel-verstärkter Komposite, welche Poly(p-phenylenpyromellitimid) (PPPI) als Verstärkung enthalten, mit folgender mechanischer, thermischer und mikrostruktureller Charakterisierung. PPPI wurde in Form hochkristalliner Partikel über Hydrothermalsynthese (HT) unter hohem Druck und hoher Temperatur hergestellt. Die Polyimidpartikel (HT-PPPI) weisen aufgrund ihrer strengen kristallinen Struktur einzigartige Eigenschaften auf, wie einen hohen theoretischen Elastizitätsmodul und eine hohe thermische Stabilität. Aufgrund dieser Eigenschaften ist PPPI ein vielversprechendes Material für die Verwendung in Polymerkompositen, mit Anwendungen in der Elektronik-, Automobil- und Raumfahrtindustrie.

Es wurden drei unterschiedliche Matrixmaterialien, darunter zwei Polyimide (P84 NT, P84) und ein Epoxidsystem untersucht.

Als erstes Matrixpolymer wurde P84 NT-Polyimidpulver für Direktformen und Heißpressen verwendet.

Als zweites Matrixpolymer wurde P84-Polyimidpulver im Heißpressverfahren (HCM) verwendet. Hier wurden drei verschiedene Partikelgrößen des P84-Pulvers sowie verschiedene Pulvermischtechniken und Pressdrücke während des HCM untersucht. Weiterhin wurde der Einfluss verschiedener Amine (Hexamethylendiamin, 1,2-Diaminocyclohexan und Polyetheramine) als Grenzflächenmodifikation untersucht.

Als drittes Matrixmaterial wurde ein heißhärtendes Epoxidharz auf Bisphenol A-Basis mit einem Aminhärter auf Basis von 1,2-Diaminocyclohexan und Diethyltoluoldiamin verwendet. Um die PPPI-Partikel in das Harz einzubringen, wurde eine Ultraschallbehandlung und Hochgeschwindigkeitsrühren angewendet.

Für die mechanische und thermische Charakterisierung der Verbundproben wurden Dreipunktbiegetests, dynamisch-mechanische Thermoanalyse, Vickers-Härte, Nanoindentation und thermogravimetrische Analyse verwendet. Zur Analyse der Mikrostruktur wurden Rasterelektronenmikroskopie und verschiedene Lichtmikroskopietechniken eingesetzt.

Die P84 NT-Verbundwerkstoffe zeigten Probleme in ihrer strukturellen Integrität und Dichte und wurden daher nicht im Detail untersucht.

Bei den P84-Kompositen nahmen die Biegefestigkeit und die Dehnung ab, während bei Zugabe von PPPI keine Änderung der Härte oder der Glasübergangstemperatur beobachtet wurde. Ein signifikanter Anstieg des Biege-, Speicher- und Eindruck-Moduls wurde beobachtet. Die Zugabe von Hexamethylendiamin als Grenzflächenmodifikation zeigte eine Zunahme der Festigkeit und Dehnung im Vergleich zu den nicht modifizierten Proben. Die thermische Stabilität wurde durch die Zugabe von PPPI in die P84-Matrix nicht beeinflusst. In diesen Proben wurde eine anisotrope, jedoch homogene Mikrostruktur beobachtet, welche bei unterschiedlichen Testrichtung die gleichen mechanischen Eigenschaften aufweist.

Bei den Epoxid-Verbundwerkstoffen wurden der Biege-, Speicher-, Eindruck- und Elastizitätsmodul mit zunehmendem Füllstoffgehalt signifikant erhöht. Die Biegefestigkeit blieb mit einem zunehmenden PPPI-Gehalt gleich, während die Biegedehnung abnahm. Bei Zugversuchen nahmen Festigkeit und Dehnung bis zum Bruch ab. Die Glasübergangstemperatur des Komposits nahm mit zunehmendem PPPI-Gehalt signifikant ab, während sich die thermische Stabilität erhöhte. In diesen Proben konnte eine isotrope und homogene Mikrostruktur beobachtet werden.

Dies lässt den Schluss zu, dass ein Einbau der HT-PPPI-Partikel in diese Matrixpolymere möglich ist. Bei den epoxidbasierten Proben konnten positive Effekte hinsichtlich der mechanischen Eigenschaften beobachtet werden, was diese Kombination zu einem interessanten Material für zukünftige Untersuchungen macht.

List of symbols and abbreviations

Symbols

σ_{fM}	Flexural strength
ε_{fB}	Flexural strain at break (“strain”)
E_f	Flexural modulus
σ_{tM}	Tensile strength
ε_{tB}	Tensile strain at break
E_t	Young’s modulus
E_s	Storage modulus
E_p	Plateau modulus
T_g	Glass-transmission temperature
V_e	Cross-link density
H_i	Hardness

Abbreviations

DGEBA	Bisphenol A diglycidylether
PPPI	poly-(p-phenylene pyromellitimide)
HMDA	Hexamethylenediamine
DACH	1,2-diaminocyclohexane
D230	Jeffamine D 230
EDR	Jeffamine EDR-176
IPA	Isopropyl alcohol
SEM	Scanning electron microscopy
BSE	Backscattered electrons
DMA	Dynamic mechanical (thermal) analysis
TGA	Thermogravimetric analysis

Index

1 Introduction and Motivation

With ongoing innovation in engineering fields like automotive-, aerospace- and electronics industry, advanced materials which combine specific properties are required. Composite materials extend the possibilities for tailoring properties over a wide range. [1, 2]
In the automotive- and aerospace sector, the use of light-weight materials with high specific strength is highly relevant. Especially polymer matrix composites are moving into focus. Historically, long fibre reinforced polymer composites have been used as light-weight components in those industries. As long fibre reinforcement yields anisotropic materials, the use of short fibre- or particle-reinforced composites is also a common strategy. [1, 3]

The polymers most used for the modification with particles are thermosets. In this category, epoxy resins and polyimides are within the most important materials. Thermoset polymers have been reinforced with all types of inorganic particles, with enhancement in their mechanical, thermal and chemical properties. One main drawback of these inorganic materials is the increasing weight due to a higher density of the inorganic particles. This has been tackled with the use of carbon-based materials, like carbon nanotubes, short carbon fibres or graphene. Here the drawbacks can be the electrical- and thermal conductivity inherent in these materials.[4]

Therefore, the introduction of polymer-particle/polymer-matrix composites shows great potential for dealing with these issues. The incorporation of different polymers into thermoset polymers has been studied quite extensively, especially with epoxy resins.[5] However, no detailed reports have been published for polyimides.
According to these considerations, poly(p-phenylene pyromellitimide) (PPPI) particles have been used as a reinforcement of polyimide and epoxy matrices in this work. These PPPI particles, produced in a novel hydrothermal polymerisation process, are an interesting possibility for the production of new composite materials, due to their unique morphology, and chemical and crystalline structure.
Therefore, this study deals with the production of these composite materials and the characterization of their mechanical, microstructural and thermal behaviour.

2 Theoretical Background

2.1 Polyimides

Polyimides are ranked in the category of "high-performance polymers" and are within the class of thermoset polymers. Here, polyimides are one of the few thermosets which are not cross linked. Their unique properties arise solely from their chemical structure. Polyimides generally contain an imide (-CO-NH-CO-) linkage group, which formally results from a substitution of the OH – groups of two carboxylic acid through one NH – group. The imide group is mostly built in a heterocyclic structure within the polymer backbone. Also, the backbone is built with aromatic structures in most cases, which leads to the formation of rigid-rod polymer chains. Conventionally, polyimides are synthesised by a two-step polymerisation. First, a diamine and dianhydride are reacted to a poly(amic acid), which is cured to the finished polyimide in a second condensation step. This process usually uses toxic solvents as a substrate for the polymerisation.[2, 6, 7]

2.1.1 Properties of polyimides

Due to their chemical structure, polyimides exhibit remarkable properties. Polyimides are within the most heat-resistant polymers and therefore have high application temperatures, with good mechanical properties over a wide range of temperatures. Also, electrical and chemical properties of polyimides are outstanding, hence their application in aerospace, defence, dielectrics, composites, or adhesives. [6, 7]
The lack of a melting point, high glass-transition temperature, and insolubility render processing of many conventional polyimides nearly impossible after curing. This applies mostly to the Kapton-type polyimides with a pyromellitimide structure.[8] To overcome these difficulties, thermoplastic polyimides have been investigated and used for adhesives, films and composite materials.[9-11] These polyimides can be fabricated by conventional thermoplastic processing techniques such as injection moulding, extrusion, compression moulding, or a processing from polymer-solutions.[8]
It is difficult to predict the mechanical properties of polyimides, because of various influencing factors, including chemical structure, molecular weight, viscosity, preparation procedure, and property determination. Especially the direction of force during fabrication could affect the mechanical properties and could also cause anisotropy within the material.[12] Thus, polyimides in general show Young's modulus values of 1500 – 3000 MPa and tensile strengths between 70 – 100 MPa, with varying elongations between 2 and 15 % corresponding to the modulus. [7, 13] In Table 1, commercially used polyimides with their properties are depicted, with Kapton© and Vespel© as representative of the conventional polyimides and Torlon© and Ultem© as references for commonly used thermoplastic polyimides.

Table 1: Typical mechanical properties of conventional polyimides

Polyimide	σ_{fM} (MPa)	σ_{tM} (MPa)	E_f (MPa)	E_t (MPa)	T_g (°C)	Ref.
Kapton© (PMDA-ODA)	117	86	3100	–	410	[6]
Vespel© (PMDA-ODA)	85-70	110-80	3100-2500	–	no T_g	[12]
Torlon© (PAI)	189	117	3600	5200	–	[6]
Ultem© (PEI)	150	105	3300	3000	–	[6]

2.1.2 Hydrothermal PPPI - Poly (p-phenylene pyromellitimide)

As mentioned before, polyimides exhibit remarkable properties, such as high specific strength, high modulus, and high temperature stability.[2] These properties can even be enhanced by increasing the crystallinity of the polymer.[14] Therefore, efforts to synthesize highly ordered

HPPs have been made in the past. [15, 16] The main disadvantages of the conventional synthesis for highly crystalline polyimides are the requirement for toxic solvents and long reaction times. A much "greener" alternative to produce highly ordered polyimides is the use of hydrothermal (HT) crystallization, under high pressure and temperature in water, as shown in the works of Baumgartner *et al.* [17] and Taublaender *et al.* [18] In their work, highly crystalline poly-(p-phenylene pyromellitimide) (PPPI) was produced via HT-synthesis in the form of particles with various morphologies.
PPPI is one of the most challenging polymers to process, because of its rigid nature, the lack of a melting point, and insolubility in most solvents.[15, 17] Even though PPPI has one of the highest moduli of known polyimides, its brittle nature inhibits the use of PPPI on its own, without modifications.[19, 20] As these properties even get enhanced with a high crystallinity, the production of finished and semi-finished PPPI parts for structural applications is difficult.

Theoretically, PPPI has one of the highest theoretical Youngs moduli of all polyimides, with a value of 500 GPa [14], albeit this does not necessarily reflect the modulus of a real technical material. Because of the high brittleness of PPPI, a mechanical characterisation has not been reported in the past. In a first assumption, the closest modification of PPPI, PMDA-MEPDA is used to set a range for the properties of PPPI. In PMDA-MEPDA, the phenylene group is substituted with toluene. This changes mechanical and thermal properties, but is the closest iteration to PPPI, as shown in Table 2. [19, 20]

Table 2: Properties of PPPI and relative polyimides [19, 20]

	σ_{tM} (MPa)	ε_t (%)	E_t (MPa)	T_g (°C)
Poly-(p-phenylene pyromellitimide)	-	-	12.2	-
PMDA-MEPDA	260	4	11.4	370

2.2 Epoxy Resins

Epoxy resins are generally considered as thermoset plastics, with a functional group consisting of a cyclic, three-atom ether called epoxide, oxirane or ethoxyline.[21] These epoxide groups are contained in a prepolymer, which is either formed by the reaction of epichlorohydrin and a hydroxyl group (polyols, aliphatic diols, phenols, dicarboxylic acids) or via a conversion of a aliphatic or cycloaliphatic alkane with peracids.[22] The derivatives of Bisphenol A (Bisphenol A diglycidyl ether – DGEBA) are the most commonly used resins (over 80 % of world production).[6] In case of DGEBA, liquid resins with a low degree of polymerisation are most commonly used. The resin is cured by a cross linking reaction of the epoxide group with various curing agents. Many compounds can be used as curing agents, such as amines (aromatic/aliphatic, primary/secondary), phenols, carboxylic acids, thiols, or anhydrides. In addition to the hardener and resin systems, epoxy resins can be modified with fillers, solvents, diluents, plasticizers, and accelerators.[21] The wide variety of these different compounds leads to the use of epoxy resins in numerous applications like adhesives, coatings, electronic insulations, and composite materials.[6]

2.2.1 Properties of epoxy systems

As this work deals with mechanical properties of epoxy composites, the mechanical properties of epoxy resins in comparison with their chemical structure will be discussed in this section. The focus lies on DGEBA resins with amine curing systems, because it has been used in this study. The main influence on mechanical and thermal properties of an epoxy system is the number of cross-links between the main chains. This cross-linking can either be varied by using primary- or secondary-; mono-, di-, or triamines as curing agents or by changing the stoichiometric ratio

between hardener and epoxy. Hence, mono- and secondary amines lowering the cross-link density and triamines increase the cross-link density, in comparison to primary diamines as curing agents. [23]

The modulus of a system decreases with higher cross-link density at temperatures over 25 °C for aromatic and aliphatic hardeners.[24] Likewise, a linear increase in glass-transition temperature with higher cross-link density is well reported in literature.[25-27] The yield strength of epoxies increases with higher cross-link density. Similarly, an increase can be noted when exchanging aliphatic groups with aromatic ones. The same increases in fracture toughness can be described as for the yield strength. In addition, fracture toughness increases with the molecular weight.[23] Figure 1 shows the structure of an epoxy-system after curing, with cross-links due to the amine hardener.

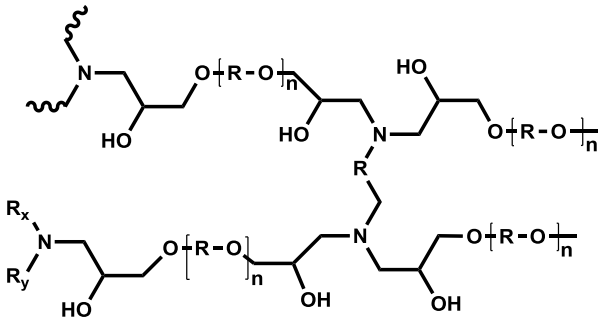

Figure 1: Epoxy structure after curing schematic (adapted from [23])

A change in chemical structure of the curing agent alters the properties of the resin. This change in properties of the resin can be observed especially when aliphatic groups are exchanged with aromatic groups. In Table 3 different DGEBA based epoxy/hardener systems are shown. Even though the absolute values can differ as a result of the curing procedure and modifications in the resin systems, they showcase the effect between aromatic and aliphatic groups in curing agents. Hence, the aromatic systems show a higher modulus, strength, and glass-transition temperature.[22, 23, 28]

Table 3: Typical mechanical properties of DGEBA resins with different hardeners

Curative	σ_{fM} (MPa)	σ_{tM} (MPa)	E_f (MPa)	E_t (MPa)	T_g (°C)	Ref.
4,4'-Methylenedianiline	80	70	2700	–	–	[22]
Hexamethylenediamine	–	60	–	2200	130	[28]
m-Phenylenediamine	–	80	–	3000	180	[28]

2.2.2 Fracture mechanism of rigid thermoset polymers

The fracture mechanism of thermosets is generally of brittle nature at room temperature. Polyimides and epoxy resins are in the range of the most brittle polymers, typical for thermosetting plastics.[29] Because of the high degree of cross-linking in cured epoxy systems, the polymer chains cannot slip against each other and form fibrils. In case of polyimides, the same effect occurs due to the high interaction between the polymer chains. This result in a deformation mechanism were crazes are the minor and shear yielding is the major form of deformation. [30, 31]

Figure 2 illustrates the difference between the two fracture mechanisms. Depending on temperature and strain rate, different fracture types can occur: stable brittle crack propagation, stable-unstable crack propagation (stick/slip), and ductile crack propagation (mostly at elevated temperatures). [23, 31]

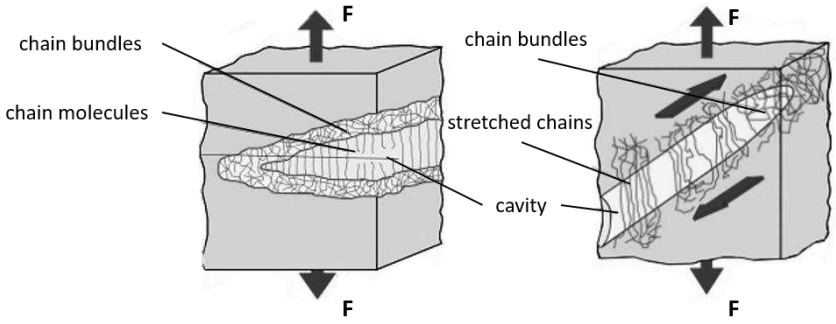

Figure 2: Craze formation (left) and Shear-Yielding (right) in plastics (adapted from [30, 31])

The brittle fracture of thermosets can be observed by fractography using scanning electron microscopy. Typically, ramps and steps are formed from brittle crack propagation regime, with the lack of plastic deformation and artifacts such as tails, foils, or strings. In a stick/slip crack propagation regime, the larger ramps are crossed with characteristic break patterns on the steps. Furthermore, the initiation of secondary cracks occurs through external or intrinsic imperfections within the material, forming break parables. [23, 32, 33]

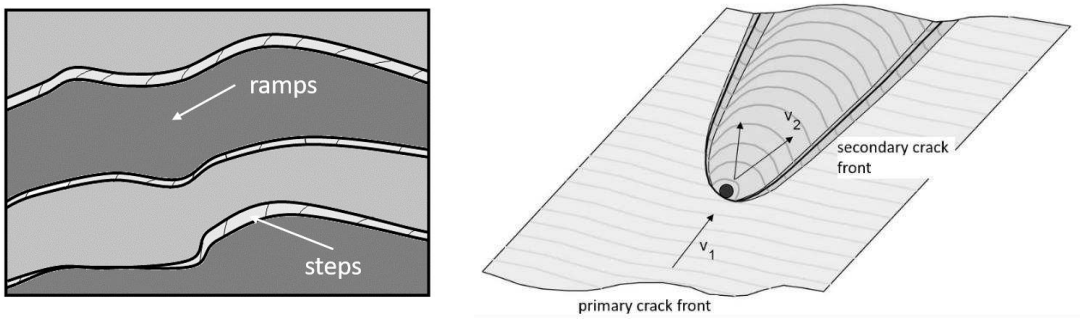

Figure 3: Brittle fracture, ramps and steps (left); break parables (right) (adapted from [32, 33])

Figure 4 depicts schematic stress/strain curves for different fracture behaviours of thermoset polymers. In quasi-static material testing, such as common tensile, flexural, or compression tests, these load/displacement curves can be observed depending on the ductility of the tested material. Stick/slip propagation is a common phenomenon for thermoset materials. Here, the crack propagation occurs at each load peak and is delayed at each load minimum.[23]

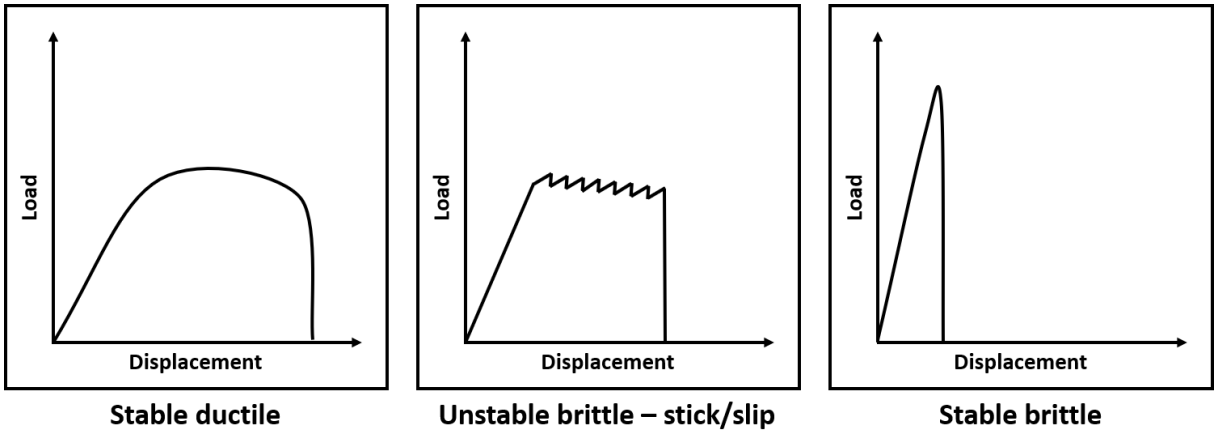

Figure 4: Fracture mechanisms displayed on stress/strain curves thermoset plastics (adapted from [23, 29])

2.3 Particulate composites and polymer blends

Composite materials generally consist of two or more phases, which consists of a matrix phase and filler or reinforcing phases. In general, composites can be distinguished by their matrix (polymer, metal, ceramic) or by the type of reinforcing phase (particles, whiskers, flakes, spheres or continuous fibres). A common motivation for the use of composite materials is in structural application, where the matrix is reinforced by a phase which has different mechanical properties, such as high stiffness, specific strength or toughness. Despite from structural reasons, functional composites are used to combine different properties in one material. Here the focus lies on electrical, thermal, catalytical, or optical properties.[4, 34]
The combinations of composites are numerous; therefore, this chapter deals with particulate reinforced polymer composites focusing on mechanical properties and failure mechanisms.
Historically, the motivation behind the addition of particles into polymers was to reduce costs and to save polymer material using natural inorganic materials like calcite, talcum or clay as additives. Later, the use of particles for the improvement of polymer properties was investigated. Inorganic materials like ceramics (Al_2O_3, SiO_2, TiO_2), glass, minerals ($Mg_3Si_4O_{10}$, $CaCO_3$), quartz, nano-clay, graphite, carbon-nanotubes, or metal (Cu, Al, Fe, Ni) particles serve as reinforcing particles as well as natural or synthetic organic materials, such as cellulose, wood, rice hulls, or starch. Inorganic ceramic or mineral particles are mainly used to improve the modulus, abrasion resistance, performance at elevated temperatures, flame retardance and decrease gas-permeability of the matrix. Metal particles on the other hand are commonly used for functional applications, like the improvement of electrical and thermal conductivity. [4, 34, 35]

In case of rigid particles, the main influences for a strengthening effect on the polymer matrices are particle size and size distribution, interface adhesion between the phases, particle loading and homogenisation. The effects on mechanical properties change quite drastically when particle size decreases from the micro- to nanoscale (< 100 nm), due to different interaction between polymer chains and particles. Also, the fracture mechanism changes when nanoparticles are used, due to the drastic reduction of the distance between particles in contrast to micro-particles. In general, an improved interfacial adhesion is necessary for a sufficient load sharing mechanism within the composite material. This factor gets more important with increasing particle sizes. These two factors have major influence on strength, toughness, and strain until break of the composite material. While strength and toughness are usually improved with smaller particles size and higher adhesion between phases, strain is naturally decreased because of the rigidity of the particles. A higher particle loading usually improves the mechanical properties when interfacial adhesion is sufficiently high. In case of large particles (> 10 µm), strength in particular is often decreased at higher particle loadings. For nanoparticles, the strength can peak at certain particle loadings in the range of a few volumetric percent. This peak in strength can also originate from inhomogeneities present at higher filler contents. [4, 36]
In all cases of rigid particle filled polymers, the modulus of the composite increases with the filler content. This follows a nearly linear function in most cases.[21, 34, 36]
These general statements can differ for each matrix/particle system, as discussed in detail in sections 2.5 and 2.6.

Aside from reinforcement with rigid inorganic or organic particles, a toughening with rubber or thermoplastic particles in polymer matrices has been investigated and used in many different variations. [5, 21]
In case of rubber toughening, different rubber (carboxyl-terminated butadiene-coacrylonitrile – CTBN, hydroxyl-terminated polybutadiene – HTPB) can be incorporated as insoluble particles or in solution, and separated during a curing of thermoset resins. In both cases, the propagating cracks get dissipated at the low-modulus rubber inclusions and therefore critical failure of the

matrix is reduced. Although a toughening effect can be achieved, drawbacks in modulus and sometimes strength can occur.[5, 21]

For thermoplastic modified polymers, an even higher toughening effect can be achieved in some cases, without a severe decrease in modulus and strength. In this case, thermoplastics like polyphenyleneoxide, poly(methyl methacrylate) or polycarbonate are often incorporated in a polymer matrix. [21, 37, 38]

2.4 Fracture mechanisms of particulate polymer composites

In case of rigid particle reinforced polymers, the combination of particle size, filler volume content and distance between the particles, as well as the ductility of the matrix polymer and the adhesion between the phases are responsible for the fracture mechanism of the composite. Therefore, the balance between those parameters predicts the outcoming mechanical properties of the composite material.
The failure mechanism for larger particles (~1 µm) under external load includes a phase separation, debonding, and void formation around the particles. These voids get elongated, depending on the flexibility of the matrix and the distance between particles. If the distance between particles is small enough and the matrix is ductile, the matrix elongates, and crazes are formed. When the voids reach the critical crack length, crack propagation and therefore fracture occurs.[39] If the interparticle distance, resulting from diameter and particle loading, is optimised, the formation of voids and occurring fibrillation can add to toughness and strength of the material. Is the matrix of brittle nature, this critical crack length decreases. In these polymers, particles can therefore initiate crack propagation, especially when the particles are large enough. A very high adhesion between particles and filler can also result in a composite with high strength and modulus, but with decreased fracture toughness and high brittleness.[4]
For smaller or nanoparticles, failure often occurs due to a formation of larger agglomerates which break up and initiate sharp cracks, leading to brittle fracture. This mechanism results in a craze-like structure.[4]

In contrast to the fracture mechanism, dominant in rigid (inorganic) filled particle composites, the situation for rubber or thermoplastic reinforced polymers largely depends on the materials in use. These kinds of reinforcements are normally used in thermoset matrices (e.g. epoxy resins). For rubber-toughened composites, a crack bridging mechanism has been described as major mechanism despite crack pinning.
Especially for thermoplastic modified thermoset composites, four different fracture mechanisms are proposed. Depending on strength, modulus and ductility of the thermoplastic in use, crack bridging, crack pinning, crack path deflection or particle-induced shear banding is possible, as illustrated in Figure 5.[4, 21, 38]

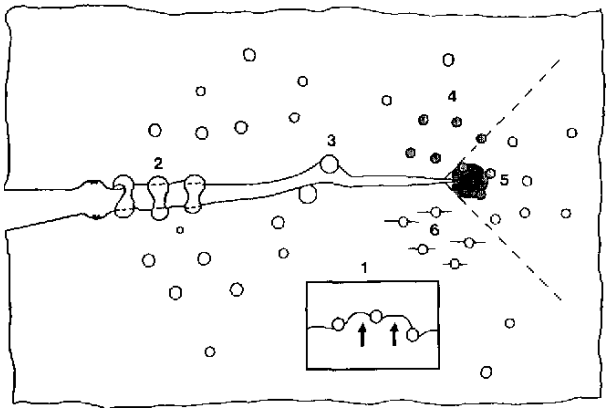

Figure 5: Fracture mechanisms for thermoplastic modified thermoset composites, (1) crack pinning, (2) particle bridging, (3) crack path deflection, (4) particle yielding, (5) particle-yielding induced shear banding, and (6) microcracking ([38], reprinted with permission by Elsevier)

In case of rigid inorganic and rigid polymer particles in a polymer matrix, crack pinning and crack path deflections are the most reported and evident fracture mechanisms.[4, 5, 21, 34, 38]
As this work deals with composites of rigid particles, but also uses polymer particles, all these fracture mechanisms are conceivable.

2.5 Polyimide-based particulate composites

Polyimides have been used as matrix polymers for composite materials in different applications, ranging from structural parts to functional materials. These materials differ widely due to different production approaches and filler varieties.
One approach is to produce composite polyimide materials from solution, *i.e.* from monomeric solutions or dissolved polymer solutions. Here, particulate nanocomposites with fillers like carbon nanotubes, nano-clays (montmorillonite, attapulgite, mica) are used and mechanical properties of polyimides can be improved. When the interfacial adhesion and homogenisation are sufficient, an increase in strength, modulus, and elongation is reported. A major drawback of this approach is that the production is limited to thin films, due to the imidization reaction itself. [40-43]

The major production route for structural parts of polyimides is the use of sintering or hot compression moulding techniques. This approach has been used in industrial applications for the production of finished and semi-finished parts.[12, 44, 45] With this approach, polyimide particle composites have been investigated in the past, with attention placed on the tribological properties of the composites. In these studies, SiO_2, graphite, short carbon nano fibres or graphitic carbon nitride were used. [46-49]
Additionally, several functional composites have been studied, produced via sintering and pressing methods, with the addition of boron nitride or graphite. [50, 51] With the addition of fillers, like short carbon fibres, improvements in strength, modulus and thermal properties have been reported.[52]

The approach on blending polyimides with different crystallinity and consequently a tailoring of mechanical properties was studied by Throne *et al.* [53] and Yokota *et al.* [54] in the past. These two studies take two different approaches on production as mentioned before. The production routes considering sintering and pressing of two different polyimides was considered by Throne and proven to work to some extent. Their approach is therefore similar to the chosen route taken in this work.

2.6 Epoxy-based particulate composites

The approach of incorporating particles into polymer matrices was proven to work with numerous different particle materials, especially in epoxy matrices. In these composite materials, the mechanical or thermal properties of the epoxy could be enhanced in most cases, using rigid particles.
The most attention in research was placed on nanocomposites, using numerous different rigid particles. The reason for this is the strengthening effect due to nanoparticles, which is often inexistent with larger particles. However, the effect on increasing modulus and fracture toughness mostly remains with microparticles. [36]

Nanoparticles like ZrO_2, SiO_2, Al_2O_3, diamond, glass, short carbon fibres and nano-clays have been studied extensively in the past.[55-63] These sorts of particles commonly increase the modulus, hardness, and fracture toughness of the composites. Here the strengthening effect depends strongly on the interfacial adhesion and size of the particles.[36]

Another strategy for improving the properties of epoxy-systems is the incorporation of organic particles like rubbers, thermoplastics or graphene.[37, 64, 65] Rubber was one of the first modifications, using particulate fillers. In case of the rubber particles, a toughening effect can be achieved, but with the drawback of reduced modulus and, at times, strength.[5]

For the thermoplastic modified epoxy systems, an even higher toughening effect occurs than for the rubber composites, without a severe decrease in modulus and strength. In this case, thermoplastics like polyphenyleneoxide, poly(methyl methacrylate) or polycarbonate were incorporated into an epoxy matrix. [37] In particular, polyetherimide has been used by Cho *et al.* [66] and Bucknall *et al.* [67] to strengthen and toughen epoxy systems, without severe drawbacks in modulus. Here the polyimide is incorporated into the epoxy resin in solution and forms separate inclusions during curing. The particles formed after curing are in the micrometre range, and are spherical. These composites or polymer blends are probably the materials most related, to the composites studied in this work, although the PPPI used in this work exhibits a higher modulus and brittleness than polyetherimide used by Cho and Bucknall.
Recently, polyimide fibre reinforced epoxy composites have been investigated by Chen *et al.* [68], with improvements in modulus and strength. Comparing these different approaches, PPPI particle reinforced composites, as investigated in this work, stand between those kinds of epoxy composites. The composite is composed only of two polymers, but uses rigid particles dispersed in the epoxy matrix, similar to the inorganic particle variations.

2.7 Models predicting properties of particulate polymer composites

The two simplest approaches to estimate properties of composite materials is to use the **rule of mixture (ROM)**, or Voigt-Modell, and the **inverse rule of mixture (inverse ROM)**, or Reuss-Modell, given in Equations (1) and (2). The Equations use the property of interest and the volume fractions of the two phases. This can be applied for a variety of properties like density, modulus, thermal- or electrical conductivity. [34]
The ROM is a linear correlation between the properties of the two phases, and can be described as a weighted mean, giving the upper limit of resulting properties. Inverse ROM moreover gives the lower bound of a property resulting from compounding two materials. ROM and inverse ROM can be described in a simple mechanical way, with the use of Hooke's law and a slab model as estimation. ROM applies an equal strain axial, while inverse ROM applies an equal stress transverse to the model slabs. Therefore, ROM is often also referred as the “iso strain” and inverse ROM as “iso stress” model.[34, 69]

In this work, all introduced models are used for the estimations of the composite modulus, and therefore all equations are written in this form. The modulus and volume fraction of the matrix E_m and V_m and of the filler E_f and V_f are used in Equations (1) and (2) .[34, 70]

$$E_c = E_f V_f + E_m V_m \tag{1}$$

$$E_c = \left(\frac{V_f}{E_f} + \frac{V_m}{E_m}\right)^{-1} \tag{2}$$

Several empirical or semi-empirical expressions have been investigated to estimate the modulus of composite materials. These equations were usually introduced for fibre composites, or originate from rheological considerations but can be applied for particulate composites as well.[36, 69]

The **Halpin–Tsai model** is one of the most used models to estimate the modulus of composite materials. This approach can be described as a self-consistent method, which takes into account reinforcement load bearing relative to the equal stress assumption.[69, 71]
It uses the moduli of the components and a factor ζ for the geometry of the filler to estimate the modulus of the composite E_c, as described in Equations (3) and (4).

$$\frac{E_c}{E_M} = \frac{1 + \zeta\eta V_f}{1 - \eta V_f} \tag{3}$$

$$\eta = \frac{\left(\frac{E_f}{E_m}\right) - 1}{\left(\frac{E_f}{E_m}\right) + \zeta} \tag{4}$$

The ζ factor is related to the ratio between length and thickness of the filler particles.
In the case of alignment in loading direction, $\zeta = 2 \cdot w/t$ is used, while for perpendicular to loading direction, $\zeta = 2$ is used. For ellipsoidal particles, the ratio is w/t =2. For a random orientation of filler particles, ζ can then be estimated with 3, between parallel and perpendicular.[36, 56, 71]

The **Kerner equation** predicts the modulus of the composite by only using the Poisson's ratio ν_m and the modulus of the matrix material, assuming spherical particles (Equation (5)). This equation also assumes a perfect interfacial adhesion and an isotropic, homogeneous composite. The Kerner equation usually only predicts the modulus of a particle composite in the range of a few volumetric percent, up to ~40 vol%. [36, 56, 70, 72]

$$\frac{E_c}{E_m} = 1 + \frac{15 V_f (1 - \nu_m)}{(1 - V_f)(8 - 10\nu_m)} \tag{5}$$

The **Lewis–Nielsen model** is a generalized and modified form of the Kerner equation. In this form the equation is comparable to the Halpin–Tsai model, but uses different assumption on filler geometry and takes filler packing into account. The factor A arises from geometrical assumptions and the Poisson's ratio of the matrix. ζ depends on the particle packing fraction; here $V_{f,max}$ must be assumed as the maximum packing of filler particles within the matrix. The limit of $V_{f,max}$ would be 0.74 for hexagonal close packing spheres, but can be assumed to be lower in accordance to

agglomerates and inhomogeneities within a real composite. [55, 70, 73] The different parts of the Lewis–Nielsen model are shown in Equations (6), (7) and (8).

$$\frac{E_c}{E_m} = \frac{1 + ABV_f}{1 + B\zeta V_f} \tag{6}$$

$$B = \frac{\frac{E_f}{E_m} - 1}{\frac{E_f}{E_m} + A} \tag{7}$$

$$\zeta = 1 + \frac{V_m}{V_{f,max}}[V_{f,max}V_f + (1 - V_{f,max})V_m] \tag{8}$$

2.8 Aminolysis reaction

In the course of this work the reaction between amines and the imide group of the polyimides will be referred to as aminolysis reaction. As this reaction most likely occurs on the polyimide surface and used amines, it is depicted showing the PPPI molecule and a primary diamine in Figure 6. The amine group reacts with the imide group, and two amid groups are formed, one of which becomes a side chain. This side chain consists of the groups within the used diamine and can then potentially react with another polyimide surface.

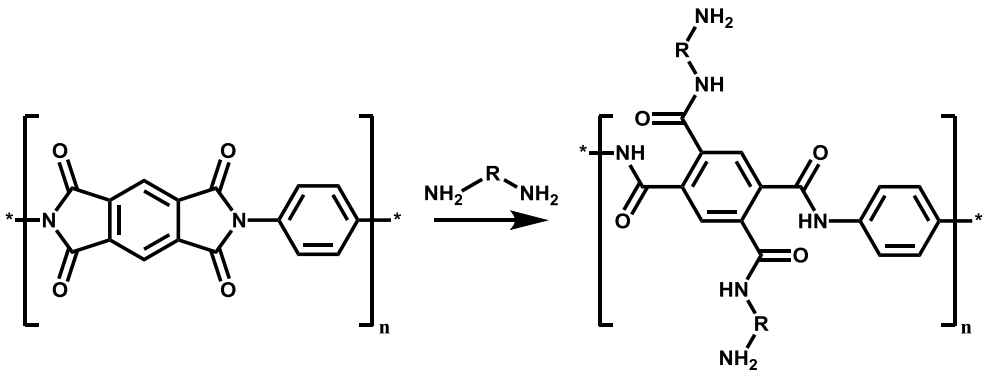

Figure 6: Aminolysis overall reaction depicted at PPPI molecule

3 Aims

The goals of this work were the preparation of polymer matrix composite materials, with the use of hydrothermal produced PPPI particles. The focus was the production of composites with an epoxy or polyimide matrix and their characterisation.

The set goals of this thesis were:

- Establishing a hot compression moulding procedure for polyimide – PPPI composites
- Testing of a direct forming (pressing and sintering) procedure for polyimide – PPPI composites
- Developing a procedure for moulding epoxy – PPPI composites
- A mechanical characterisation of the produced composites, with main focus on classic mechanical testing including three-point bending, tensile and hardness testing
- An understanding of the fracture behaviour with fractography
- An investigation of the microstructure with various plastographic methods via light and scanning electron imaging
- A thermal characterisation with dynamic mechanical thermal analysis and thermogravimetric analysis

4 Experimental Procedures

4.1 Preparation of polyimide particles

The synthesis of the PPPI particles has been done by Michael Taubländer (of advanced organic materials research group). The materials used for the synthesis of the PPPI particles are depicted in Table 4.

Table 4: Materials for preparation of polyimide particles

Name	Supplier	specification
p-phenylenediamine	Sigma-Aldrich	97%
pyromellitic dianhydride	Sigma-Aldrich	98%

To produce the monomer salt, 42.4 g (194.4 mmol, 1.08 eq.) of pyromellitic dianhydride (PMDA) were added to 600 mL of degassed distilled H_2O. After stirring at 80 °C under Ar atmosphere for one hour, the solution cleared, indicating the finished hydrolysis to pyromellitic acid (PMA). Then, 19.5 g (180 mmol, 1 eq.) of p-phenylenediamine (PDA) were added, which led to the precipitation of the monomer salt as an off-white solid. The monomer salt $H_2PDA^{2+}PMA^{2-}$ was separated by vacuum filtration and was washed with distilled H_2O. [18]

In a 1 L steel autoclave, 23.9 g of the monomer salt (66 mmol) were suspended in 330 mL of distilled water. The mixture was heated to 250 °C for 3 h under magnetic stirring at 600 rpm. The reaction was stopped by rapid cooling to room temperature with cold water. The product was separated by vacuum filtration and was then washed with distilled water and ethanol. Finally, the PPPI was dried in a vacuum oven at 80 °C overnight. [18]

From former works with PPPI particles, produced at the advanced organic materials research group, specific properties are known, which are listed in Table 5. Figure 7 illustrates the structure of PPPI. For calculations and comparison with finished materials, these properties have been used in this work.

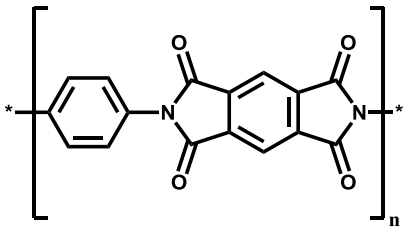

Figure 7: Structure of poly-(p-phenylene pyromellitimide) – PPPI, [17]

Table 5: Properties of PPPI particles

Property		Ref.
Theoretical density	1,73 g/cm³	[74]
Size distribution	D_{10}: 2.2 D_{50}: 6.1 D_{90}: 11 µm	[74]
Decomposition onset	630 °C	[17]

The produced PPPI particles used in this work have a sheet-like structure as shown in Figure 8. The particles show a sheet-like morphology, with a size of around 6 µm in length/width, and a thickness of about 0.1 µm. The particle size was determined by dynamic light scattering and is found to be a multimodal distribution from 11 µm down to under 1 µm, with a D_{50} of 6.1 µm.

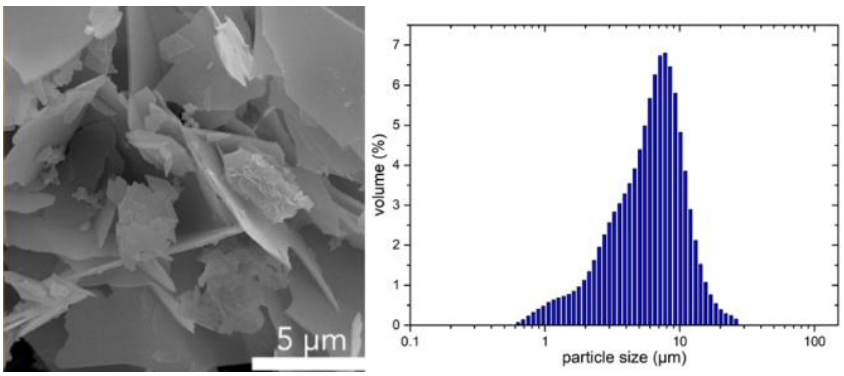

Figure 8: PPPI particles size distribution and morphology, [74]

4.2 P84 - Composites

4.2.1 Materials

In Table 6, materials and their source of supply for production of the P84 – composites are depicted.

Table 6: Materials for the production of P84 - composites

Name	Supplier
P84 Polyimide Powder – 425 mesh HCM	HP Polymer GmbH
P84 Polyimide Powder – 325 mesh HCM	HP Polymer GmbH
P84 Polyimide Powder – 200 mesh HCM	HP Polymer GmbH
P84 NT	Evonik
PPPI Powder poly-(p-phenylene pyromellitimide)	Unterlass Lab
Silicone Spray AK	Wacker Silicones
Isopropanol	-
Hexamethylenediamine (HMDA)	-
1,2-Diaminocyclohexane (DACH)	Fluka Chemika
JEFFAMINE® D-230 Polyetheramine	Huntsman
JEFFAMINE® EDR-176 Polyetheramine	Huntsman

4.2.2 Properties of P84

P84 HCM powder from HP Polymer GmbH was used as the first of three matrix materials in this work. This polyimide is fully imidized and therefore suitable for hot compression moulding. In Figure 9 and Table 7, the structure of this polyimide and its manufacturer's specifications are shown.

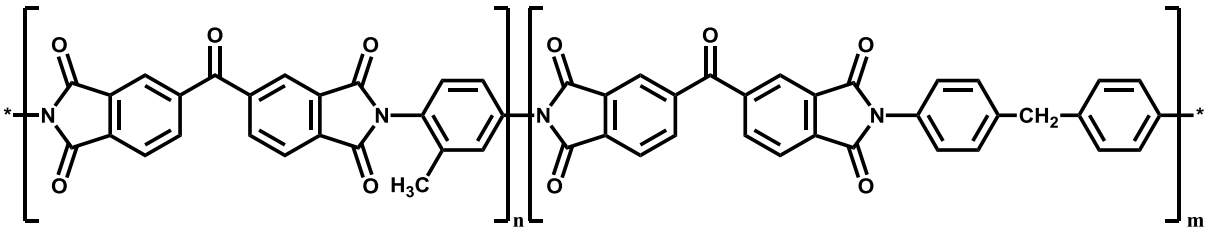

Figure 9: P84 structure[74]

Table 7: Properties of P84 HCM [44]

Properties	
Density	1,34 g/cm³
Tensile strength	140 MPa
Tensile elongation at break	9 %
Tensile modulus	4000 MPa
Flexural strength	205 MPa
Flexural elongation at break	7 %
Glass-transition temp.	330 °C

4.2.3 Properties of P84 NT

P84 NT powder from Evonik Industries was used as the second of three matrix materials in this work. This polyimide is not fully imidized and is therefore suited for direct forming (cold pressing and sintering) and hot compression moulding. In Table 8, the manufacturer's specifications are listed.

Table 8: Properties of P84 NT[45]

Properties	
Density	1,38 g/cm³
Tensile strength	140 MPa
Tensile elongation at break	10 %
Tensile modulus	3581 MPa
Flexural strength	188 MPa
Flexural modulus	3705 MPa
Flexural elongation at break	15 %
Glass-transition temp.	337 °C

4.2.4 P84 - Composite production

4.2.4.1 Powder mixing

For the polyimide – polyimide composites, P84 and P84 NT were used as matrix materials. To determine the suitable particle size for the production of the composites, preliminary tests were conducted with different mesh grade powders. Also, different mixing strategies of the various powders were tested as described subsequently.

Tumbling Mixer:

The P84 - and PPPI - powders were weighted in a wide neck bottle (PE) and 30 zirconium dioxide grinding balls (d: 10.5 mm) were added. The powders were blended for 20 minutes in the tumbling mixer (Turbula, WAB). To separate the mixed powder from the grinding balls, a 0.5 mm sieve was used. The powder mixture was dried for at least 18 h in a drying oven at 110 °C in a crystallizing dish.

Dry ball milling:

The polyimide powders were weighted in a wide neck bottle and 30 zirconium dioxide grinding balls were added. The powders were mixed for 4 hours in a ball mill. Then the mixture was sieved through a 0.5 mm sieve. The powder mixture was dried for at least 18 h in a drying oven at 110 °C in a crystallizing dish.

Wet ball milling:

The powders were weighted in a wide neck bottle and a suitable amount of isopropanol (IPA) was added (e.g. 100 mL IPA for 20 g powder). 30 zirconium dioxide grinding balls were added. The mixture was shaken by hand and then placed in the ball mill for four hours. Afterwards, the grinding balls were separated by a sieve, and the isopropanol powder mixture was dispersed by ultra-sonication (Hielscher, UP400S) for 15 minutes (amplitude: 70%, cycle: 0.5). The isopropanol was removed using a rotary evaporator at 100 mbar and 60 °C. To dry the powder completely, it was placed in a drying oven for at least 18 h at 110 °C. To break up agglomerates potentially built during the drying procedure, another dry ball milling step was carried out for 2 hours. After sifting (0.5 mm), the powder mixture was dried for 2 hours at 110 °C.

4.2.4.2 Surface modification

Surface modification of P84- and PPPI- powders was performed using a variety of diamines. The diamines and their respective abbreviations are hexamethylenediamine (HMDA), 1,2-diaminocyclohexane (DACH), and two different polyetheramines (Jeffamines), Jeffamine D 230 (D230) and Jeffamine EDR-176 (EDR).
The amines were incorporated in three different ways, depending on the powder mixing procedure. For a surface modification of only the PPPI, the powder was put into a round bottom flask with distilled water and 1 wt% of the amine (with respect to the PPPI compound). The suspension was subsequently stirred at reflux for one hour. To modify both polyimide powders at once, the amines were put into the powder mixture and either wet- or dry-ball-milled. The modification was done solely with composite samples of 10 vol% PPPI.

4.2.4.3 Hot compression moulding

To produce a monolithic part out of the polyimide mixture, hot compression moulding was used. The inside of the hot-pressing tool and punches were lightly coated with silicone spray. 19 g of the powder were put into the die cavity, with the lower punch already in place. The upper punch was put on top of the powder and pressed into the die cavity by hand. The pressing tool was put inside the press (P/O/Weber, Type PW 40S) in between isolating blocks, as shown in Figure 10. For the hot-pressing procedure, the heat mantle was plugged in and the thermocouple was put in place. The heating program was started on the controller (Dold – Prozessorregler, DPP 96 C) with a heating rate of 6 °C/min from 25 to 350 °C and a holding time of 30 min at 350 °C. The pressure was applied simultaneously at 35 MPa or 70 MPa. For one surface-modified sample, an additional temperature step (2 h at 250 °C) was added during heating. During the hot compression, the pressure dropped constantly and was adjusted throughout the procedure. Higher decreases in pressure were noted especially from 280 to 320 °C. At the end of the temperature program, the pressing tool was left to cool on its own over several hours. The cooled compacted sample was demoulded at low force. Resulting samples had a size of 40 mm diameter and a height of 11 mm.

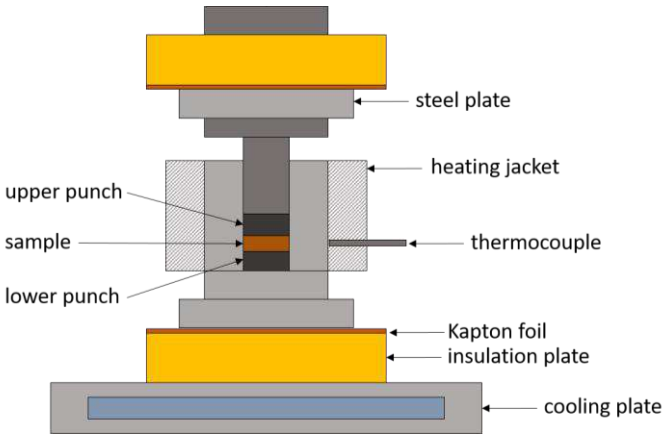

Figure 10: Setup used for hot compression moulding

Figure 11 shows examples of the finished hot compression moulded P84/PPPI composites and cut out test specimens for flexural testing.

Figure 11: P84/PPPI composite, hot compression moulding samples and cut out test specimens

4.2.4.4 Direct forming

The mixed powders were filled into silicone moulds, which were closed thereafter. The moulds were sealed with cut-of latex gloves fingers, while taking care that no air was enclosed. Cold isostatic pressing (P/O/Weber, Type PW 40S) was performed in synthetic oil at pressures of 250 MPa, 300 MPa and 350 MPa. The pressure was held for 5 minutes and then released slowly over 5 minutes. Pressed “green parts” were subsequently sintered at 350 °C for 1 and 3 hours under air, using a heating rate of 2 °C/min.

4.3 Epoxy - Composites

4.3.1 Materials

In Table 9, materials and their source of supply for production of the epoxy – composites are depicted.

Table 9: Materials for the production of epoxy - composites

Name	Supplier
Araldite LY 1564	Huntsman
Hardener XB 3473*	Huntsman
PPPI Powder poly-(p-phenylene pyromellitimide)	Unterlass Lab
Isopropanol	
Silocon Spray AK	Wacker Silicones
Elastosil M 4641	Wacker Silicones

4.3.2 Properties of Araldite

Araldite LY 1564 is a Bisphenol A/diglycidyl ether-based, low viscosity epoxy resin, suited for the use in filament winding, resin transfer moulding (RTM), pressure moulding, or pultrusion. The resin was cured with a formulated amine hardener – Hardener XB 3473 – consisting of 2,4-diethyl-6-methyl-1,3-phenylenediamine (60-90 %) and 1,2-diaminocyclohexane (7-13 %). The structures of epoxy resin and hardener system and its properties can be found in Figure 12, Figure 13 and Table 10.

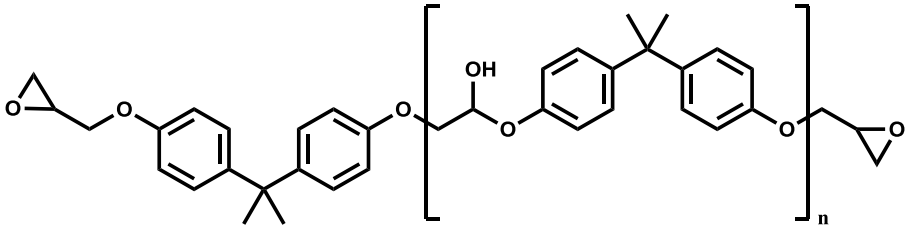

Figure 12: Bisphenol A diglycidyl ether (DGEBA) used as epoxy resin prepolymer

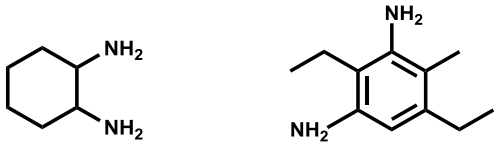

Figure 13: 1,2-diaminocyclohexane and 2,4-diethyl-6-methyl-1,3-phenylenediamine used as hardener system

Table 10: Properties of Araldite LY 1564 / Hardener XB 3473 – epoxy resin[75]

Properties	
Average molecular weight (Araldite LY 1564)	<700 g/mol
Density (Araldite LY 1564)	1.10 – 1.20 g/cm³
Density (Hardener XB 3473)	0.99 – 1.02 g/cm³
Initial mix viscosity	1000 – 1200 mPa s (25 °C) 200 – 250 mPa s (40 °C)
Pot life	84 – 88 h (100g)
Glass-transition temp. (DMA)	165 – 175 °C
Flexural strength	100 – 110 MPa
Ultimate flexural elongation	5.5 – 6.5 %
Flexural modulus	2500 – 2700 MPa

4.3.3 Preparation of silicone moulds

For the production of tensile and flexural testing specimens, different silicone moulds were prepared. The silicone (Wacker Silicones, Elastosil M 4641 B) was mixed with 10 wt.% of the according curing agent (Wacker Silicones, Elastosil M 4641 A) by hand. To end up with a negative mould, the positive forms of the specimens were poured over with the silicone mass in an acrylic glass box, as depicted in Figure 14. The silicone was subsequently degassed in a vacuum oven at 3 mbar for 40 minutes. The remaining air bubbles were removed with a spatula, and the surface was straightened. After 24 hours of curing at room temperature, the moulds were released and preheated to 160 °C for several hours before they could be used.

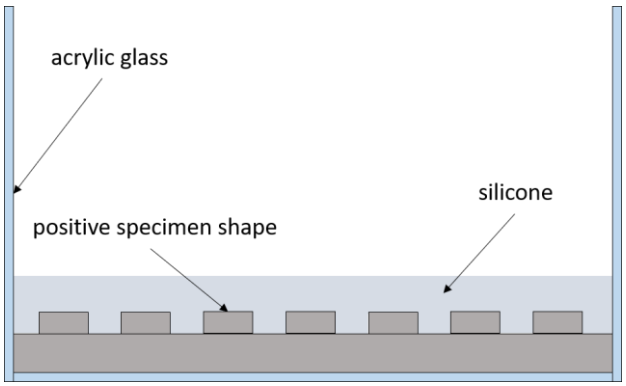

Figure 14: Silicone moulds production scheme

4.3.4 Compounding procedure

To produce the unmodified epoxy resin, the epoxy prepolymer (diglycidylether of Bisphenol-A – DGEBA) was mixed with the curing agent (2,4-diethyl-6-methyl-1,3-phenylenediamine; 1,2-diaminocyclohexane) in a weight ratio of 100 to 26 parts. The mixture was stirred in a planetary mixer (Thinky, ARE-250) for 4 minutes at 2000 rpm. Degassing and casting was done the same way as for the composite samples.

For the preparation of the composites, the dried PPPI particles were mixed in isopropanol, in accordance to the intended content of the finished samples. To break up any agglomerates, the mixture was kept in an ultrasonic bath for 60 minutes, and under a probe sonicator (Hielscher, UP400S) for 15 minutes (70 % amplitude, 0,5 cycle). The epoxy prepolymer (DGEBA) was admixed using a dispersing instrument (Ultra Turrax, T25 basic) for 60 minutes at 1900 rpm. Then the isopropanol was removed using a rotary evaporator at 60 °C for 90 minutes. To incorporate the curing agent into the prepolymer/PPPI mixture, the planetary mixer was used for 4 minutes at 2000 rpm. The mixture was degassed in the planetary mixer for 10 minutes at 800 rpm and for 10 minutes in a vacuum oven at 20 mbar. Before casting, the silicone moulds were coated with a thin film of silicone spray. Then the mixture and silicone moulds were preheated to 90 °C in the vacuum oven for 30 minutes, and the hot epoxy composite was poured carefully in the open moulds. Curing was done for 3 hours at 130 °C and for 12 hours at 160 °C. The whole procedure is summarized in Figure 15. After a slow cooling in the oven to room temperature, the samples were released from the mould.

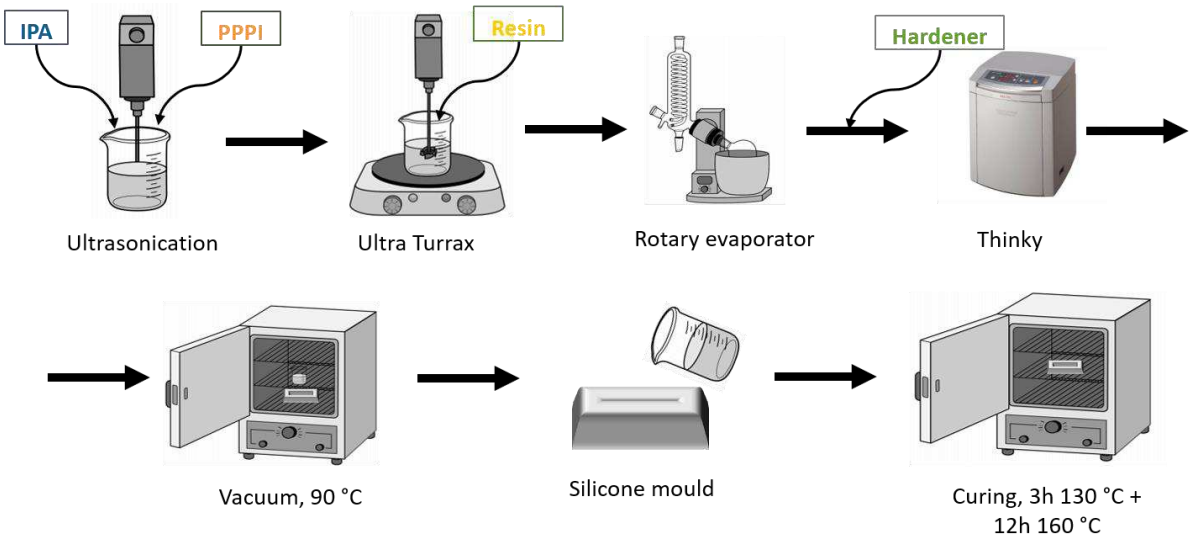

Figure 15: Processing scheme for the production of epoxy-based composites

Figure 16 shows different casted neat epoxy and epoxy-based composite samples. The “dog bone” shaped samples are for the use in tensile testing and the rectangular samples for the production of flexural test specimens.

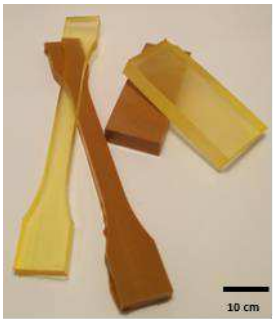

Figure 16: Epoxy resin and epoxy/PPPI composite samples for tensile testing and flexural testing before cutting and grinding

4.4 Characterization

4.4.1 Density evaluation

Density of the different samples was measured geometrically, by a calliper and an analytical scale. For Archimedes density, the samples were weighted in air and under distilled water using an Archimedes setup. The temperature of the water was determined after the density measurement.

4.4.2 Microstructural analysis

To analyse the microstructure of the composite samples, various plastographic techniques were used. For imaging with a reflected light microscope (Olympus GX51), sample pieces were cold embedded (Struers, Epo Fix Kit) and polished according to the procedure in Table 11 on a semi-automatic grinding and polishing machine (Struers, Tegra Pol-31) using SiC and diamond media. The polished samples were etched with an aqueous solution of 50 weight % NaOH for 10 min, and were examined under the reflected light microscope.
Thin-ground sectioning was done by hand on thin cut sample pieces. First, one side was polished similar to the procedure in Table 11. The polished side was glued on a glass specimen holder with epoxy glue (UHU PLUS, Schnellfest). Then, the second side was grinded until just a thin film of the sample remained on the specimen holder, and was polished with the same procedure. The prepared thin-ground samples were analysed using a transmitting light microscope and polarised light (λ/n - plate).
Scanning electron micrographs of fracture surfaces and polished samples were recorded with a FEI ESEM Quanta 200 in secondary and backscattered electron mode.

Table 11: Polishing procedure

Substrate	Grit size (µm)/(mesh)	Speed (rpm)	Load (N)	Time (min)
SiC	P 400	150	10/60	1
SiC	P 1000	150	10/60	1
Stuers, Plan	15	150	10/60	2
Stuers, Dac	6	150	10/60	5
Stuers, Dac	3	150	10/60	25
Struers, Nap	1	150	10/60	15

4.4.3 Nanoindentation

Nanoindentation was done using a loading of 0.5 mN, a loading rate of 0.05 mN/s, 30 s holding time, and 0.1 mN/s release on the embedded and polished samples (Hysitron, UBI 750L). The load-displacement curves during the indentation were recorded. On each sample, ten indentations were made.

4.4.4 Vickers hardness

Vickers hardness testing was performed on cold embedded (Struers, Epo Fix Kit) and polished samples using an EMCO, M4U-025 hardness tester. The diagonals of the hardness impressions were measured using a light microscope (Olympus GX51). In this work, the hardness of the reference material and composites was determined via the HV1 method, this translates to a force of 1 kg (9.81 N) applied onto the Vickers indentation pyramid. On each sample, 5 indentations were made. To test the materials on fracture mechanics, higher loads up to 10 kg were used.

4.4.5 Three-point bending tests

Three-point bending tests were conducted following the EN ISO 178 [76] protocol, using a Zwick 1474 universal testing machine. The cast samples (100 x 35 x 10 mm) were cut into test specimens using a nickel bonded diamond cutting wheel (AB Technics, nickel bond diamond wafering blade) and ground to 35 mm length x 5 mm width x 1.60 mm thickness using silicon carbide grinding paper (P400, P1000) and a diamond grinding disk (Cameo disk, P120 - 180).
For the hot moulded samples, the cylinders (d: 40 mm, h: 11 mm) were cut in half to obtain two discs with 5 mm height. The cylinders were then cut into 1.60 mm thick test specimens, with a varying length between 30 and 40 mm. Strength testing was done perpendicular to the pressing direction applied during hot compression moulding.
To test the strength parallel to pressing direction in hot compression moulding, test specimens were cut into disks with a thickness slightly over 1.60 mm. Test pieces of 5 mm width were then cut out of these disks. In Figure 17, the described specimen types are shown.
The bottom side was polished in 15 µm, 3 µm and 1 µm steps using diamond paste and polishing cloths similar to the procedure in Table 11. For each PPPI content, 10 samples were tested at room temperature (25 °C) with a length of span between supports of 25.4 mm and a testing speed of 1 mm/s.

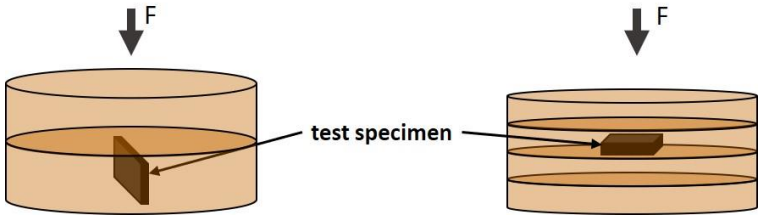

Figure 17: Three-point bending test specimens, P84 samples perpendicular (left) and parallel (right) to pressing force

4.4.6 Tensile tests

Tensile tests were conducted according to the EN ISO 527 [77] protocol, using a Zwick 1474 universal testing machine. The cast samples (test specimen 1BA, Table 12) were grinded with silicon carbide grinding paper (P400, P1000) and a diamond grinding disk (Cameo disk, P120 - 180) to achieve plane parallel sides. Finally, the samples were polished with polishing cloths and diamond paste in 15 µm, 3 µm and 1 µm steps. Figure 18 and Table 12 contain the dimensions of test specimen type 1BA in detail.

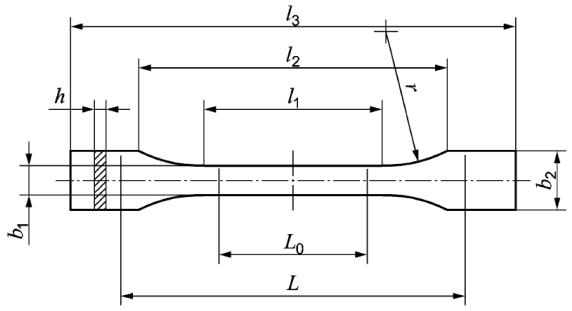

Figure 18: Dimensions of test specimen type 1BA [77]

Table 12: Dimensions of test specimen type 1BA

		Dimensions (mm)
l_3	Overall length	75
l_1	Length of narrow parallel part	30.0
r	Radius	≥ 30
l_2	Distance between broad parallel sides	58
b_2	Width at end	10
b_1	With of narrow part	5
h	Height	3

4.4.7 Dynamic mechanical analysis

Dynamic mechanical analysis (DMA) was performed in a three-point bending set up, with a length of span between supports of 20 mm (test specimens: 35 mm length x 5 mm width x 1.25 mm thickness) at 1 Hz and 0.06 % dynamic strain (TA Instruments, DMA Q800). The temperature was varied from 30 °C to 400 °C with a heating rate of 3 °C/min.

Due to the phase shift (delta- δ) between stress and strain the resulting modulus (E^*) is a complex number. As shown in Equation (9), it consists of the storage (E') and loss modulus (E'') of the analysed material. The ratio between storage and loss modulus results in the tangent of delta, as depicted in Equation (10) and Figure 19. The tangent of delta reflects the damping behaviour. When observed at varying temperature, it is indicating the glass-transition temperature of a polymer material. Therefore, this ratio is referred as "tan delta" in the diagrams concerning dynamic mechanical analysis (in Chapter 5.3.3.7, 5.3.4.7, and 5.4.9).[78]

$$E^* = E' + iE'' \tag{9}$$

$$\tan\delta = \frac{E''}{E'} \tag{10}$$

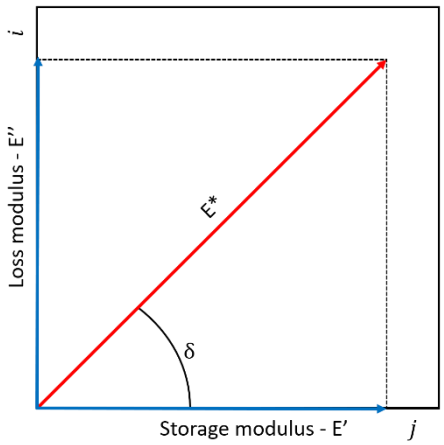

Figure 19: Depiction of phase shift, storage and loss modulus on the complex plane (adapted from [78])

4.4.8 Thermogravimetric analysis

Thermogravimetric analysis (TGA) was performed using a PerkinElmer TGA 8000 instrument with a ramp of 10 °C/min from 30 °C to 700 °C under nitrogen atmosphere (20 ml/min). For TGA, the samples were pulverised with a vibration mill and liquid nitrogen cooling (Retsch, Mixer Mill MM 400). The crushed samples were then sieved and the fraction between 200 µm and 90 µm was used for analysis.

4.4.9 Experiments on thermal degradation of P84 composites

To determine the thermal degradation behaviour of the P84 material and P84/PPPI composites, bending specimens were put into a chamber oven under air, at 200 and 300 °C. After three hours, the heating was turned off and the oven cooled naturally to room temperature. The samples were removed from the oven and tested using a three-point bending set up. The fracture surfaces were examined under the scanning electron microscope.

4.5 Parameters used for models on predicting properties

In all models, except for the Kerner equation, the Young's modulus of PPPI (E_f) was necessary. Here the indentation modulus, measured on the PPPI particles in the epoxy matrix via nanoindentation was used, with a value of 8700 ± 1060 MPa. This value only estimates the Young's modulus of the PPPI particles, but as long as there are no other techniques to determine the mechanical properties of the particles on their own, it was used to calculate the models.
Another possibility would be the use of the more theoretical estimated modulus of PPPI with a value of 12.2 GPa.[20]

For the Poisson's ratio (ν_m) of the matrix materials, 0.35 was assumed, since both matrix polymers are within this range of lateral strain.[55]
The ζ factor in the Halpin–Tsai equation was approximated as 3 for the geometric considerations taken in Chapter 2.7.[56]
In the Nielsen equation, $V_{f,max}$ was assumed as 0.37 to estimate agglomerations and lower particle packing. The A factor in this equation was estimated with 4.86 for a ellipsoidal filler geometry. [55]

5 Results

5.1 P84 NT – Composites – Direct forming

The following chapter describes the results of the P84 NT – composite samples produced by direct forming. For the production of directly formed P84 NT composites, the wet ball milling procedure was chosen.
The resulting "sample code" contains the matrix material (P84 NT), process type (direct forming DF, hot compression moulding HCM), PPPI content in volume percentage, mixing technique (IPA), and the moulding pressure in MPa (35, 250, 300, 350). For example, P84NT_DF_0_IPA_350.

5.1.1 Density

The density of the P84 NT samples was determined before and after sintering. The results of these measurements are described in this section subsequently.

5.1.1.1 Green Density

In Figure 20, the densities of cold isostatic pressed samples are shown. Cylindrical and rectangular bar shaped samples were pressed from neat P84 NT and composite powder. The geometrically determined green density values indicate a lower density for the rectangular samples than for the cylindrical samples.

A loss of relative density and therefore a rise in porosity in the composite samples becomes apparent, upon addition of PPPI. Also, with the addition of PPPI a decrease in absolute density can be observed. No difference in density can be noted between various applied pressures.

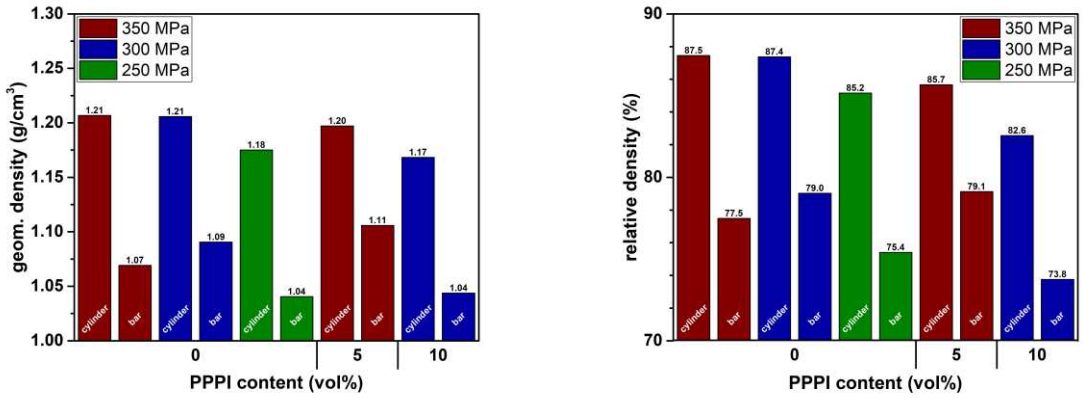

Figure 20: Green absolute and relative density of P84 NT direct forming unfilled and composite P84NT_DF_IPA samples

5.1.1.2 Density after sintering

Density after sintering was determined using the Archimedes method. As it can be seen in Figure 21, all samples show similar relative densities, and no trend between composite and reference samples is observable. The rectangular samples show slightly higher densities than the cylindrical samples. A rise in absolute density can be noticed for the composite samples, due to the higher density of the PPPI. The application of different pressures for sample pressing doesn't seem to have any impact on the sample density.

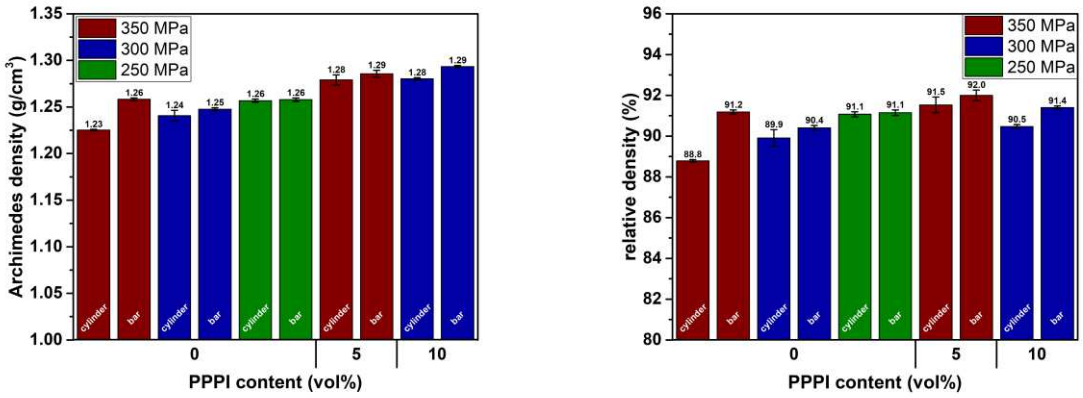

Figure 21: Archimedes, absolute and relative density after sintering of P84 NT direct forming unfilled and composite P84NT_DF_IPA samples, 350 °C for 1 h

To investigate the influence of sintering time on density at 350 °C, a dwell time of 3 h was used. No rise in density of the sintered samples can be observed, which is pictured in Figure 22. This was only investigated with unfilled P84 NT samples.

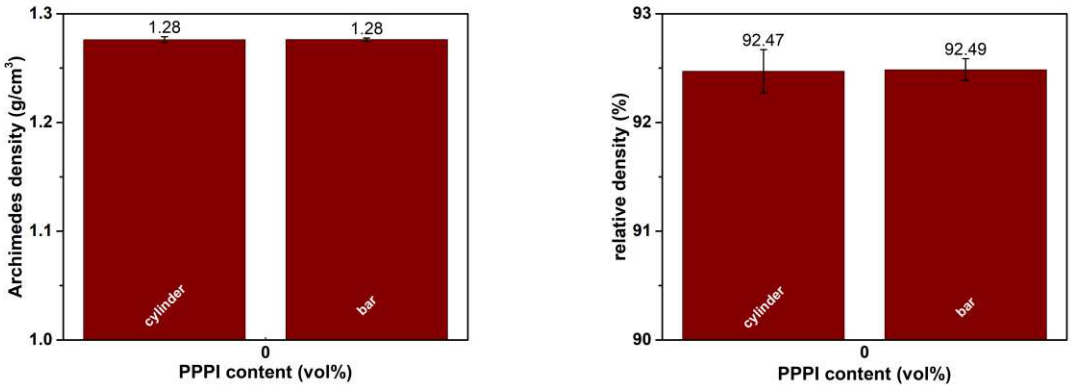

Figure 22: Archimedes, absolute and relative density after sintering P84 NT direct forming unfilled P84NT_DF_IPA_350 samples, 350 °C for 3 h

5.1.2 Microstructural analysis

The fracture surface of the "direct formed" P84 NT sample (0 vol% PPPI, 350 °C, 3 h) is illustrated in Figure 23 and shows individual particles and no uniformly sintered material. The formation of sintering necks can be observed only at an early stage. As the image in Figure 23 a particle packing rather than a uniform sintered material, the sintering can be assumed as incomplete with this sintering program and time.

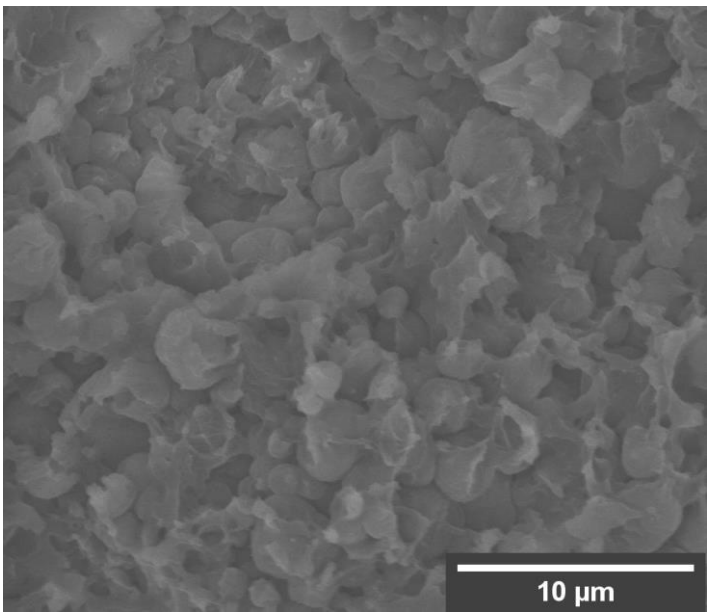

Figure 23: SEM-image of fracture surface P84 NT direct forming sample (0 vol% PPPI), sintered at 350 °C for 3 h; P84NT_DF_0_IPA_350

5.2 P84 NT – Composites – Hot compression moulding

The following chapter describes the results of the P84 NT – composite samples produced by hot compression moulding. For the preparation of these composites, the wet ball milling procedure was chosen and a pressure of 35 MPa was applied during hot compression moulding.

5.2.1 Density

The absolute density of the hot compression moulded samples slightly increases with the addition of PPPI, due to the higher density of PPPI. On the other hand, the relative density decreases with PPPI content. This drop in compaction during hot pressing leads to increased porosity of the composite material. Figure 24 gives an overview of the determined densities.

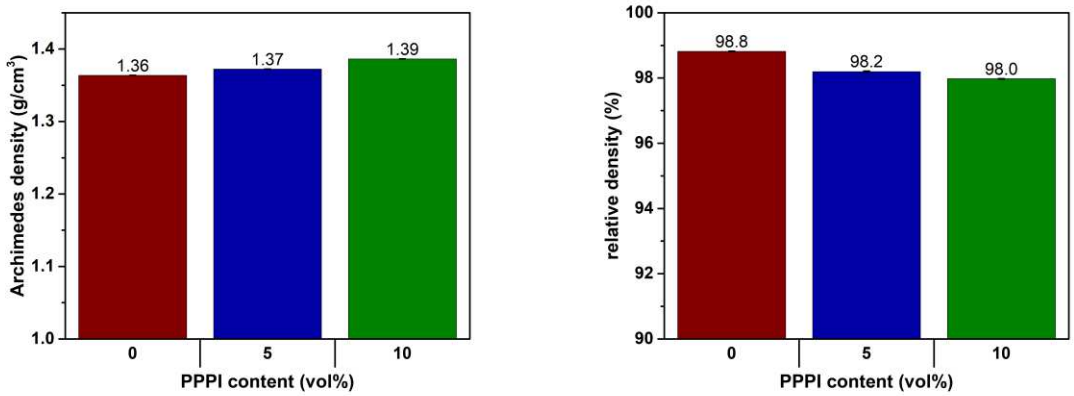

Figure 24: Archimedes and relative density of P84 NT unfilled and composite samples, after hot compression moulding, P84NT_HCM_IPA_35

5.2.2 Microstructure – SEM fracture surfaces

The three-point bending test fracture surfaces of the hot compression moulded P84 NT samples indicate a rather brittle fracture in case of the neat P84 NT and with the addition of 5 vol% PPPI. In the unfilled P84 NT sample, areas with small voids are observed as it is illustrated in the left

picture of Figure 25. A step-like surface appears in the neat and 5 vol% PPPI sample (Figure 25, right image). The voids can also be observed in the 5 vol% composite sample, but at a lower concentration and not as clustered as in the unfilled samples.

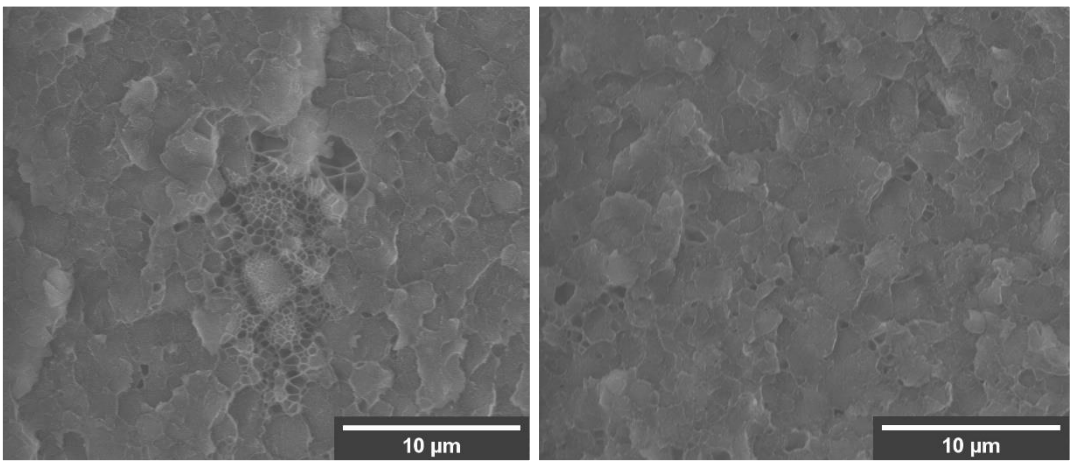

Figure 25: Fracture surfaces of P84 NT, hot compression moulding unfilled sample P84NT_HCM_0_IPA_35 (left) and composite sample P84NT_HCM_5_IPA_35 (right)

5.2.3 Three-point bending test

Figure 26 displays representative stress/strain curves of P84 NT samples and the composites containing 5 and 10 vol% PPPI, Table 13 and Figure 27 contain the flexural strength and strain of these samples. The fluctuation in the curves is due to the force sensor used in these tests. The standard deviation of strength and strain is relatively low. The variation of strength and strain between the test samples most likely originates from imperfections of each test sample and varies within an expected range.

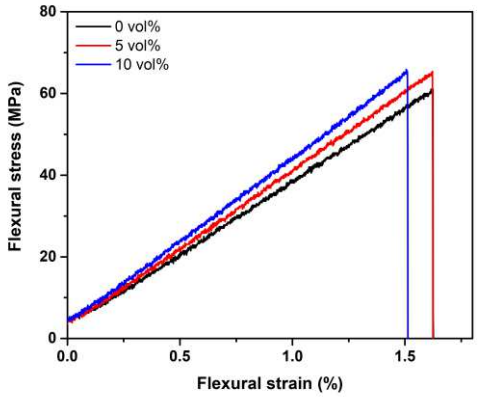

Figure 26: Flexural stress/strain curves of P84 NT hot compression moulded unfilled and composite samples, P84NT_HCM_IPA_35

With the addition of PPPI, no significant change in flexural strength and strain can be determined. The strength and strain values measured are significantly below the producer's specifications of P84 NT.

Table 13: Flexural strength, strain and modulus of P84 NT hot compression moulded unfilled and composite samples; P84NT_HCM_IPA_35

PPPI content (vol%)	σ_{fM} (MPa)	ε_{fB} (%)	E_f (MPa)
0	64.6 ± 9.3	1.69 ± 0.23	3258 ± 121
5	65.2 ± 9.8	1.67 ± 0.26	3326 ± 186
10	72.8 ± 8.1	1.69 ± 0.18	3747 ± 131

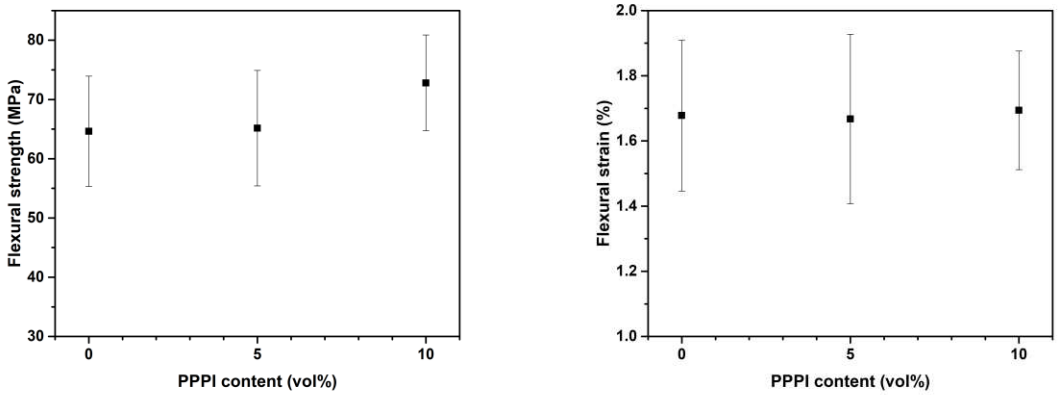

Figure 27: Flexural strength and strain versus PPPI content P84 NT hot compression moulded unfilled and composite samples, P84NT_HCM_IPA_35

The flexural modulus of these samples can be found in Figure 28 as well as in Table 13. It is only increased in the 10 vol% PPPI sample, as predicted by ROM (Chapter 2.7). Samples with 5 vol% PPPI and the unfilled P84 NT exhibit the same modulus, which is also lower than the values provided by the producer. In this case, the modulus of PPPI was also assumed using the measured value from nanoindentation, as described in Chapter 4.5.

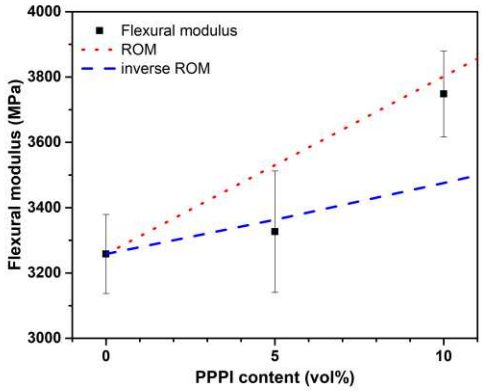

Figure 28: Flexural modulus versus PPPI content P84 NT hot compression moulded unfilled and composite samples, with ROM/inverse ROM model; P84NT_HCM_IPA_35

5.3 P84 – Composites

5.3.1 Direct forming

A direct forming procedure of the P84 powder was tested with cold isostatic pressing and die pressing. The resulting samples exhibited no structural integrity, and therefore the route of pressing and sintering was not pursued further. No densification can be observed in sintering experiments at 350 °C under air.

5.3.2 Hot compression moulding - Preliminary tests

In the preliminary tests, three different powder grades were tested for their applicability in hot compression moulding. Also, three different mixing techniques were investigated. Additionally, the influence of moulding pressure was evaluated. This leads to the sample names “T” for tumbling mixer, “IPA” for wet ball milling under isopropanol and “DB” for dry ball milling. The applied pressure is marked with “35” and “70” (in MPa).
The different P84 powders are ranked from the highest particle size (200 mesh) to the lowest (425 mesh).
The resulting “sample code” contains the matrix materials (P84), PPPI content in volume percentage, mesh-size, mixing technique (T, IPA, DB), hot compression moulding pressure (35 or 70), and an abbreviation for an amine-modification. In case the sample is not modified, it is marked as “unmod”. For example, P84_10_425_DB_35_unmod.

5.3.2.1 P84 /PPPI powder mixtures

In Figure 29, SEM-images of PPPI and P84 powders are shown. The PPPI particles have a micro-sheet shape, with dimensions between 1 and 10 µm in length and width. The thickness of the sheets appears to be thin (under 0.1 µm). Also, larger clusters of particles appear due to the preparation for SEM imaging.
The P84 particles appear rounded in oval shapes, with larger particles of about 20 µm and smaller spheres in the range of 2 µm.

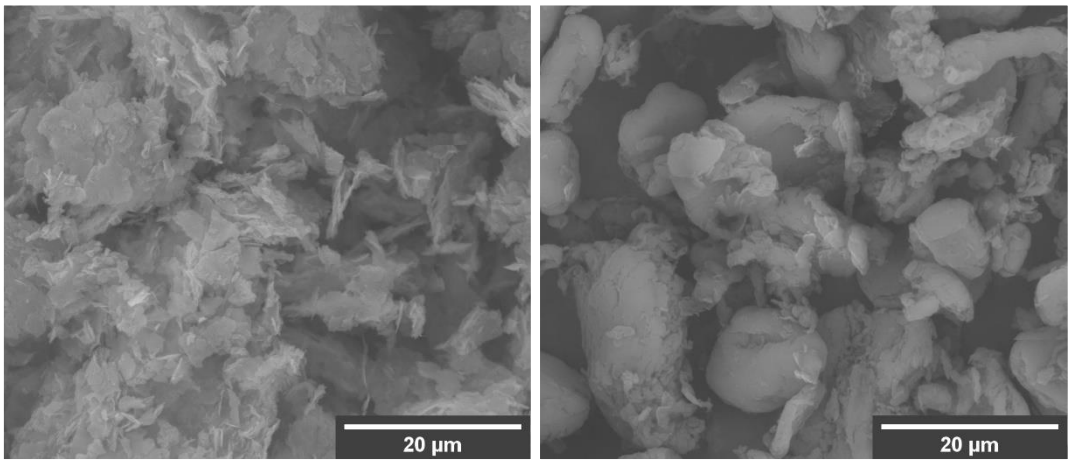

Figure 29: PPPI powder (left) and P84 425 mesh powder (right), as supplied

SEM-images of all different powder mixtures can be found in Figure 30 where it can be seen, that the PPPI particles appear evenly distributed in between the P84 particles. No mixing induced damage of the P84 or PPPI particles can be observed.

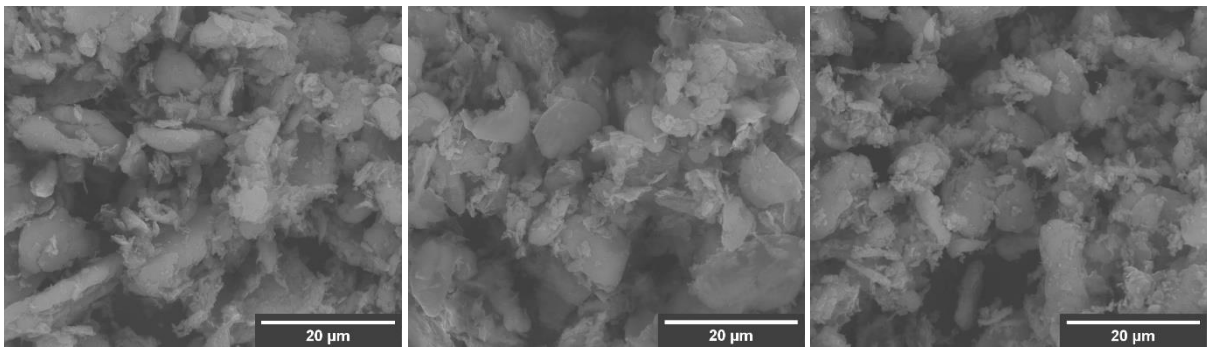

Figure 30: P84 powder mixtures with 10 vol% PPPI; tumbling mixer (left), wet ball mill (middle), dry ball mill (right)

5.3.2.2 Density

The absolute density of the samples was determined using the Archimedes method, Figure 31 contains the determined absolute and relative densities of P84 samples with varying PPPI content and different mesh grades. For the neat P84 samples, high compaction is observable, while the density does not show an extensive variation between samples with different powders. Here, an increase in moulding pressure from 35 to 70 MPa does not change the density significantly.
Only the 20 vol% PPPI sample shows a difference between the mesh grades, with increasing density when using finer P84 powder.
The absolute density of the composites mixed by wet or dry ball milling slightly increases due to the higher density of the added PPPI. A higher relative density is noticeable in the ball milled samples compared to the tumbling mixed samples, with increases of 0.7 % for wet ball milling and 1.2 % for dry ball milling, respectively.
An increase in relative density is observable with a higher moulding pressure of the dry and wet ball milled samples, with increases of 0.7 % in the wet ball milled samples and 0.4 % for the dry ball milled samples, respectively.
In case the tumbling mixer was used, the absolute density of the samples decreases even with the addition of 20 vol% of the denser PPPI. Consequently, the relative density decreases severely in these samples.
In all composite samples, a decrease in relative density can be observed. This decrease in relative density and thus an increase in porosity is most pronounced in the sample containing 50 vol% PPPI with a relative density of only 79 %.

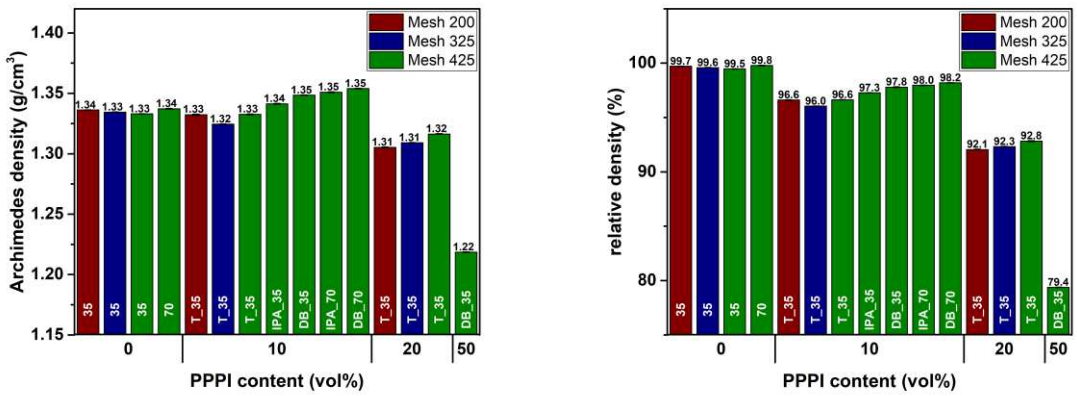

Figure 31: Archimedes and relative density of different preliminary test P84 unfilled and composite samples

5.3.2.3 Microstructure – plastographic analysis

Figure 32 shows plastographic preparations of preliminary test samples of P84 composites. The darker spots resemble either pores or can also be caused by particle outbreaking during polishing. Image analysis of these pictures resulted in relative densities of 89 % for the DB_35 and 91 % for

the IPA_35 sample. In the 10 vol% PPPI samples, no anisotropy or preferred direction of the particles is noticeable.
This underestimation of relative density is most likely due to a break-out of PPPI particles occurring while polishing the samples. Also, scratches remaining from polishing are contributing to these results, hence their equally dark appearance.

Figure 33 shows the image analysis of the samples with 20 vol% PPPI, which results in a relative density of 87 %. Here, an elongation of the matrix P84 particles can be observed. The pores and most likely the PPPI particles are concentrated around the P84 particles.
An analysis of the 10 vol% PPPI sample pressed with 70 MPa results in 92 % relative density.

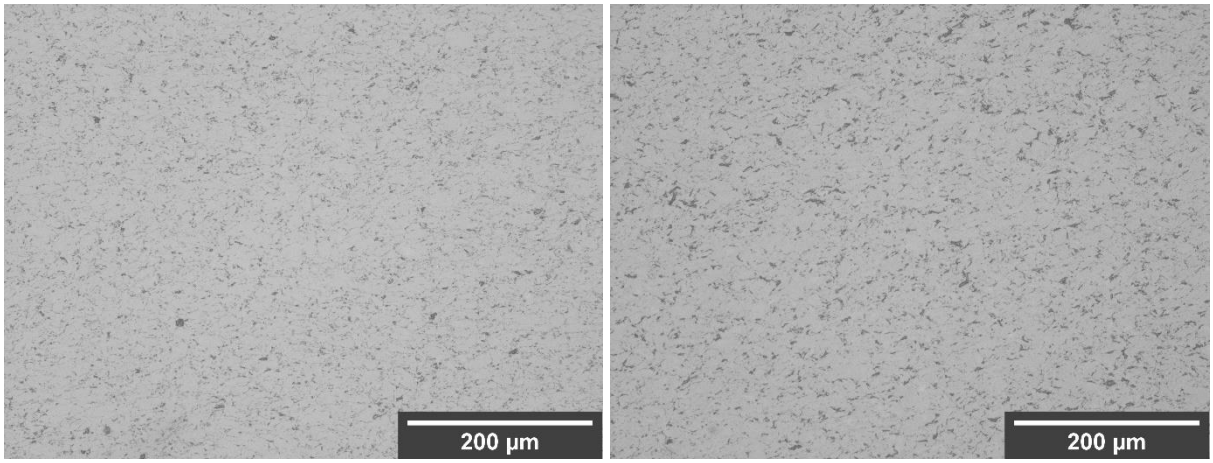

Figure 32: Reflected light microscopy; Sample 10 vol% PPPI, 425 mesh, P84_10_425_DB_35_unmod (left) and P84_10_425_IPA_35_unmod (right)

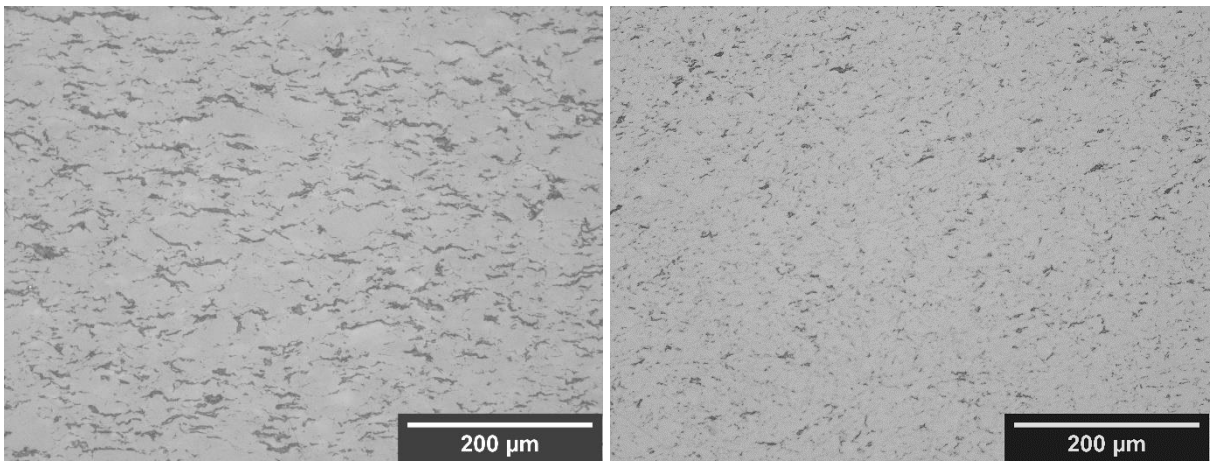

Figure 33: Reflected light microscopy; Sample 20 vol% PPPI, 425 mesh, P84_10_425_T_35_unmod (left) and 10 vol% PPPI P84_10_425_IPA_70_unmod (right)

5.3.2.4 Three-point bending tests

For the preliminary three-point bending tests, a force sensor not ideally suited for the measured force range was used. Therefore, the sensitivity of the measurements is insufficient for an absolute determination of the flexural modulus. Nevertheless, the trends of strength and strain of different mesh-grades and mixing techniques can be evaluated.

Figure 34 illustrates the trends in flexural strength and strain for the neat P84 samples in comparison to the samples containing PPPI. For the neat P84 samples, a clear trend in strength and strain is observable. With reduced particle size of the P84 powder, strength and strain increase significantly. An increased applied pressure during hot compression moulding leads to a

decrease in strength of more than 50 %, and a decrease in strain of nearly 70 %.
A significant decrease in strength and strain with the addition of PPPI is observed for all different composite samples. This decrease can be illustrated in the 10 vol% PPPI samples when compared to the neat P84 sample of the same mesh grade. Here, the decrease is much more pronounced for the finer P84 powder than for the coarser 200 mesh powder. The decreasing trend continues for the composite samples with 20 vol% PPPI.
When comparing the different particle size of P84 powders in the composites with PPPI, a similar increase in strength and strain is noticeable for finer powders, as this was the case for the unfilled P84 samples.

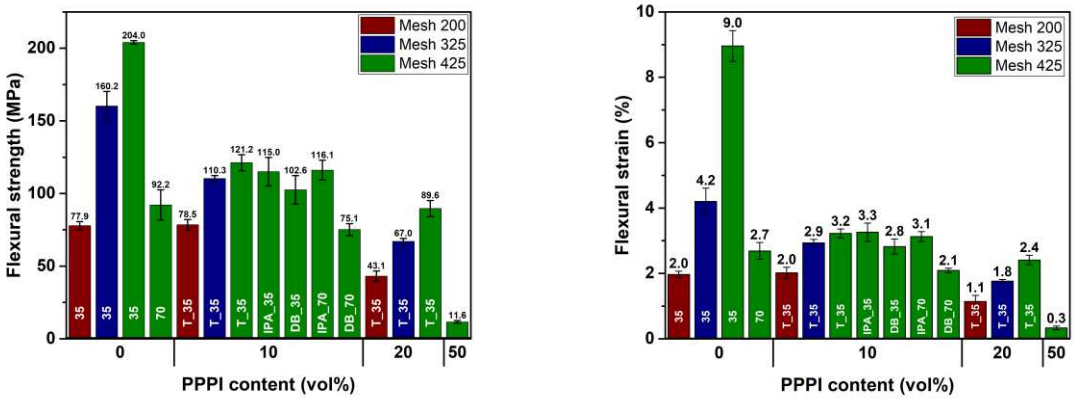

Figure 34: Flexural strength and strain versus PPPI content and mesh size of different preliminary test P84 unfilled and composite samples

In comparison, the different mixing techniques have no significant impact on the strength and strain of the composite materials. A slight decrease in strength and strain is noticeable for the dry ball milling approach (DB_35), but in consideration of the standard deviations, the values lie within the range of the other mixing techniques.
In the composite samples, a decrease in strength and strain is measured for the dry ball milled samples compacted with 70 MPa. In case of the wet ball milled samples, no difference is noticeable. Furthermore, the addition of 50 vol% PPPI to the composite decreases the strength and strain of the material to a near-complete lack of structural integrity.

5.3.2.5 Microstructure – SEM fracture surfaces

This chapter describes the microstructural analysis of neat P84 and composites per fractography. The fracture behaviour of these samples was evaluated using the obtained images.
Figure 35 and Figure 36 show representative fracture surfaces of neat P84 samples. The comparison of 200 and 425 mesh samples displays no difference in morphology. Also, no difference between samples compacted at 35 and 70 MPa can be found in the corresponding SEM-images. In general, all P84 samples show a brittle fracture with ramps, steps, and “breaking parabolas”, which are visible at higher magnifications. Figure 36 shows a good example of these breaking parabolas, which are formed during the initiation of secondary cracks.

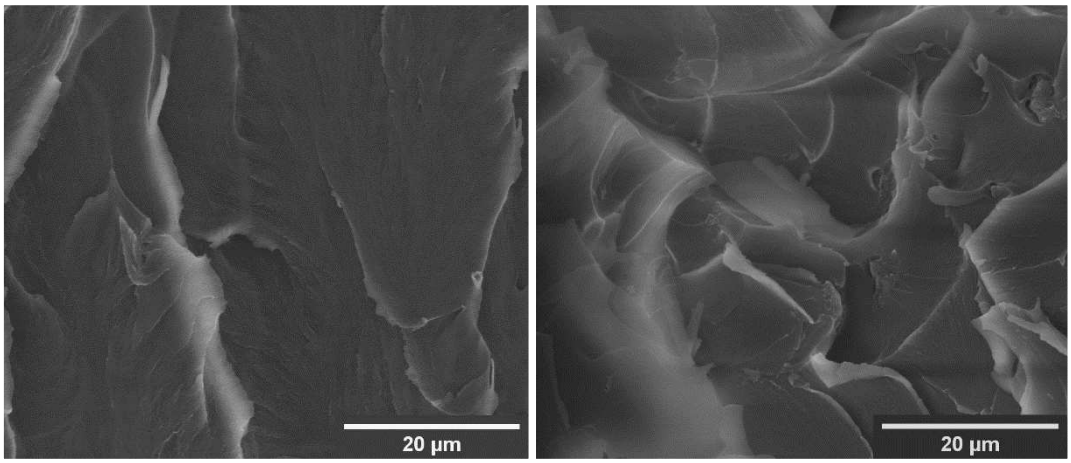

Figure 35: Fracture surface of P84, 35 MPa; P84_0_200 _35 (left) and P84_0_425 _35 (right)

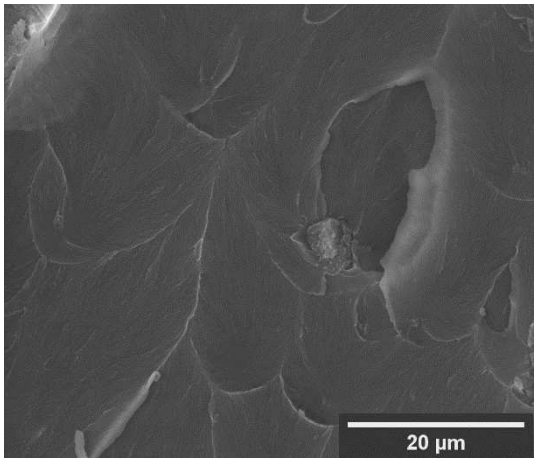

Figure 36: Fracture surface of P84, 70 MPa; P84_0_425 _70

Comparing the three different mixing procedures, the morphology of the fracture surfaces appears similar, which is demonstrated by the SEM-images in Figure 37 and Figure 38. Areas with P84 matrix, characterised by the same “smooth-brittle” fracture as in the reference samples, are detectible. Between and around these areas, a rough surface structure appears. This surface is either caused by the PPPI sheets on the fracture surface or the result of PPPI particles which were pulled out of the P84 matrix. Also, a fracture of the PPPI particles on their own can be a plausible explanation for the occurring morphology.

In the tumbling mixer and dry ball milling approach, larger areas of P84 matrix are observable than in samples produced using wet ball milling. There, deeper voids and an overall rougher surface can be observed while the edges of these samples appear sharper than in dry mixed samples. No difference in morphology occurs between samples compacted at 35 and 70 MPa.

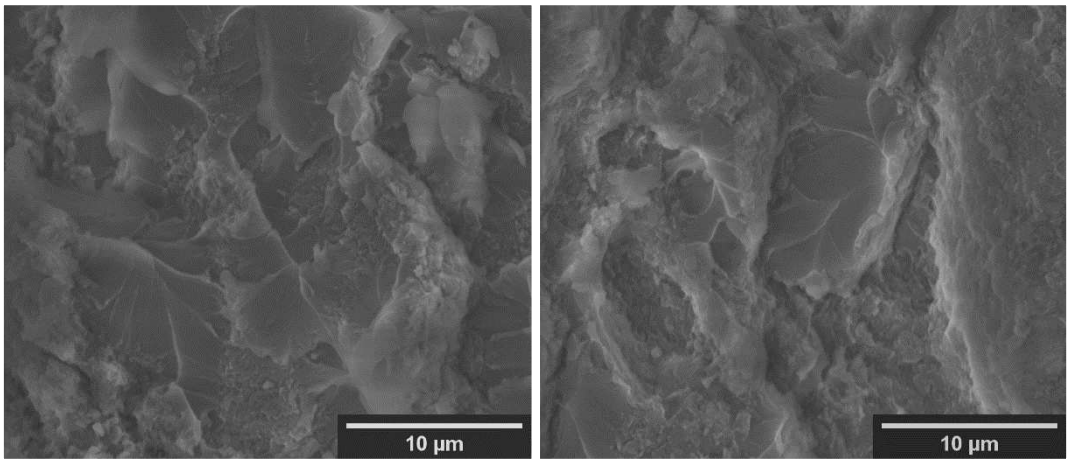

Figure 37: Fracture surface of P84 10 vol% PPPI, 35 MPa, Mesh 425 samples; P84_10_425 _T_35_unmod (left) and P84_10_425_DB_35_unmod (right)

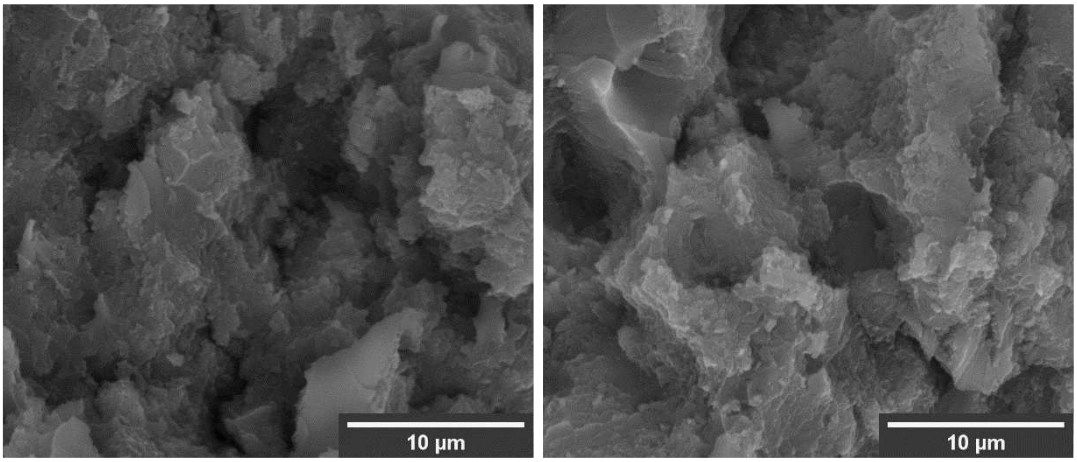

Figure 38: Fracture surface of P84 10 vol% PPPI, Mesh 425 samples; P84_10_425_IPA_35_unmod (left) and P84_10_425_IPA_70_unmod (right)

Comparing the SEM-images of the samples with 20 % PPPI content, (exemplary) contained in Figure 39, a difference between samples with the coarse 200 mesh P84 powder and the finer 425 mesh P84 powder appears. In the 200 mesh sample (Figure 39, left image), the majority of the fracture shows a rough surface and only small areas of "P84 fracture" are observable. The 425 mesh sample appears similar to the 10 vol% PPPI samples in Figure 38, with "smooth-brittle" fracture and rough surfaces in between. In both cases of the 20 vol% PPPI samples, the particles on the rough areas appear to be larger than in the 10 vol% samples.

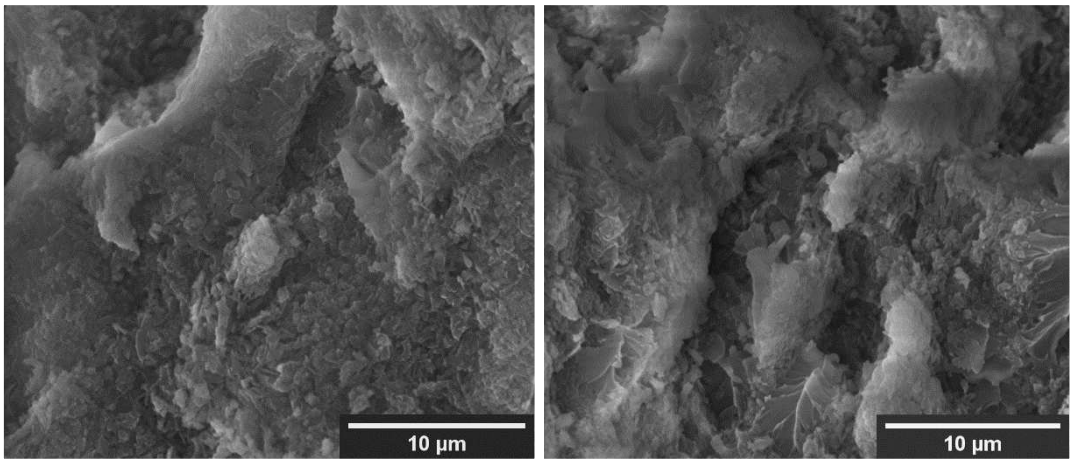

Figure 39: Fracture surface of P84 20 vol% PPPI, 35 MPa samples; P84_10_200_T_35_unmod (left) and P84_10_425_T_35_unmod (right)

5.3.3 Hot compression moulding - Unmodified Samples

This section presents the properties of the P84/PPPI composites produced by hot compression moulding For the production of these composites, the wet ball milling procedure, 425 mesh P84 powder and an applied pressure of 35 MPa during hot compression moulding was chosen according to the results of preliminary tests (see section 5.3.2).

5.3.3.1 Density

Figure 40 shows the absolute and relative densities of samples with 0 vol%, 5 vol% and 10 vol% PPPI content. The absolute density of the 5 vol% PPPI composite is increased compared to the unfilled P84 sample due to a higher density of the PPPI, while the relative density of this sample remains the same compared to the reference sample. In the 10 vol% PPPI sample, the absolute density decreases even with the addition of the denser PPPI. Therefore, the relative density is decreased and a higher porosity in this sample is observed.

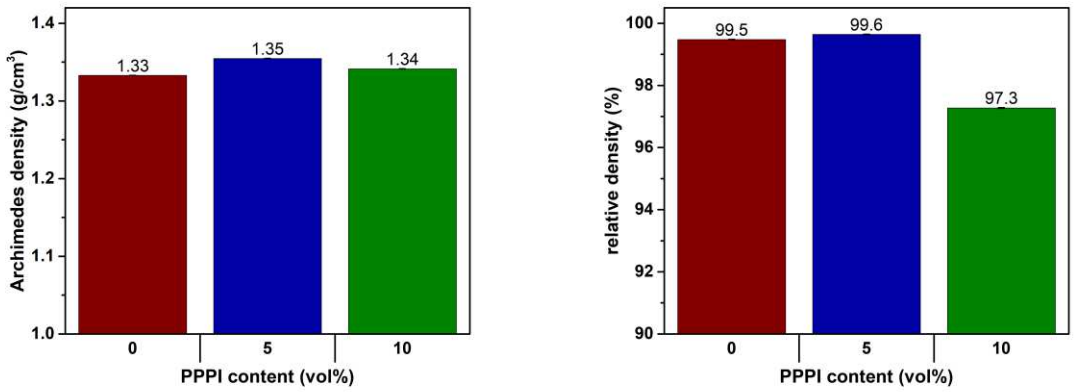

Figure 40: Archimedes and relative density of unmodified P84 unfilled and composite samples; P84_425_IPA_35_unmod

5.3.3.2 Microstructure

For a better understanding of the microstructure within the composites, three different imaging techniques were used, Examples of the obtained images can be found in Figure 41 and Figure 42. A thin-grinded and polished sample was analysed with polarised light (Figure 41, left image). Here, the PPPI appears yellow due to its high crystallinity. The P84 matrix occurs in violet, due to its amorphous nature. With this technique, pores cannot be detected as they consist of air which occurs amorphous like the P84 matrix itself.

The same sample was then etched with NaOH for 10 min and examined using reflected light (Figure 41, right image), where a clear contrast between P84 and PPPI particles is visible. Due to the etching, the PPPI particles appear darker while the P84 matrix is not affected. The larger dark spots resemble either pores or outbroken particles, which were present in the images before etching. Another origin of the large dark spots could be PPPI particles orientated in plane with the polished surface.

A similar structure is observed in the backscattered electron image in Figure 42, where the P84 matrix is darker than the surrounding PPPI particles. Here, pores or broken out particles can be detected was well. Most likely, the larger spots are P84 particles which were removed from the surface during polishing and etching.

Comparing the obtained images, the microstructure of P84/PPPI composite samples can be described in the following way: the smaller PPPI sheets surround the P84 particles, forming a sort of P84-“cores” enclosed by PPPI-“shells”. A clear elongation of the P84 particles is observable, perpendicular to the direction of pressing force.

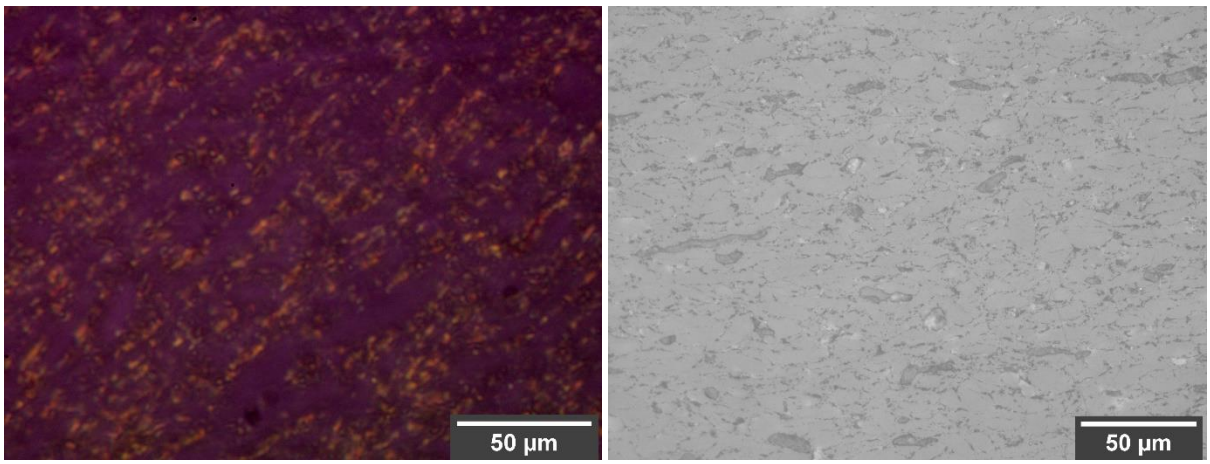

Figure 41: Micrographs of a P84 - 10 vol% PPPI composite sample, P84_10_425_IPA_35_unmod; transmitted, polarised light (left) and NaOH - etched, reflected light (right)

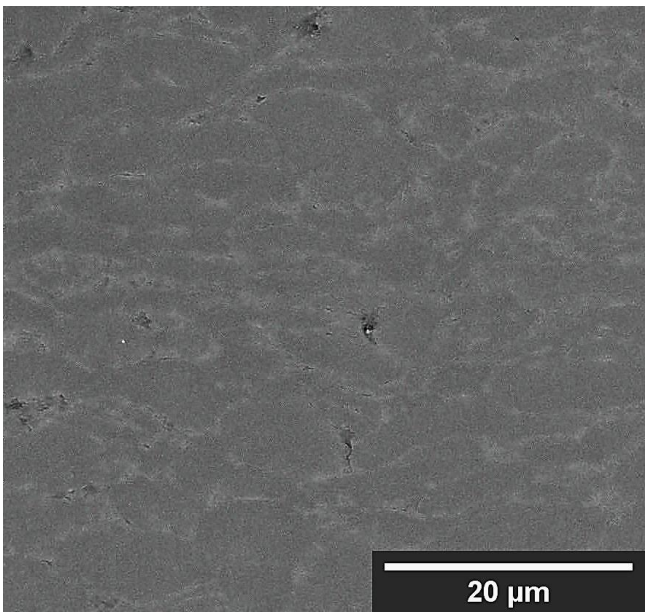

Figure 42: Micrographs of a P84 - 10 vol% PPPI composite sample, P84_10_425_IPA_35_unmod; backscattered electrons image

5.3.3.3 Hardness

The macroscopic hardness was tested using the Vickers HV 1 indentation method. As no cracks can be observed on the edges of the indenter impressions, a very brittle fracture mechanism can be ruled out for the P84 composites.

Table 14 summarizes the determined values of Vickers hardness of the different unfilled and composite samples. The hardness decreases from 385 MPa in the neat P84 sample to 370 MPa in the 5 vol% PPPI sample. The hardness of the 10 vol% PPPI sample, does not change significantly to the reference P84 sample.

For the ROM and inverse ROM model (see Chapter 2.7), the hardness of PPPI particles was determined by nanoindentation (see section 5.3.3.4). As depicted in Figure 43, the hardness cannot be enhanced by adding PPPI as predicted by the models.

Table 14: Vickers hardness of P84 unfilled and composite samples, P84_425_IPA_35_unmod

PPPI content (vol%)	H_i (MPa)
0	386 ± 12
5	367 ± 8
10	391± 10

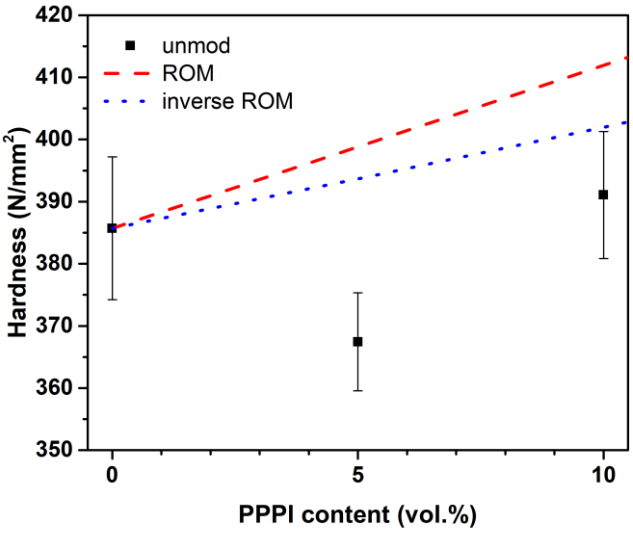

Figure 43: Vickers HV 1 hardness versus PPPI content and ROM/inverse ROM model, P84 unfilled and composite samples, P84_425_IPA_35_unmod

5.3.3.4 Nanoindentation

The indentation modulus of the 10 vol% PPPI composite sample is slightly higher than the modulus of the P84 reference sample, with an increase of 250 MPa. The modulus of 10 vol% PPPI composite is conforming to the calculated ROM model, as it can be seen in Figure 44.
Table 15 contains the values of indentation modulus and nanoindentation hardness of samples with different PPPI content. With selective indentations on the PPPI particles within the P84 matrix, an indentation modulus of pure PPPI can be determined with a value of 8700 MPa. As this method had to be performed on the partially broken out PPPI particles, the value shows a high standard deviation of 1060 MPa.

Table 15: Indentation modulus and nanoindentation hardness of P84 unfilled P84_0_425_IPA_35_unmod and composite P84_10_425_IPA_35_unmod samples, PPPI measured in composite sample P84_10_425_IPA_35_unmod

PPPI content (vol%)	E_i (MPa)	H_i (MPa)
0	5740 ± 60	563 ± 16
10	5990 ± 167	516 ± 14
100	8700 ± 1060	648 ± 83

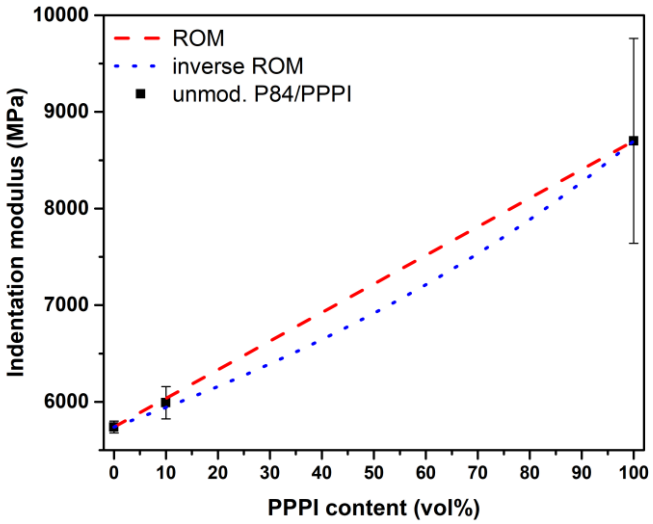

Figure 44: Indentation modulus versus PPPI content of P84 unfilled P84_0_425_IPA_35_unmod and composite P84_10_425_IPA_35_unmod samples, PPPI measured in composite sample P84_10_425_IPA_35_unmod

Figure 45 depicts the nanoindentation hardness of samples with various PPPI content. The hardness of the composite samples with 10 vol% PPPI, measured via nanoindentation, is significantly lower than the hardness of the P84 matrix, with a decrease of 47 MPa. The hardness measured on the PPPI particles increases by 85 MPa compared to the modulus measured on the P84 matrix material. Even though the PPPI particles exhibit a higher mean value, the even high standard deviation of 83 MPa does not indicate a significantly higher hardness of the PPPI to the P84 matrix.

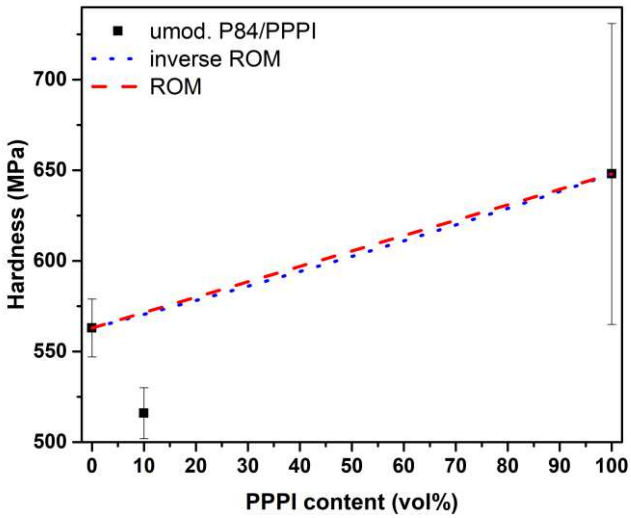

Figure 45: Nanoindentation hardness versus PPPI content of P84 unfilled P84_0_425_IPA_35_unmod and composite P84_10_425_IPA_35_unmod samples

5.3.3.5 Three-point bending tests

In Figure 46, representative stress/strain curves of a P84 reference sample and composite samples are depicted. For these bending tests, the specimens were cut perpendicular to the pressing force direction during hot compression moulding.

The neat P84 sample shows a large elastic region up to a strain of 5 % before the behaviour changes to plastic deformation, without a distinguished transition. Plastic deformation takes place

up to a sharp fracture at around 9 % strain.
This plastic behaviour of the matrix P84 is suppressed by the addition of PPPI. In the 5 vol% PPPI composite, no plastic deformation of the material can be observed. After a steeper elastic deformation, the material fractures, implying much more brittle behaviour with a higher modulus. This behaviour gets even more pronounced in the 10 vol% sample. The strength of the composite decreases significantly compared to the P84 reference sample.

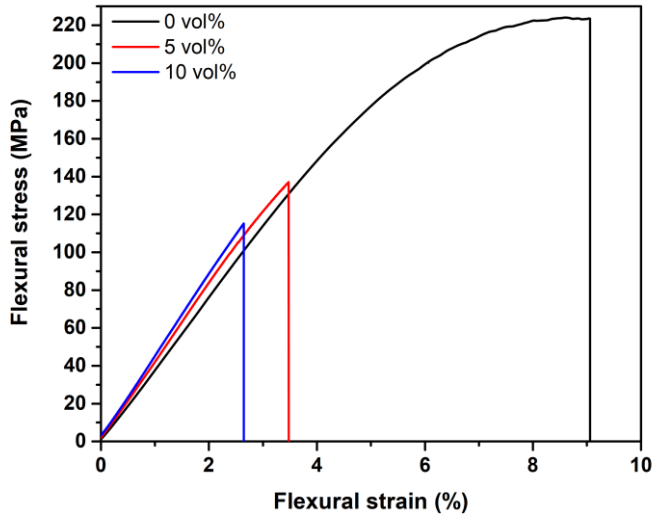

Figure 46: Flexural stress/strain curves P84 unfilled and composite samples, P84_425_IPA_35_unmod

The flexural strength and strain could be measured with a low standard deviation. In Table 16, strength, strain and modulus of the P84 samples are shown, furthermore, the values of flexural strength and strain are illustrated in Figure 47. The strength decrease from the P84 sample to the composite with 5 vol% PPPI is about 40 %, from 221 MPa to 127 MPa. This trend continues with the 10 vol% sample, but the decrease is not as severe. The same trend can be seen in strain of the composite materials, with a decrease of nearly 70 % for the 5 vol% PPPI sample. The decreasing trend also continues with the addition of more PPPI, but is not as pronounced as in the 5 vol% sample.

Table 16: Flexural strength, strain and flexural modulus of P84 unfilled and composite samples, P84_425_IPA_35_unmod

PPPI content (vol%)	σ_{fM} (MPa)	ε_{fB} (%)	E_f (MPa)
0	221 ± 5	8.96 ± 0.47	3350 ± 120
5	127 ± 6	3.09 ± 0.19	3750 ± 200
10	104 ± 7	2.38 ± 0.17	4000 ± 130

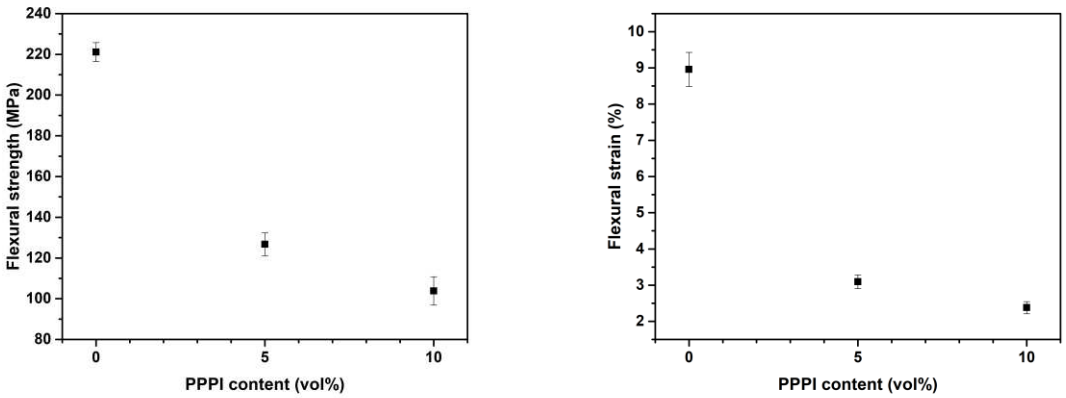

Figure 47: Flexural strength and strain versus PPPI content P84 unfilled and composite samples, P84_425_IPA_35_unmod

Figure 48 depicts the flexural modulus calculated from the stress and strain curves of the bending test, as well as calculations of common models for the prediction of composite moduli, as described in Chapter 2.7. Considering the standard deviations, the increase in average modulus from the neat P84 samples to the composite containing 5 vol% PPPI is not significant. However, the average modulus of samples containing 10 vol% PPPI increases significantly compared to the modulus of the reference sample. Here, an increase of 20 % from 3350 to 4000 MPa occurs.
The trend of an increase in modulus corresponds to the Kerner equation, while the other models slightly underestimate the rise in modulus. These models were calculated using the indentation modulus determined by nanoindentation (see section 5.3.3.4).

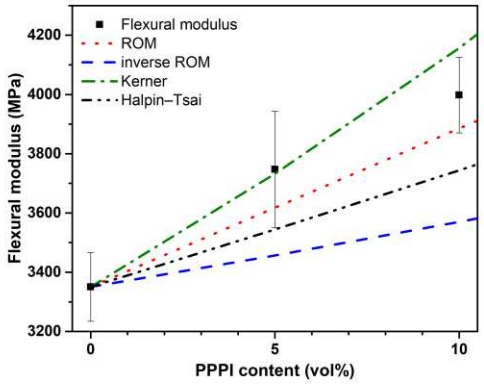

Figure 48: Flexural modulus versus PPPI content P84 unfilled and composite samples, P84_425_IPA_35_unmod and common models

Orientation dependent – Three-point bending tests

Due to the observed anisotropy in the material, bending tests perpendicular and parallel to the pressing direction during hot compression moulding were conducted.
Figure 49 and Figure 50 show the results from 10 vol% PPPI composites tested in parallel and perpendicular to the pressing direction. No significant change in flexural strength, strain or modulus can be observed depending on the orientation of the test specimens.

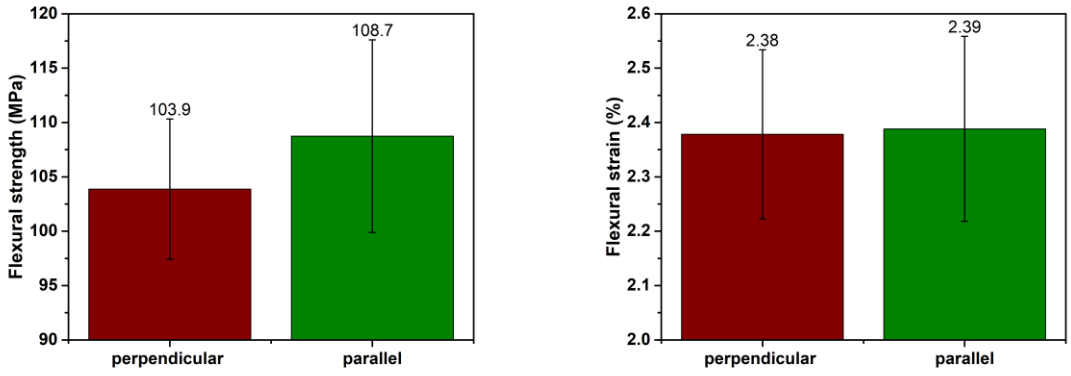

Figure 49: Flexural strength and strain, measured perpendicular and parallel to pressing direction, P84 composite sample P84_10_425_IPA_35_unmod

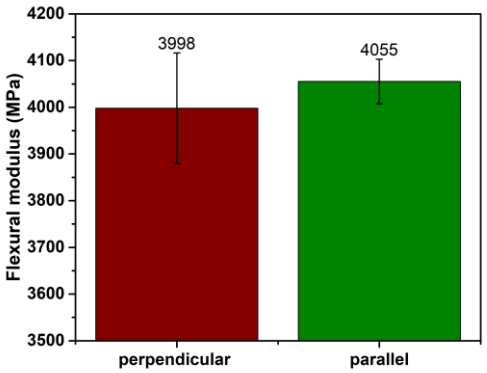

Figure 50: Flexural modulus, measured perpendicular and parallel to pressing direction, P84 composite sample P84_10_425_IPA_35_unmod

5.3.3.6 SEM fracture surfaces – fracture mechanisms and microstructure

The fracture surfaces examined in this section originate from three-point bending tests at room temperature. Figure 51 shows low magnification images of fracture surface with the tensile loaded side on the upper side of the image.

In the neat P84 sample a glass-like, "smooth" fracture surface can be observed. The failure originates from the upper edge of the picture, indicated by the large parallel striations formed. These parallel striations run parallel to the crack propagation at first, and then turn perpendicular to it at the end of the crack. Formation of secondary cracks can be observed in the lower section of the fracture, with characteristic parabola shapes, giving a "fish scale"-like morphology. In the upper section, a morphology typical for unstable crack propagation (stick-slip) is observable, with finer fracture lines perpendicular to the larger striations which originate from the point of failure. Furthermore, a lack of crazes confirms the brittle fracture behaviour, and at higher magnifications, the parabola shapes and fracture steps become apparent.

Images of the composite samples are illustrated in Figure 51 (10 vol% PPPI) and Figure 52 (5 vol% PPPI). All of them show a similar fracture morphology, with characteristically rough surfaces. This rough fracture surface is typical for materials were the initial crack gets either deflected or a debonding occurs. Here, a debonding of the particles seems plausible as the shapes on the rough surfaces resemble the morphology of the PPPI particles, with their sheet-like appearance. Another reason for the rough surface can be fractures of the PPPI particles themselves since brittle polymers exhibit a similar fracture behaviour as the observable fracture

surfaces. In all cases, the smooth fracture surfaces of the P84 matrix appear in separated areas of the composites with all studied PPPI contents, as also shown in Chapter 5.3.2.5.

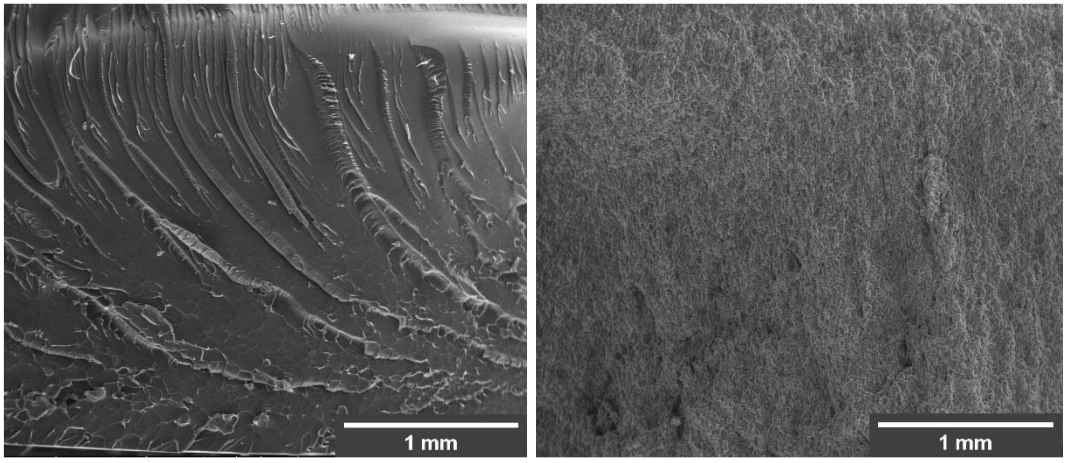

Figure 51: Fracture surface of P84 reference sample, P84_0_425_IPA_35_unmod (left) and of 10 vol% PPPI sample, P84_10_425_IPA_35_unmod (right)

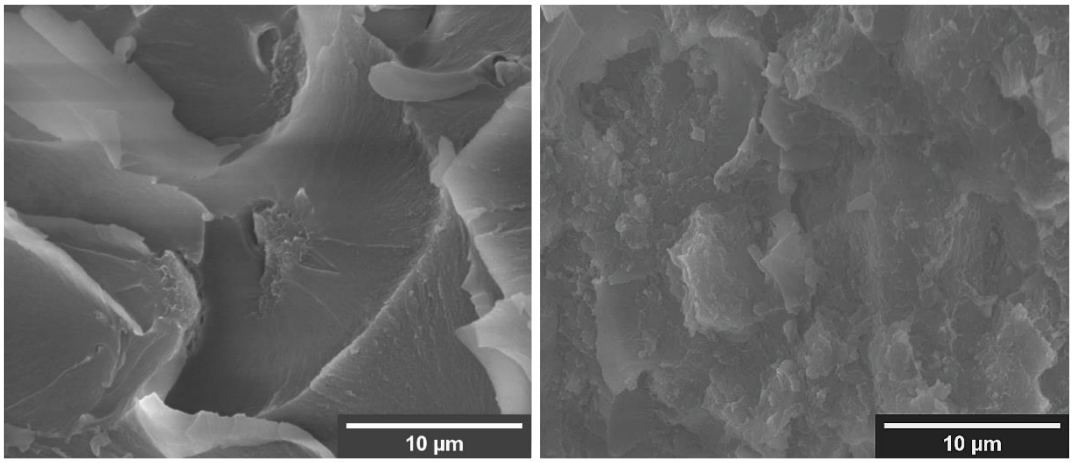

Figure 52: Fracture surface P84 reference sample, P84_0_425_IPA_35_unmod (left) and 5 vol% PPPI sample, P84_5_425_IPA_35_unmod (right)

5.3.3.7 Dynamic mechanical analysis

The test pieces for DMA testing were cut perpendicular to the pressing direction during hot compression moulding.

In Figure 53 (left), the progress of the storage modulus in dependence of temperature, measured via dynamic mechanical analysis, is plotted. For all samples, the same trend is noticeable. The decrease of modulus with higher temperature follows a comparable slope. The storage modulus increases with the addition of PPPI.

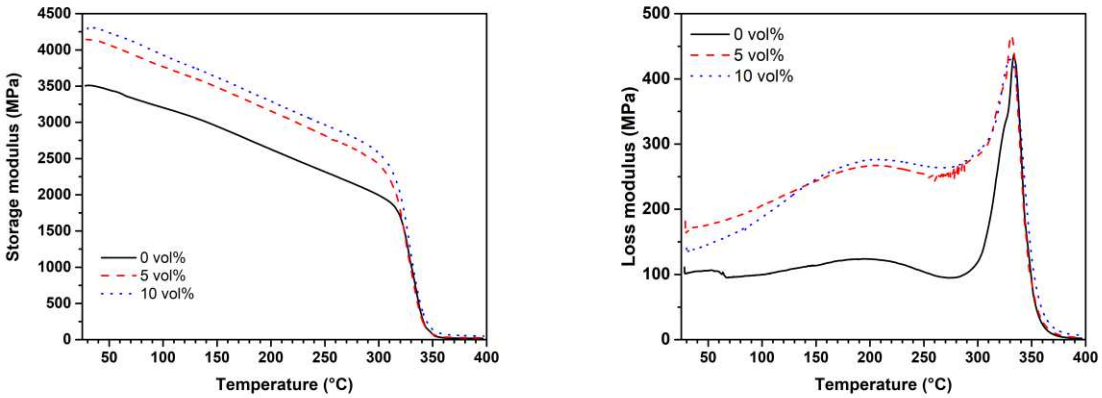

Figure 53: Storage modulus (left) and loss modulus (right) versus temperature of unfilled and composite P84 samples, P84_425_IPA_35

Table 17: Storage modulus, plateau modulus and glass-transition temperature of unfilled and composite P84 samples, P84_425_IPA_35

PPPI content (vol%)	E_s (MPa) at 30 °C	E_p (MPa) at T_g + 30 °C	T_g (°C)
0	3510	18	352
5	4140	28	348
10	4290	56	348

The values of storage modulus, glass-transition temperature and plateau modulus (30 °C above glass-transition temperature) are listed in Table 17. The glass-transition temperature (T_g) is indicated by the tangent delta of the phase angle between storage and loss modulus. The peak of tan delta, illustrated in Figure 54, corresponds to the glass-transition temperature T_g of the material. In case of the P84 and composites with different PPPI contents, T_g does not change. An influence of the PPPI particles in the composite material is observed by different tan delta peak heights. The peak height decreases with the addition of PPPI, and therefore, the dampening of the material is decreased. This effect is more pronounced for the 10 vol% PPPI sample. A broadening of the peak width is often contributed by an increase of inhomogeneity, which does not occur in the composite samples, as their peak width is comparable to the P84 reference sample.
The loss modulus shown in Figure 53 (right) depicts the glass-transition temperature in a similar way as the tan delta peaks in Figure 54. The dampening is also correlated with the peak height of the loss modulus curves. In this case, a higher dampening is indicated by a lower peak height of the loss modulus.

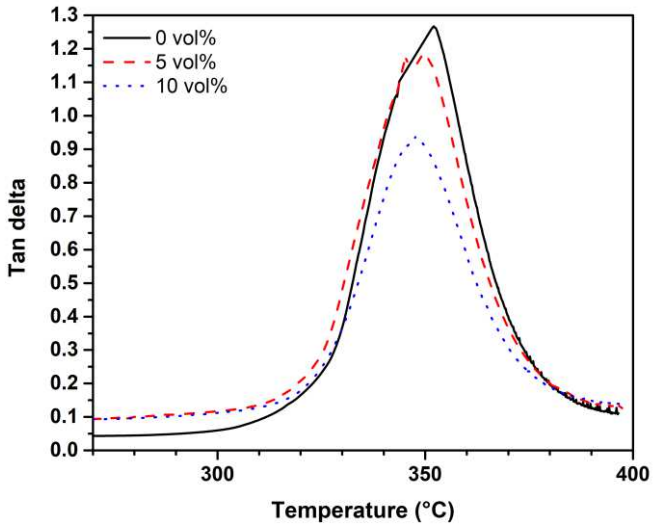

Figure 54: Tan delta versus Temperature of unfilled and composite P84 samples, P84_425_IPA_35

In Figure 55 (left), the storage modulus at 30 °C was plotted against the PPPI content of the samples, with common model predictions. The relative increase in storage modulus from the P84 reference sample to the 5 vol% PPPI composite is higher than the further increase to a content of 10 % PPPI. As it can be seen in Figure 55, the Kerner equation (from Chapter 2.7) delivers the best approximation of trend in storage modulus.

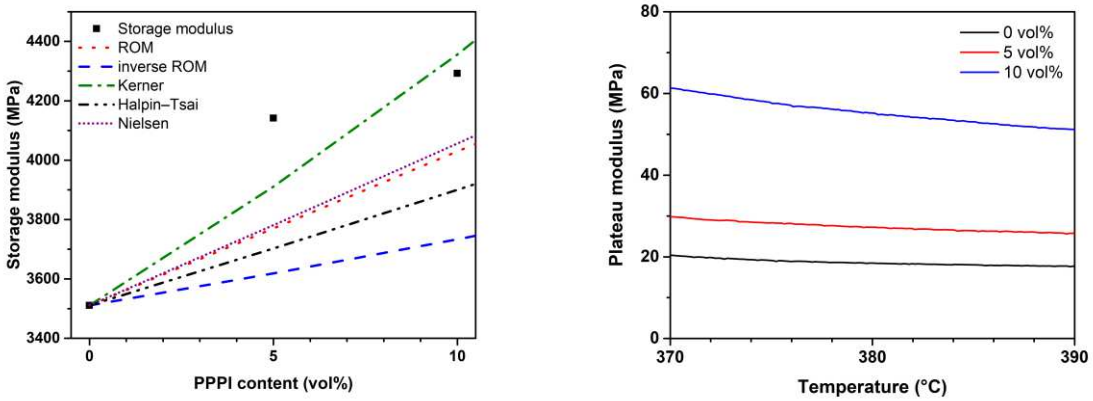

Figure 55: Storage modulus versus PPPI content of unfilled and composite P84 samples, P84_425_IPA_35 and common models (left); Plateau modulus versus temperature of unfilled and composite P84 samples, P84_425_IPA_35 (right)

The storage modulus above the glass-transition temperature is often referred to the plateau modulus. In Figure 55 (right), the plateau modulus of the composites and unfilled P84 samples is depicted. An increase in modulus with the addition of PPPI can be observed. Here, the relative increase of the plateau modulus is more pronounced for the 10 vol% PPPI sample. The higher plateau modulus in the composite samples indicates a hindered material movement at the rubbery state. The increase in plateau modulus implies a better creep resistance of the composite material at temperatures above the glass-transition temperature of the composite material.

5.3.3.8 Thermogravimetric analysis

The results from the thermogravimetric analysis of the P84 samples show no significant change in the onset of degradation temperature of the composite samples compared to the neat P84 as listed in Table 18 and illustrated in Figure 56. A slight increase of 10 °C can be observed with the addition of 10 vol% and 20 vol% PPPI.

Table 18: Degradation onset - temperature of unfilled and composite P84 samples, P84_425_IPA_35

PPPI content (vol%)	Onset of degradation (°C)
0	524
5	527
10	538
20	538

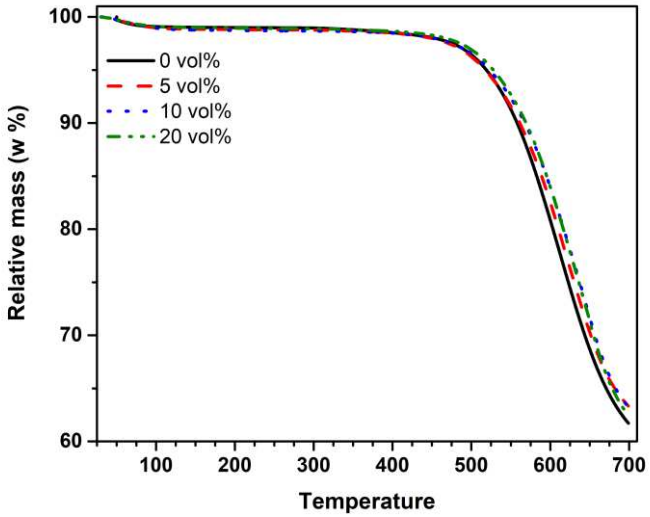

Figure 56: Thermogravimetric analysis of unfilled and composite P84 samples, P84_425_IPA_35

5.3.3.9 Experiments on thermal degradation of P84 composites

The fracture surfaces of the unfilled sample, P84_0_425_35 and composite sample P84_10_425_IPA_35_unmod, exposed to 200 °C for 3 hours (Figure 58) show differences in morphology when compared with fracture surfaces of the untreated samples (Figure 57). The fracture surface of the unfilled P84 sample (Figure 58, left) shows a similar fracture behaviour than the reference sample without heat treatment. The composite sample (Figure 58, right) also shows a quite similar fracture surface to the composite samples without heat treatment, except for a more pronounced rounding of several edges.

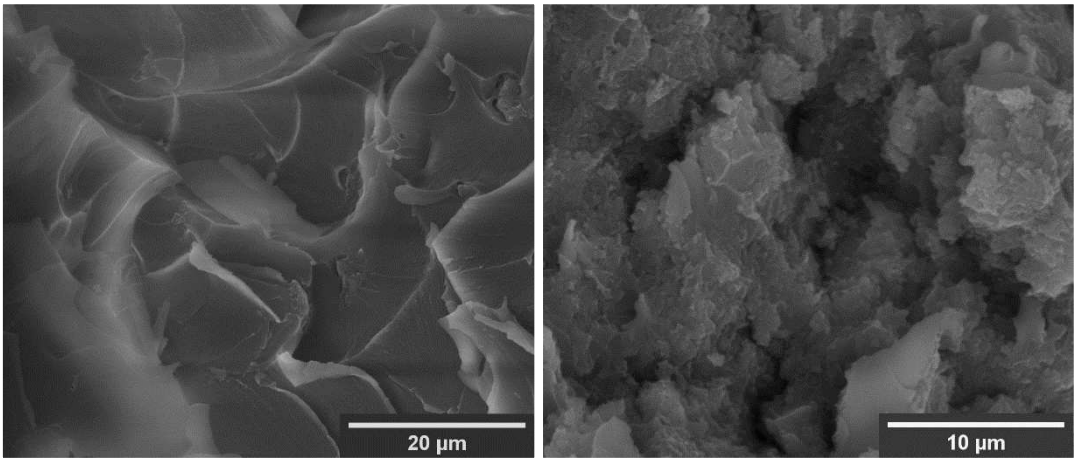

Figure 57: Non-heat treated reference unfilled and composite samples, P84_0_425_35 (left) and P84_10_425_IPA_35_unmod (right)

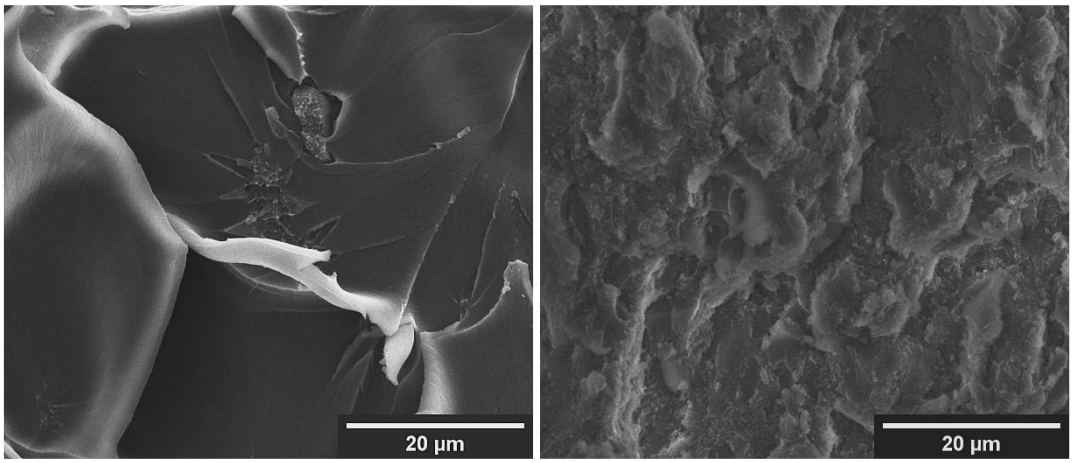

Figure 58: Thermal degradation experiment of unfilled and composite samples at 200 °C for 3 h under air, P84_0_425_35 (left) and P84_10_425_IPA_35_unmod (right)

After exposure to 300 °C both samples display large voids. In case of the neat P84 sample, the voids look smaller and resemble a "honeycomb"-like structure. These voids seem to cluster, and surrounding areas resemble the same fracture behaviour as the untreated samples. The unfilled P84 sample after 300 °C heat treatment shows a more ductile fracture behaviour, than the reference sample, which can be recognized by the increased occurrence of "tails". In the composite sample, large "craters" can be observed. The large craters are spread across the sample, while in areas between the "craters", the fracture structure remains the same as in untreated samples.

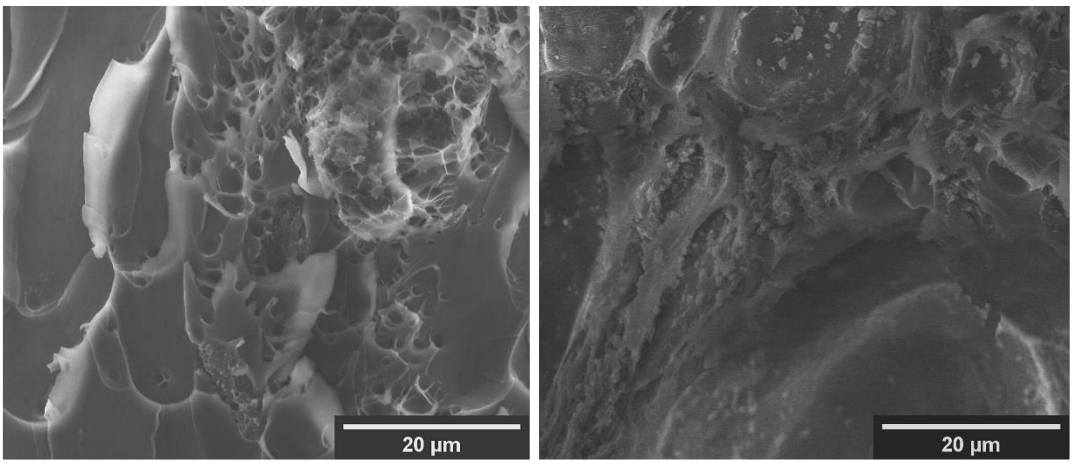

Figure 59: Thermal degradation experiment of unfilled and composite samples at 300 °C for 3h under air, P84_0_425_35 (left) and P84_10_425_IPA_35_unmod (right)

5.3.4 Hot compression moulding – Amine-modified samples

In this section, the influence of different amines used for modification of the P84 composites is described.
The abbreviations used in this section stand for the different used amines: hexamethylenediamine "HMDA", 1,2-diaminocyclohexane "DACH" and two different polyetheramines (Jeffamines), Jeffamine D 230 "D230" and Jeffamine EDR-176 "EDR". The respective weight percentage of the amine is noted after the abbreviation.
Different incorporation methods were used. The modification in aqueous solution in a round bottom flask is noted with "Syn". This method was used for modifications of just the PPPI and P84/PPPI mixtures. Otherwise, dry ball milling "DB" and wet ball milling in isopropanol "IPA" were used, in which the amines were mixed with the same procedure as for the unmodified samples. In addition, a period of 30 minutes was held at 250 °C during hot compression moulding of one sample, abbreviated with "HT".
The modifications were done solely using composite samples containing 10 vol% PPPI.

The resulting "sample code" contains the matrix material (P84), PPPI content in volume percentage(10), mesh-size, mixing technique (T, IPA, DB, Syn), hot compression moulding pressure in MPa (35), and an abbreviation for an amine-modification. In case of no modification the sample is marked with "unmod". For example, P84_10_425_IPA_35_unmod or P84_10_425_IPA_35_HMDA 1%.

5.3.4.1 Density

The effects of the modification on the P84 composites' density are depicted in Figure 60. With an addition of 1 % amine, the density does not decrease significantly compared to the unmodified 10 vol% PPPI composite samples, except for the HMDA modification via mechanical stirring (HMDA_1%_Syn) and the wet ball milled sample (HMDA_1%_IPA). The addition of 2 and 5 % HMDA or Jeffamine D230 decreases the density of the composite gradually. The most severe decrease comes with the addition of 5 % HMDA, from 98 % to 93 % relative density.

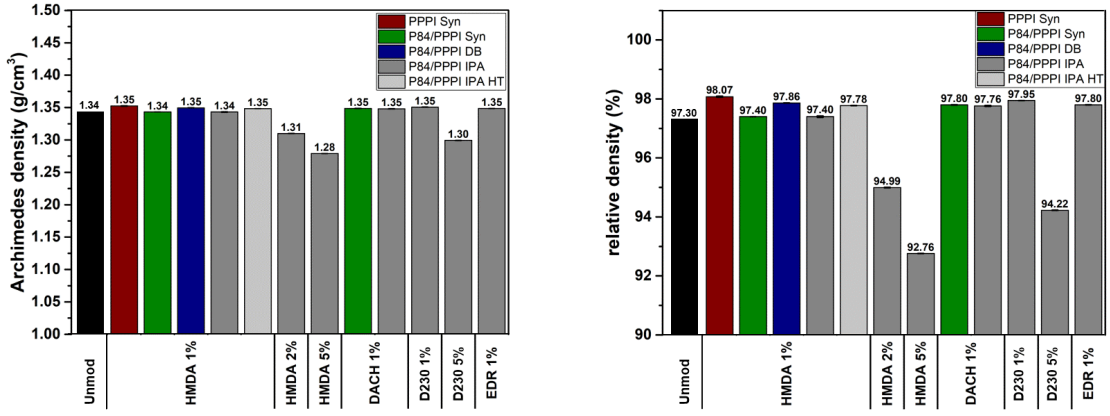

Figure 60: Archimedes and relative density of amine-modified P84 composite samples, P84_425_35_mod. Unmodified composite sample P84_10_425_IPA_35_unmod for comparison

5.3.4.2 Microstructure

In Figure 61, reflected light and BSE micrographs of a sample modified with 1 % HMDA are depicted. The microstructure of the interfacial surface modified composites with 1 % amine shows no differences to the unmodified P84 composites (Chapter 5.3.3.2, Figure 41). This sample is representative for all 1 % amine modified samples, which all exhibit the same structure. In these samples, the distinction between P84 "grains" and PPPI particles around the "grains" are observable.

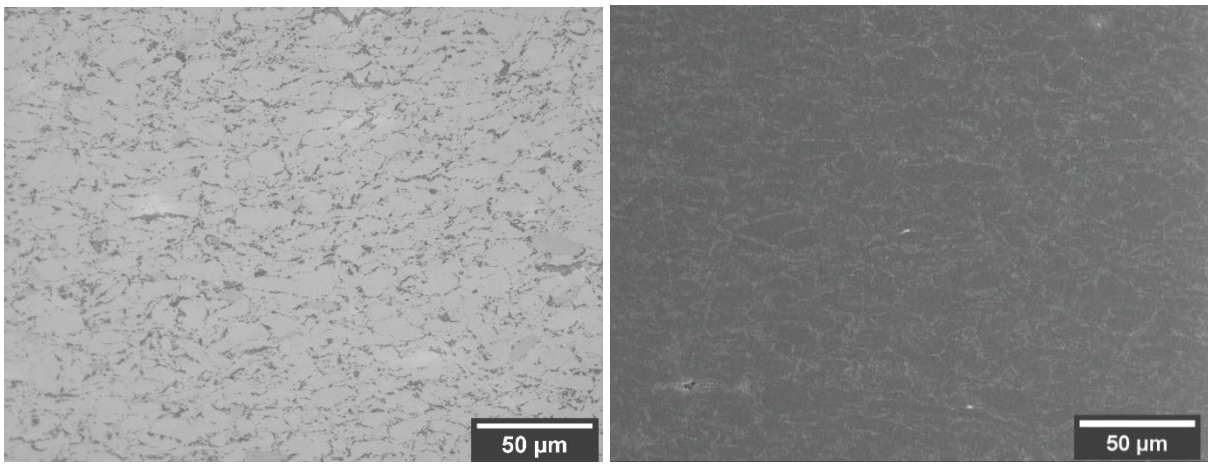

Figure 61: Micrographs of P84_10_425_ IPA _35_HMDA 1% sample, reflected light/etched (left) and P84_10_425_ DB _35_HMDA 1% sample, BSE (right)

In all 5 % amine modified samples, a formation of pores on the edge of the samples was found, as shown in Figure 62. This pore formation confirms the decrease in density measured by the Archimedes method.

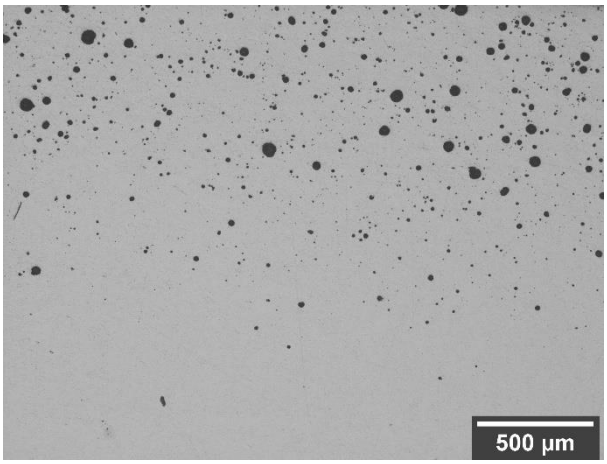

Figure 62: Pore formation on sample edge of P84_10_425_ IPA _35_HMDA 5%

5.3.4.3 Nanoindentation

As depicted in the left diagram of Figure 63, the indentation modulus of the 1 % HMDA modified, 10 vol% PPPI composite sample does not change significantly, compared to the modulus of the unmodified10 vol% PPPI composite.
Compared to the unmodified composite containing 10 vol% PPPI, the nanoindentation hardness does not change significantly to the 1 % HMDA-modified sample with 10 vol% PPPI (Figure 63, right). All respective values of indentation modulus and nanoindentation hardness are listed in Table 19.

Table 19: Indentation modulus and nanoindentation hardness of amine-modified P84 composite sample, P84_10_425_ IPA _35_HMDA 1%. Unmodified composite P84_10_425_IPA_35_unmod and unfilled sample P84_0_425_IPA_35_unmod for comparison

PPPI content (vol%)	E_i (MPa)	H_i (MPa)
0	5740 ± 60	563 ± 16
10	5990 ± 167	516 ± 14
10 (HMDA 1%)	6030 ± 163	531 ± 14

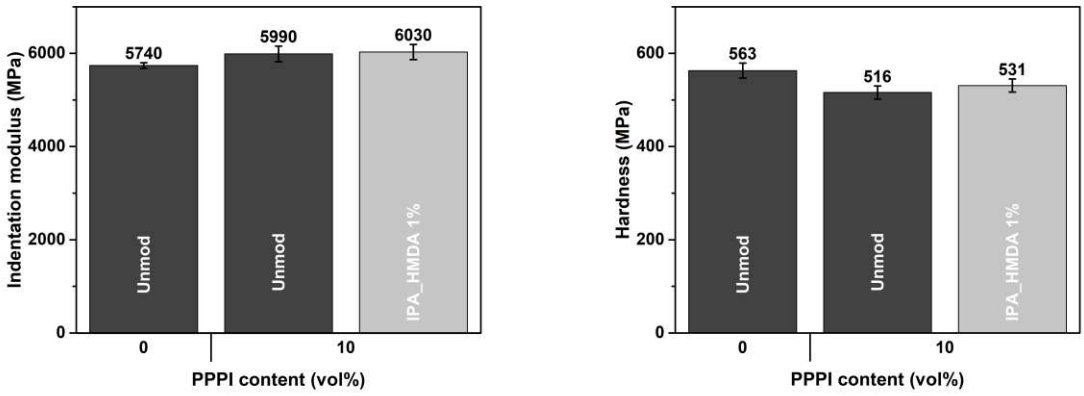

Figure 63: Indentation modulus and nanoindentation hardness of amine-modified P84 composite sample, P84_10_425_ IPA _35_HMDA 1%. Unmodified composite sample P84_10_425_IPA_35_unmod and unfilled P84_0_425_IPA_35_unmod are shown for comparison

5.3.4.4 Hardness

The Vickers HV 1 hardness of selected modified samples is shown in Figure 64. Hardness did not change significantly with the addition of different amines, or different concentrations. No significant difference between the different mixing techniques can be observed in composite hardness.

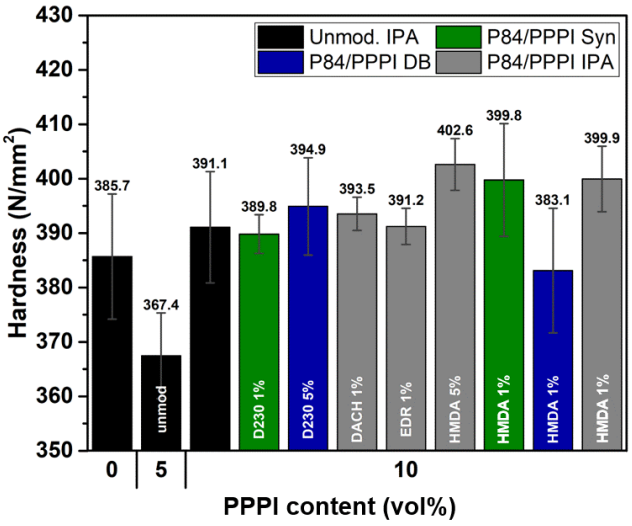

Figure 64: Vickers HV 1 hardness of different amine-modified P84 amine-modified composite samples, P84_425_35 Unmodified composite P84_10_425_IPA_35_unmod, P84_5_425_IPA_35_unmod and unfilled sample P84_0_425_IPA_35_unmod for comparison

5.3.4.5 Three-point bending tests

The influence of the amine-modification on the mechanical properties, measured with three-point bending tests, is summarised in Table 20 and Figure 65. For these bending tests, the specimens were cut perpendicular to the pressing direction during hot compression moulding.

In case of the 1 % HMDA modifications applied by stirring in water under reflux (Syn), a decrease in strength and strain is evident. The same trend, but less pronounced, is observable with the modification 1 % DACH under the same conditions, while the wet ball milled DACH-modification shows no significant change.

The modifications with Jeffamines show no significant change in strength and strain, regardless

of amine concentration or mixing procedure.
The addition of 1 % HMDA results in a strength increase of 20 % in the dry ball milled sample and an increase of 30 % in the wet ball milled variation, from 104 to 123 MPa and 139 MPa, respectively. The strain in these two variations also exhibits a similar increasing trend of 10 % (DB) and 30 % (IPA), from 2.4 to 2.7 % and 3.2 %, respectively.
For 2 or 5 % HMDA, the strength and strain of the material are comparable to the unmodified sample.
The conduction of a ramping time at 250 °C with the addition of 1 % HMDA reduces the flexural strength and strain slightly below the values of the unmodified sample. This is in contrast to the modified sample without ramping time, suggesting that the temperature has an influence on the processes.

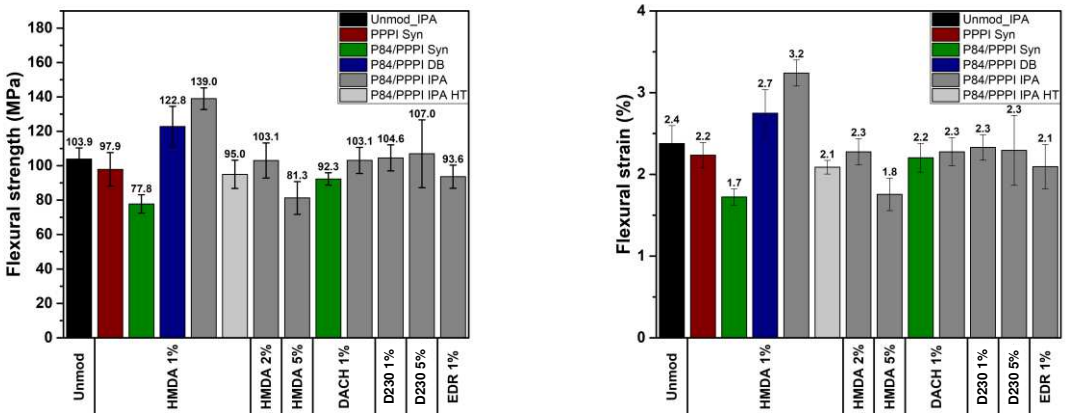

Figure 65: Flexural strength and strain of amine-modified P84 composite samples, P84_10_425_35. Unmodified composite sample P84_10_425_IPA_35_unmod for comparison

Table 20: Flexural strength, strain and flexural modulus of amine-modified P84 composite samples, P84_10_425_35. Unmodified composite sample P84_10_425_IPA_35_unmod for comparison

Modification	σ_{fM} (MPa)	ε_{fB} (%)	E_f (MPa)
Unmod_IPA	104 ± 6	2.37 ± 0.22	4028 ± 74
HMDA 1%_PPPI_Syn	97.9 ± 9.8	2.23 ± 0.16	3998 ± 118
HMDA 1%_P84/ PPPI_Syn	77.8 ± 5.3	1.72 ± 0.10	3985 ± 97
HMDA 1%_P84/PPPI_DB	123 ± 11	2.75 ± 0.29	4098 ± 106
HMDA 1%_P84/PPPI_IPA	139 ± 6	3.24 ± 0.16	4091 ± 62
HMDA 1%_P84/PPPI_IPA_HT	95.0 ± 8.2	2.09 ± 0.08	4102 ± 55
HMDA 2%_P84/PPPI_IPA	103 ± 10	2.28 ± 0.16	4122 ± 85
HMDA 5%_P84/PPPI_IPA	81.3 ± 9.5	1.75 ± 0.20	4204 ± 72
DACH 1%_P84/PPPI_Syn	92.3 ± 3.6	2.20 ± 0.18	3738 ± 90
DACH 1%_P84/PPPI_IPA	103 ± 8	2.28 ± 0.17	4134 ± 98
D293 1%_P84/PPPI_IPA	105 ± 8	2.33 ± 0.16	4011 ± 83
D239 5%_P84/PPPI_IPA	107 ± 19	2.29 ± 0.43	4230 ± 142
EDR 1%_P84/PPPI_IPA	93.6 ± 6.7	2.09 ± 0.27	3886 ± 72

Figure 66 (left) compares the flexural modulus of the modified composite samples, which does not change drastically with the addition of different amines in different concentrations, except for a decrease observed in the 1 % DACH sample stirred in water under reflux. In this sample, a decrease to 3738 MPa was found.
In Figure 66 (right), examples of stress/strain curves of different modified samples are shown. All samples show a brittle fracture behaviour, with a lack of plasticity.

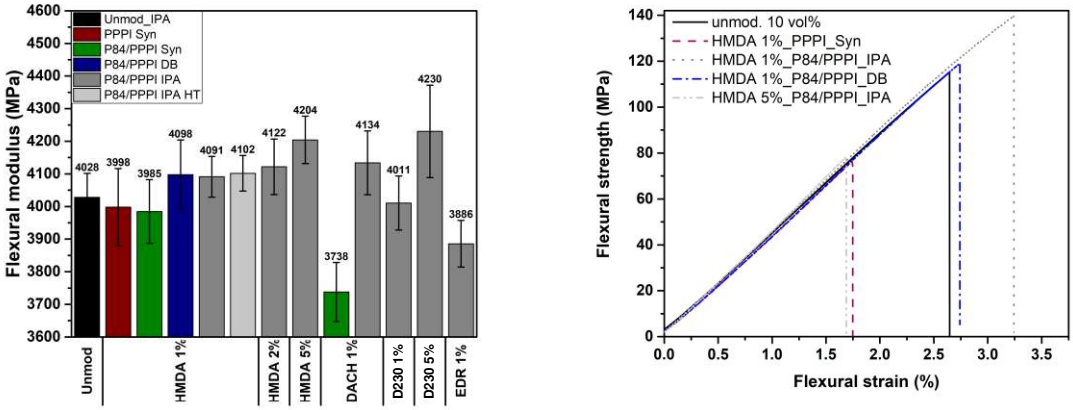

Figure 66: Flexural modulus of amine-modified P84 samples, P84_10_425 _35 (left); stress/strain curves of chosen modified P84 samples, P84_10_425 _35 (right); Unmodified composite sample P84_10_425_IPA_35_unmod for comparison

5.3.4.6 SEM fracture surfaces – Fracture mechanisms and microstructure

All fracture surfaces of the different modified composite samples all show a similar morphology. In Figure 67 and Figure 68, representative SEM micrographs are depicted. The fracture surface is comparable to the unmodified samples (Chapter 5.3.2.5, Figure 51), with brittle fracture surfaces similar to the fracture of neat P84 samples. Also, rougher surfaces can be observed, which resemble the structure of PPPI particles on the surface. Areas with a "smooth" brittle fracture take up the majority of the pictures, which is in contrast to the unmodified samples, where the overall surface was of a rougher nature. This difference seem to be more pronounced in the 5 % HMDA sample. The variations with just 1 % of amine are in closer resemblance to the unmodified samples, with more rough areas and morphologies, looking like sheet particles.

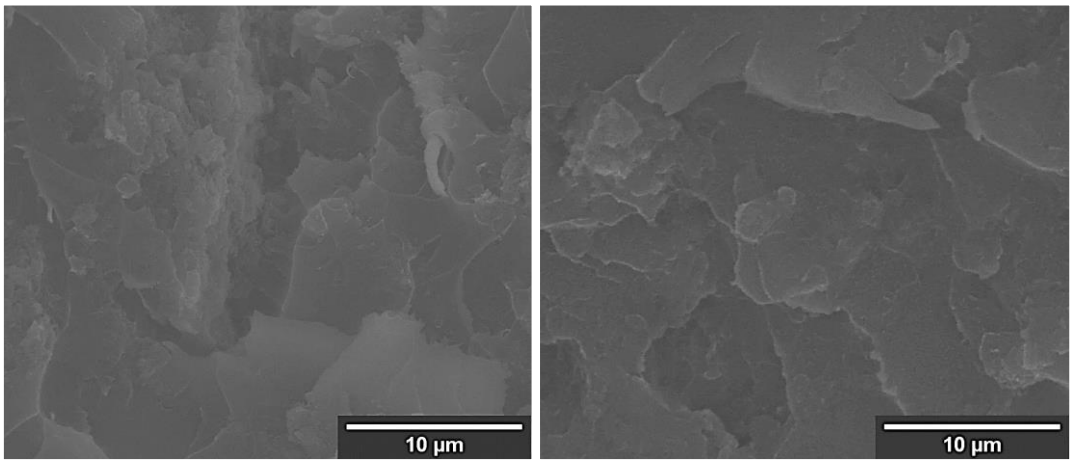

Figure 67: Fracture surface modified P84 composite sample, P84_10_425_ IPA _35_HMDA 1% (left) and P84_10_425_ IPA _35_HMDA 5%(right)

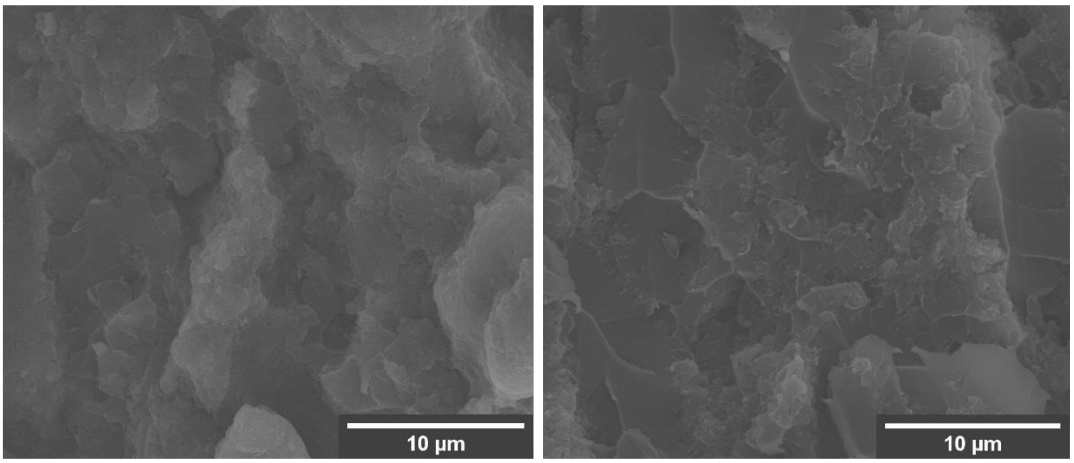

Figure 68: Fracture surface modified P84 composite sample, P84_10_425_ Syn _35_DACH 1% (left) and P84_10_425_ DB _35_HMDA 1% (right)

5.3.4.7 Dynamic mechanical analysis

The test pieces for DMA testing were cut perpendicular to the pressing during hot compression moulding.

In Figure 69 (left), the progress of the storage modulus in dependence of temperature, measured via dynamic mechanical analysis, is plotted. Unmodified and HMDA-modified composite samples follow the same trend: Slopes of the decrease of modulus with higher temperatures are comparable. The decrease of modulus with higher temperature follows a comparable slope. The storage modulus at 30 °C increases with the addition of PPPI, and is slightly increased with the addition of 1 % HMDA.

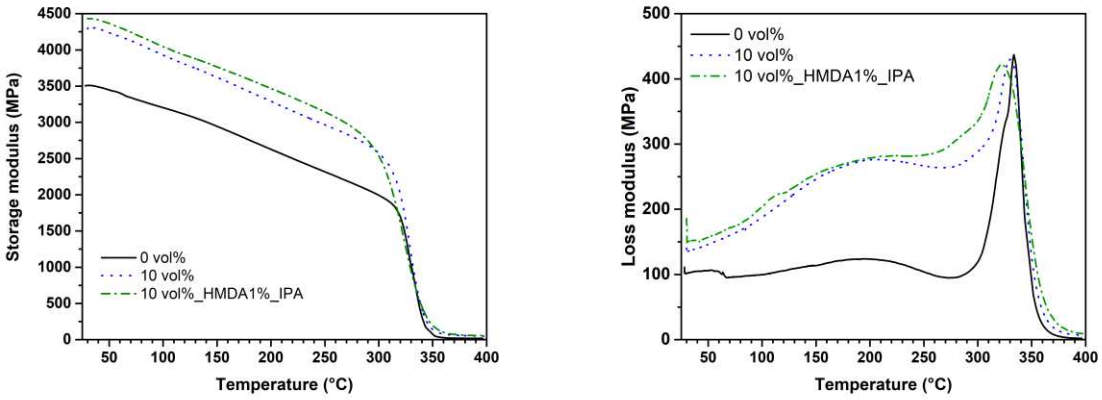

Figure 69: Storage modulus (left) and loss modulus (right) versus temperature of amine-modified P84 composite sample, P84_10_425_IPA_35_HMDA 1%. Unmodified composite P84_10_425_IPA_35_unmod and unfilled sample P84_0_425_IPA_35_unmod for comparison

Table 21: Storage modulus, plateau modulus and glass-transition temperature of amine-modified P84 composite, sample P84_10_425_ IPA _35_HMDA 1%. Unmodified composite P84_10_425_IPA_35_unmod and unfilled sample P84_0_425_IPA_35_unmod for comparison

PPPI content (vol%)	E_s (MPa) at 30 °C	E_p (MPa) at T_g + 30 °C	T_g (°C)
0	3510	18	352
10	4290	56	348
10 (HMDA 1%)	4430	61	349

The values of storage modulus, glass-transition temperature and plateau modulus are listed in Table 21. The glass-transition temperature (T_g) is indicated by the tangent delta of the phase angle

between storage and loss modulus. The peak of tan delta corresponds to the glass-transition temperature T_g of the material. An influence of the PPPI particles in the composite material is observed by different tan delta peak heights. The peak height decreases with the addition of PPPI and therefore, the dampening of the material is decreased. This effect is more pronounced for the 1 % HMDA modified sample. A broadening of the peak width is often contributed by an increase of inhomogeneity, which does occur in the HMDA modified composite, when compared with to the P84 reference and unmodified composite sample.
The loss modulus shown in Figure 69 (right) depicts the glass-transition temperature in a similar way as the tan delta peaks in Figure 70. The dampening is also correlated with the peak height of the loss modulus curves. In this case, a higher dampening is indicated by a lower peak height of the loss modulus.

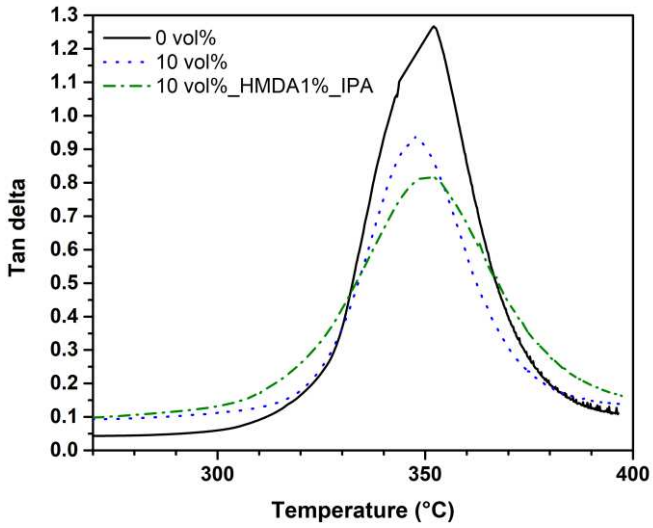

Figure 70: Tan delta versus Temperature of amine-modified P84 composite, sample P84_10_425_ IPA _35_HMDA 1%. Unmodified composite P84_10_425_IPA_35_unmod and unfilled sample P84_0_425_IPA_35_unmod for comparison

Figure 71 (left) compares the storage modulus at 30 °C of the modified composite to the unmodified one and to the reference sample. Only a slight increase in storage modulus from the unmodified to the HMDA modified sample is observed. A similar relative change is noticeable in the plateau modulus shown in Figure 71 (right). As these measurements were only conducted once, the significance of this change cannot be evaluated.

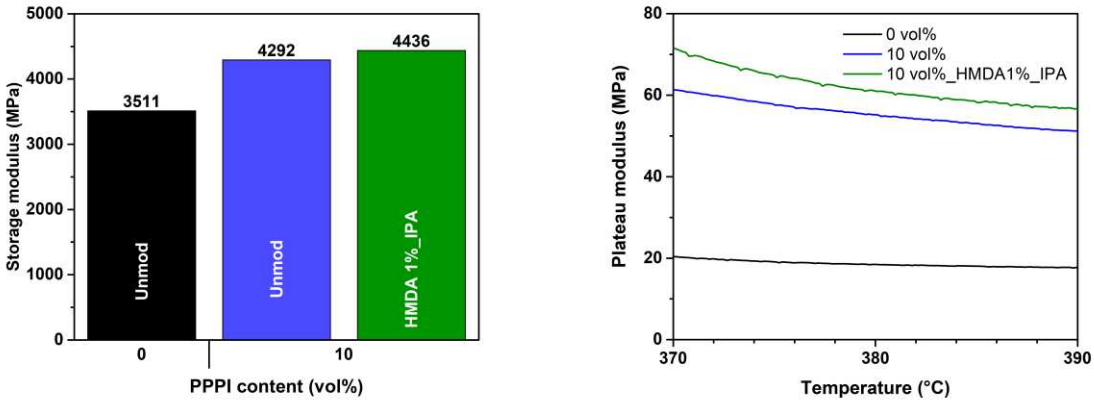

Figure 71: Storage modulus versus PPPI content amine-modified P84 composite sample P84_10_425_ IPA _35_HMDA 1% (left); Plateau modulus versus temperature (right); Unmodified composite P84_10_425_IPA_35_unmod and unfilled sample P84_0_425_IPA_35_unmod for comparison

5.3.4.8 Thermogravimetric analysis

The results from the thermogravimetric analysis of the 1 % HMDA modified composite sample (Figure 72 and Table 22) show no significant change in the onset of degradation compared to the P84 reference sample. A slight decrease of 15 °C in the onset of degradation can be observed in comparison with the unmodified 10 vol% PPPI composite.

Table 22: Degradation onset - temperature of amine-modified P84 composite, sample P84_10_425_ IPA _35_HMDA 1%. Unmodified composite P84_10_425_IPA_35_unmod and unfilled sample P84_0_425_IPA_35_unmod for comparison

PPPI content (vol%)	Onset of degradation (°C)
0	524
10	538
10 (HMDA 1%)	523

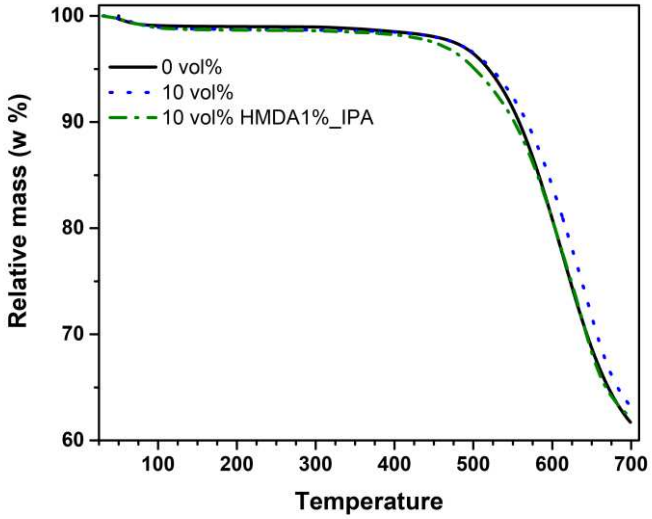

Figure 72: Thermogravimetric analysis of amine-modified P84 composite, sample P84_10_425_ IPA _35_HMDA 1%. Unmodified composite sample P84_10_425_IPA_35_unmod and unfilled P84_0_425_IPA_35_unmod for comparison

5.4 Epoxy – Composites

In case of the epoxy composites, additions of 5, 10, and 15 vol% PPPI were tested. Due to assumed interactions between the PPPI particles and the amine hardener, non-stoichiometric mixtures were prepared with the addition of 5 wt% hardener.

The resulting "sample code" contains the matrix material (epoxy), PPPI content in volume percentage, and an abbreviation for the over-stoichiometric addition of 5 wt% hardener as "mod". In case of a stoichiometric hardener addition, the sample is marked with "unmod". For example, Epoxy_10_unmod.

5.4.1 Density

The density of the unfilled epoxy and composite samples was measured using the Archimedes method, Figure 73 presents the results of absolute and relative density. The Archimedes density of the neat epoxy, cured with a stoichiometric amount of hardener, was used as the theoretical density for the calculation of relative densities. Therefore, the relative density of the unfilled epoxy is 100 %. The addition of 5 % hardener does not drastically change the density of the material, neither in the composite nor in the neat epoxy.

An increase in absolute density is observable due to the higher density of the PPPI (1.73 g/cm³). The relative density of the composite material gradually decreases with the addition of PPPI.

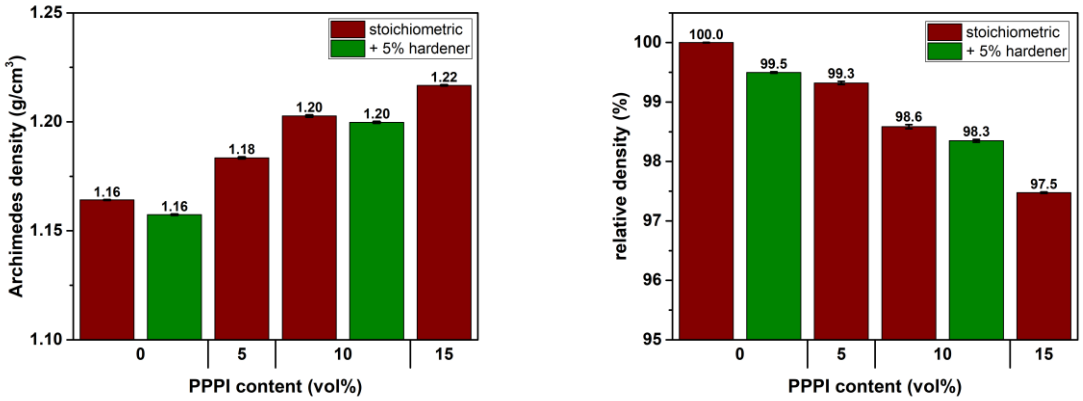

Figure 73: Archimedes and relative density of unfilled and composite, non-stochiometric and stochiometric epoxy samples (stoichiometric and + 5 % hardener), Epoxy_unmod and Epoxy_mod

5.4.2 Microstructural analysis

For a better understanding of the microstructure of the composite material, the plastographic preparations were examined with backscattered electron imaging and reflected or transmitting light microscopy. With all imaging methods, a clear contrast between PPPI particles and epoxy matrix is detectible.
In Figure 74 and Figure 75, the back-scattered electron (BSE) images of the polished sample surfaces show the PPPI particles as brighter spots in contrast to the surrounding epoxy matrix. A homogenous distribution of the particles in a random orientation can be observed on these images. Also, the size and geometry of the PPPI is comparable to the starting particles. Furthermore, an out-breaking of the PPPI particles during polishing can be observed.

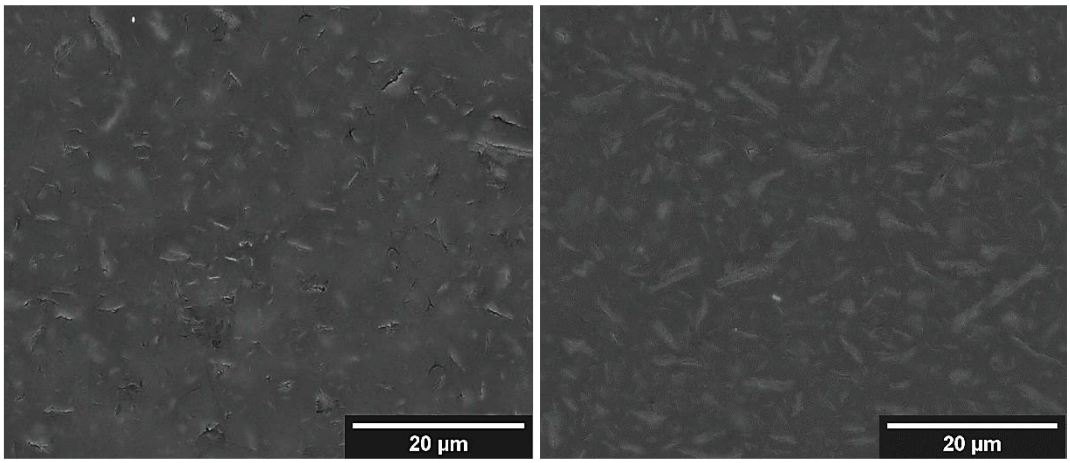

Figure 74: Micrographs of unmodified epoxy composite samples, Epoxy_5_unmod BSE (left) and Epoxy_10_unmod BSE (right)

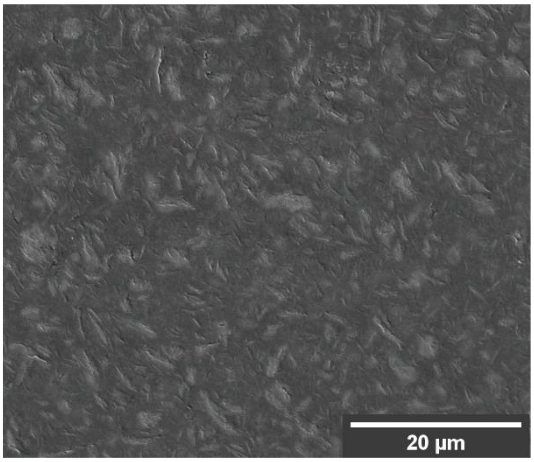

Figure 75: Micrographs of unmodified epoxy composite samples, Epoxy_15_unmod BSE

In Figure 76 (right), the reflected light image of a 10 vol% PPPI epoxy composite is shown. The darker spots show the PPPI particles, which are partially etched with sodium hydroxide. The brighter epoxy matrix isn't affected by the etching. Here, a homogenous distribution can be observed as well. No pores can be detected in these samples, though some of the larger spots in the image could consist of pores.

The transmitted polarised light image of a thin grinded sample is shown in Figure 76 (left). In this image, the crystalline PPPI appears yellow, while the amorphous epoxy matrix is violet. A similar morphology as in the other images can be observed, confirming the findings of the other two techniques. The distribution of the particles does not seem as homogeneous as observed in the other images.

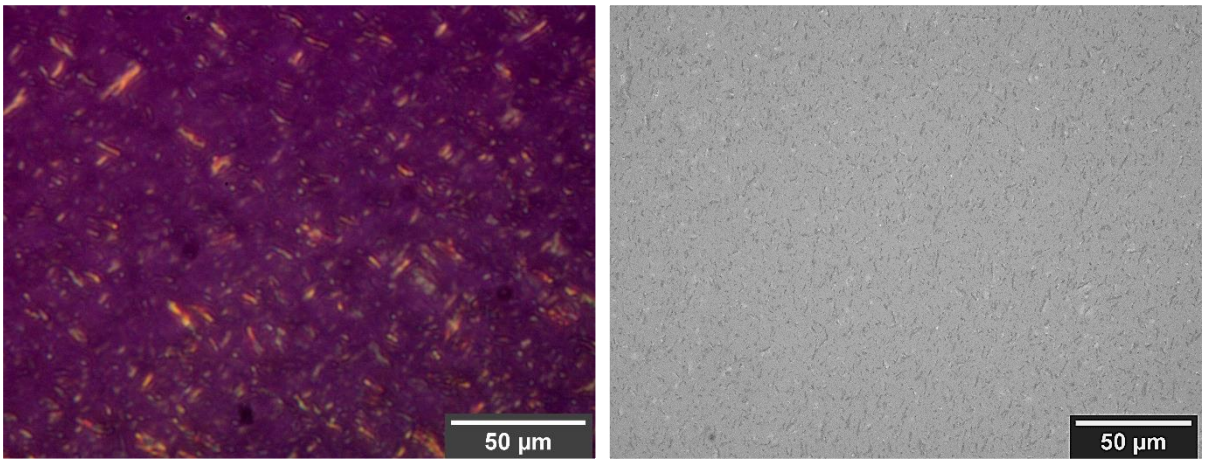

Figure 76: Micrographs of unmodified epoxy composite samples, Epoxy_10_unmod, transmitted, polarised light (left) and Epoxy_10_unmod NaOH - etched, reflected light (right)

5.4.3 Nanoindentation

The indentation modulus and hardness were determined via nanoindentation, the results are shown in Table 23, Figure 77, and Figure 78. A neat epoxy sample and an epoxy composite sample with 10 vol% PPPI were analysed. Also, the modulus and hardness of the PPPI particles was measured on this composite sample. The values of the indentation modulus of the 10 vol% PPPI composite fit well with the ROM model, calculated using the indentation modulus and hardness of the PPPI particles.

Table 23: Indentation modulus and nanoindentation hardness of unmodified, unfilled and composite epoxy samples, PPPI measured in composite sample Epoxy_10_unmod

PPPI content (vol%)	E_i (MPa)	H_i (MPa)
0	2960± 67	265 ± 13
10	3590 ± 83	290 ± 14
100	8700 ± 1060	648 ± 83

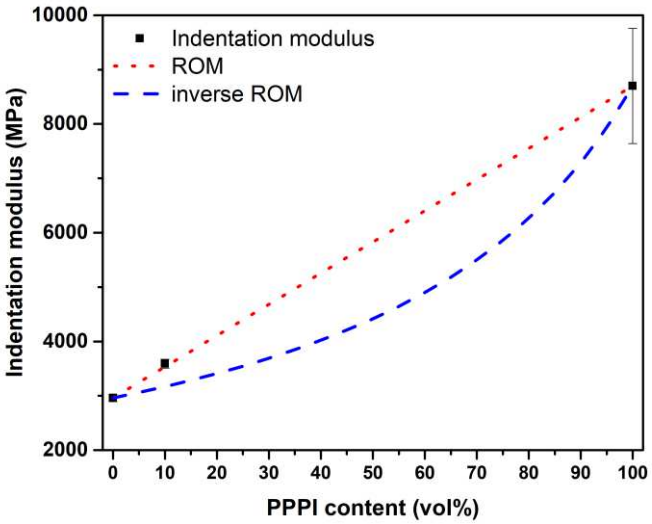

Figure 77: Indentation modulus versus PPPI content of unmodified, unfilled, and composite epoxy samples, PPPI measured in composite sample Epoxy_10_unmod and ROM models

The hardness of the composite sample is between the expected ratio of calculated ROM and inverse ROM (from Chapter 2.7) and follows the expected increasing trend, as illustrated in Figure 78.

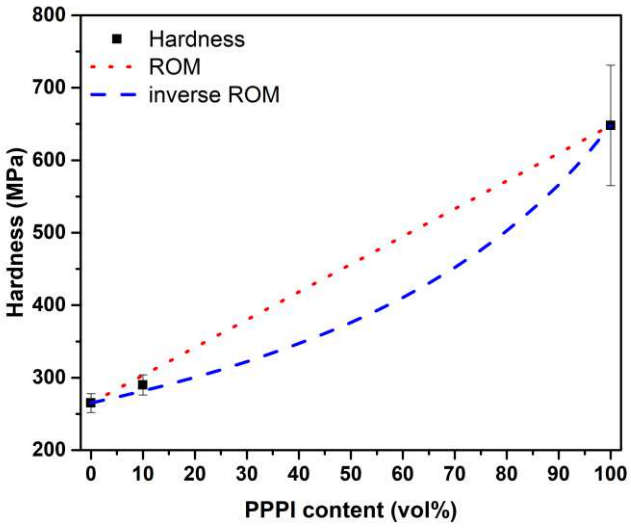

Figure 78: Nanoindentation hardness versus PPPI content of unmodified, unfilled, and composite epoxy samples, PPPI measured in composite sample Epoxy_10_unmod and ROM models

5.4.4 Hardness

The Vickers HV 1 hardness of unfilled epoxy and composite samples is shown in Figure 79, the respective values are listed in Table 24. No cracks were formed at the edges of the indents.
The Vickers hardness of the composite increases almost linearly with the PPPI content. An increase of 25 %, from 175 MPa to 218 MPa, was observed from the neat epoxy to the 15 vol% PPPI composite. To estimate the quality of the hardening through PPPI, a ROM model and an inverse ROM model were used. To calculate the models, the nanoindentation hardness of the PPPI particles (648 ± 83 MPa) was used. The composite hardness lies between the values predicted by ROM and inverse ROM (from Chapter 2.7).

Table 24: Vickers hardness of unmodified, unfilled, and composite epoxy samples, Epoxy_unmod

PPPI content (vol%)	H_i (MPa)
0	175 ± 3
5	186 ± 3
10	206 ± 3
15	218 ± 2

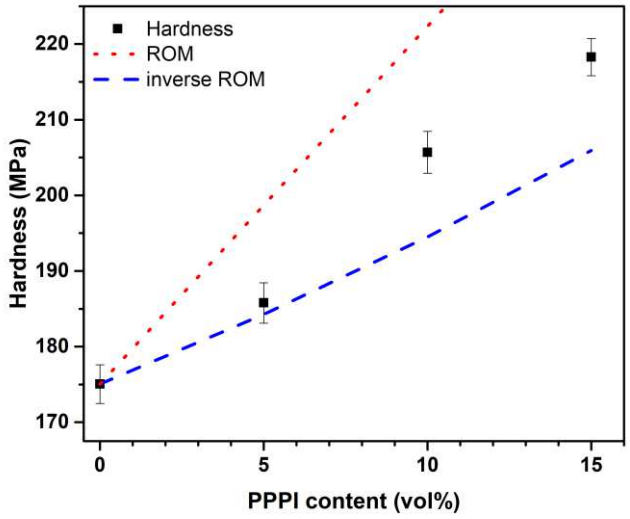

Figure 79: Hardness versus PPPI content of unmodified, unfilled, and composite epoxy samples, Epoxy_unmod

5.4.5 Three-point bending tests

In Figure 80, representative stress/strain curves of the composites and the neat epoxy are shown. The change of flexural properties with the addition of PPPI is also shown in Table 25 and Figure 81. A clear change of properties with the addition of PPPI becomes apparent, with a decrease of flexural strain and an increase in flexural modulus. The plasticity of the composite decreases progressively with the amount of PPPI, until a nearly complete lack of plastic behaviour emerges in the 15 vol% composite. The transition between elastic and plastic behaviour is continuous, no distinctive transition point can be observed.

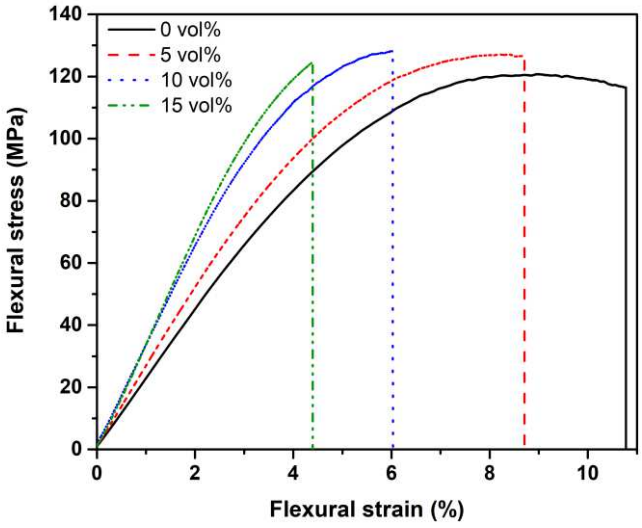

Figure 80: Flexural stress/strain curves of unmodified, unfilled and composite epoxy samples, Epoxy_unmod

The flexural strength of the composite material does not change significantly in comparison to the unfilled epoxy. The lack of plasticity becomes clear with the nearly linear decrease of strain in Figure 81.

Table 25: Flexural strength, strain and flexural modulus of unfilled and composite epoxy samples, Epoxy_unmod

PPPI content (vol%)	σ_{fM} (MPa)	ε_{fB} (%)	E_f (MPa)
0	120 ± 2	10 ± 0.8	2200 ± 98
5	124 ± 2	9.3 ± 1	2480 ± 77
10	126 ± 3	6.0 ± 0.6	2910 ± 110
15	123 ± 4	4.5 ± 0.4	3200 ± 95

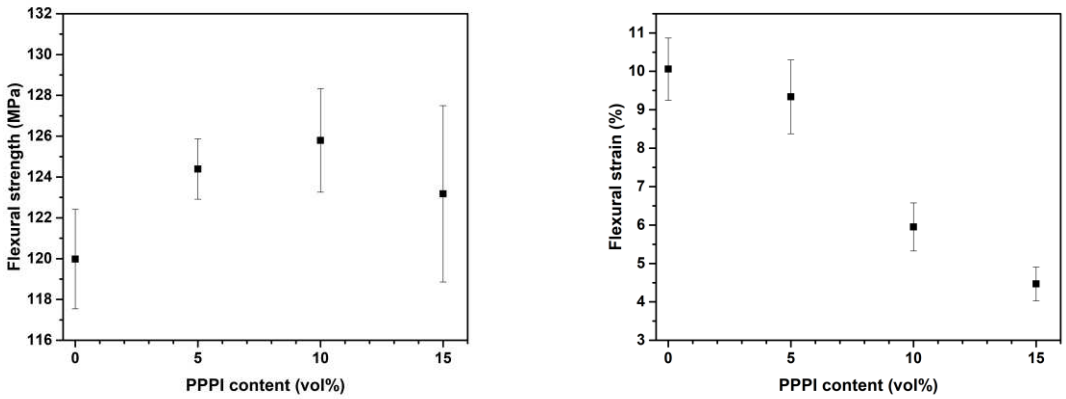

Figure 81: Flexural strength and strain versus PPPI content unfilled and composite epoxy samples, Epoxy_unmod

As visible in Figure 82, the flexural modulus increases nearly linearly with PPPI content. To estimate the theoretical boundaries of modulus enhancement, different models were used. In these models the modulus of the PPPI is required. Here, the indentation modulus measured for the PPPI particles in the epoxy matrix via nanoindentation was used (with a value of 8700 ± 1060 MPa).
The increasing modulus of the composite is in good accordance with the value calculated by ROM (from Chapter 2.7).

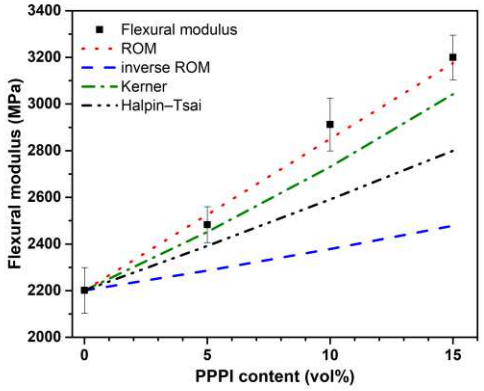

Figure 82: Flexural modulus versus PPPI content epoxy unfilled and composite samples and common models, Epoxy_unmod

Three-point bending tests – Over-stoichiometric hardener addition

Due to assumed interactions between the PPPI particles and the amine hardener, non-stoichiometric mixtures were prepared with the addition of 5 wt% hardener.

To investigate the influence of hardener in the epoxy composites, the unfilled epoxy and a 10 vol% PPPI filled sample were cured with the addition of 5 wt% hardener. No significant change in strength, strain, or modulus can be observed as shown in Figure 83and Figure 84. Concerning strength and modulus, the standard deviation of over-stoichiometric and stoichiometric unfilled composite samples lies in the same range. The strain of the non-stoichiometric 10 vol% PPPI composite, on the other hand, varies over a much higher range than in the stoichiometric epoxy

composite.

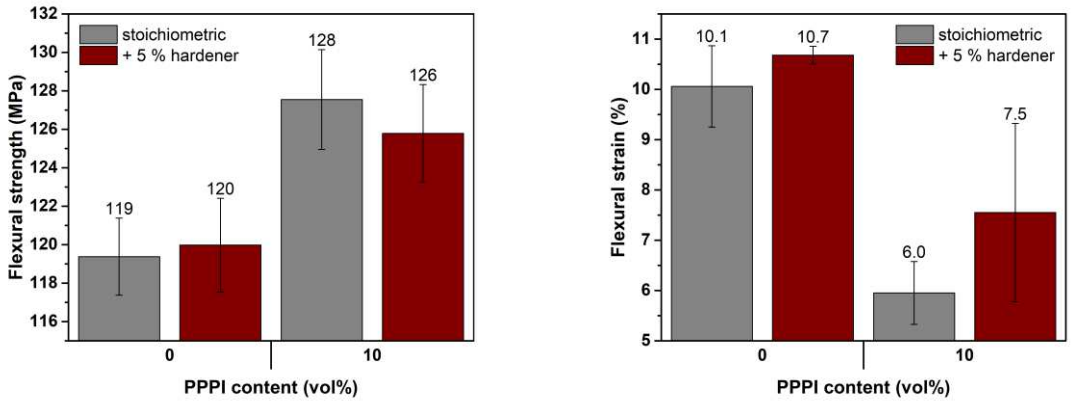

Figure 83: Flexural strength and strain versus PPPI content of stoichiometric, and non-stoichiometric, unfilled, and composite epoxy samples, Epoxy_mod and Epoxy_unmod

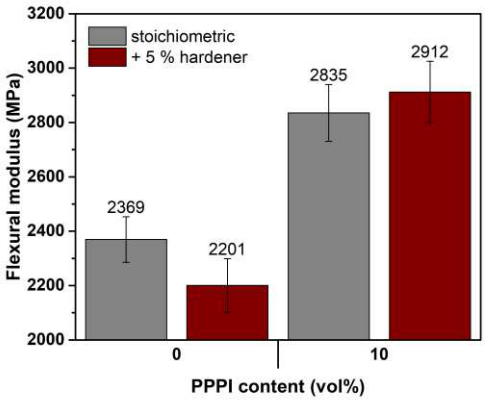

Figure 84: Flexural modulus versus PPPI content of stoichiometric, and non-stoichiometric, unfilled, and composite epoxy samples, Epoxy_mod and Epoxy_unmod

5.4.6 Fracture surfaces – three-point bending

The SEM fractograms in Figure 85 - Figure 88 give a better understanding of the failure mechanisms in the matrix and composite. The epoxy matrix displays a brittle fracture surface. The point of failure is clearly visible on the upper right side of Figure 85 as a smooth surface, from which large parallel striations spread radially. The smooth surface is the initial fast crack propagation, and the parallel lines follow this propagation through the material until large rifts can be observed parallel to the crack propagation direction.

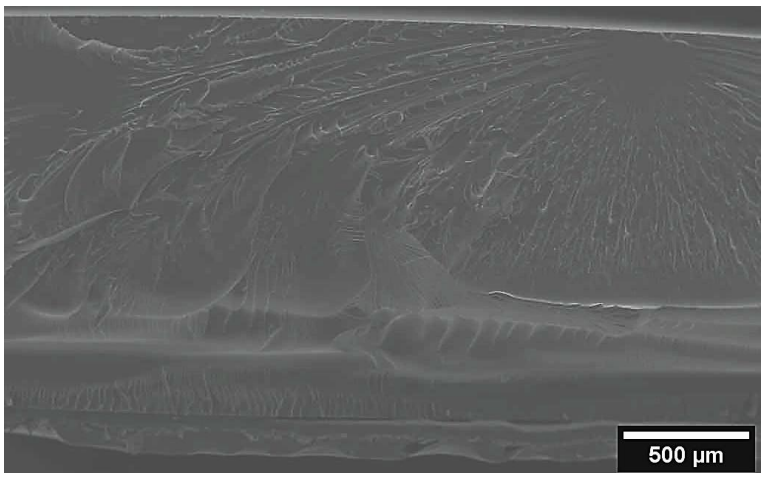

Figure 85: Fracture surface three-point bending test of unmodified, unfilled epoxy, Epoxy_0_unmod sample (overview)

In case of the epoxy composite material with an addition of 5 vol% PPPI, no distinctive point of failure is visible in Figure 86. The failure starts from the upper edge of the sample with a smooth surface, due to fast crack propagation. Large parallel striations, parallel to crack propagation, can be observed. These parallel lines turn perpendicular to the crack propagation at the centre of the sample, until an overall rough surface appears at the bottom of the sample. The surface of the fracture looks much rougher, indicating the presence of particles and the formation of numerous secondary cracks.

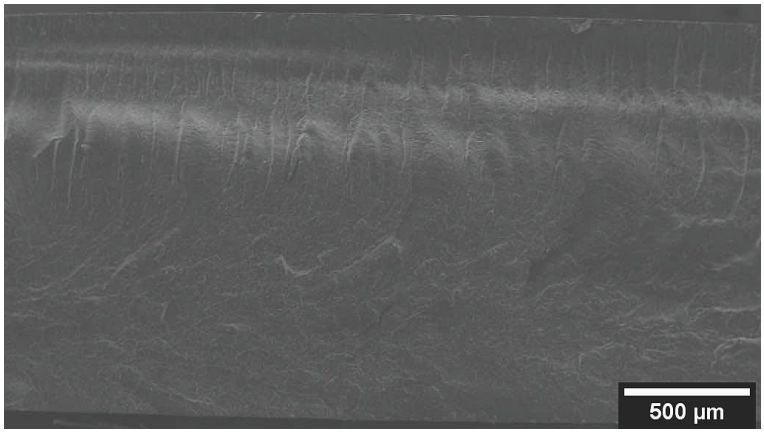

Figure 86: Fracture surface three-point bending test of unmodified, epoxy-based composite, Epoxy_5_unmod sample (overview)

In the unfilled epoxy (Figure 87, left), brittle fracture is indicated by the smooth, glass-like surface, observed under higher magnification. A formation of secondary cracks cannot be observed. The fracture surface is dominated by the formation of ramps, also indicating brittle fracture and lacking plastic deformation.
In the composite material (Figure 87, right) a “step-like” fracture surface appears. This indicates deboning of particles, which forms craters on the fracture surface. Also, crack deflection on the particle surface is plausible. A fracture mechanism which includes the cutting of the particles does not seem plausible in this case.
The transition between the fracture behaviour becomes apparent when comparing the composite with 5 vol% and 10 vol% PPPI. In the 5 vol% sample, only small areas show a rough surface with small steps. Between those regions, areas which resemble the parallel ramps of the epoxy can be observed. The 10 and 15 vol% PPPI composites (Figure 88) display only the step-like behaviour, indicating a debonding of particles as primary failure mechanism.

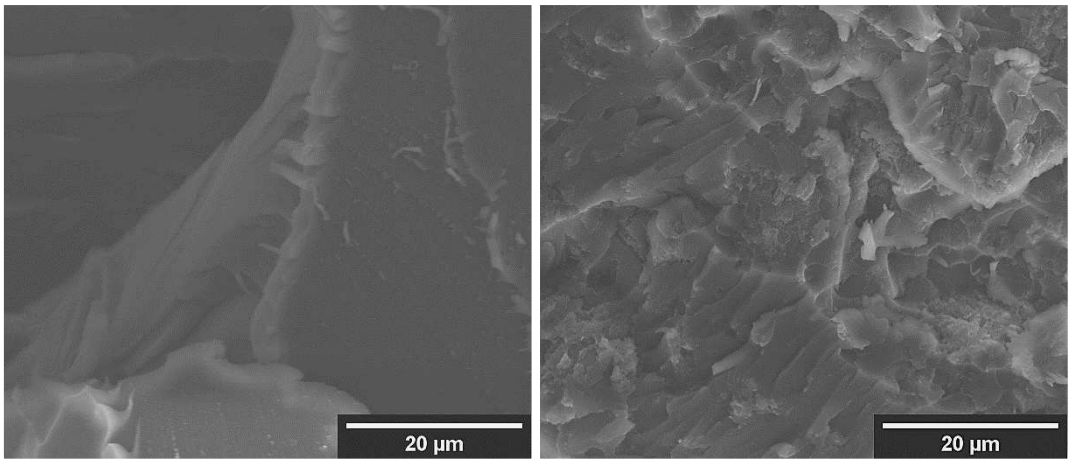

Figure 87: Fracture surface of three-point bending test of unmodified epoxy samples, unfilled Epoxy_0_unmod (left) and composite Epoxy_5_unmod (right)

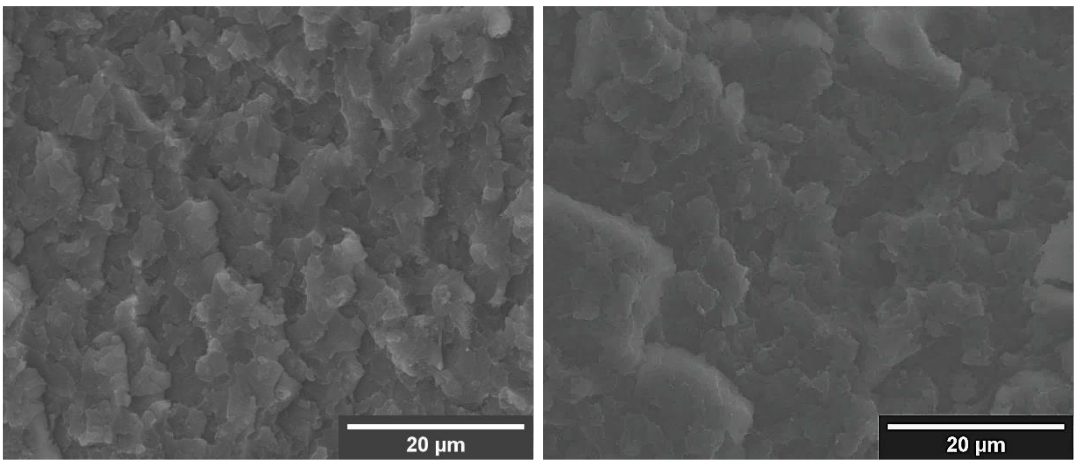

Figure 88: Fracture surface of three-point bending test of unmodified, epoxy-based composite, Epoxy_10_unmod (left) and Epoxy_15_unmod sample (right)

5.4.7 Tensile tests

In Figure 89, representative stress/strain curves of tensile tests, performed for neat epoxy and epoxy-based composites are depicted, the corresponding values are listed in Table 26. A clear change in mechanical behaviour becomes apparent. The strain until break of the composite is decreased from 5 % in the unfilled epoxy to 2.5 %. Only a slight decrease of strain from the 5 vol% to 10 vol% PPPI sample is observable. A decrease of tensile strength in the composite material is also measured, from 56 MPa in the neat epoxy, to 43 MPa in the 5 vol% composite.
The Young's modulus of the composite material is increased compared to the unfilled epoxy samples. Here, an increase of 20 % is observed, from 2160 MPa in the neat epoxy, to 2556 MPa in the 10 vol% PPPI composite.

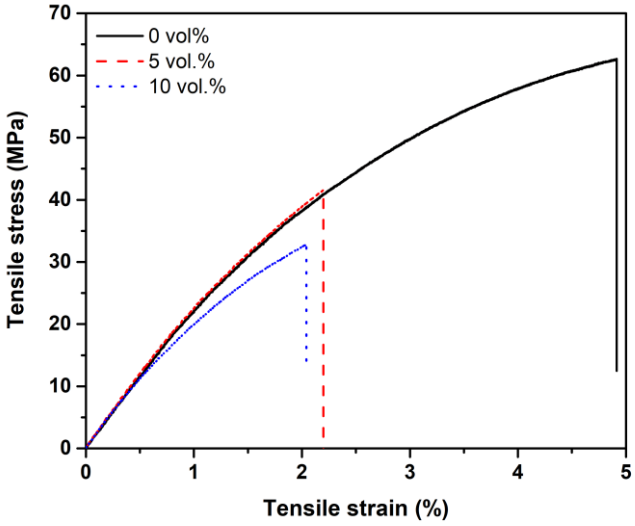

Figure 89: Tensile stress/strain curves of unmodified, unfilled and composite epoxy samples, Epoxy_unmod

Table 26: Tensile strength, strain and Young's modulus of unmodified, unfilled and composite epoxy samples, Epoxy_unmod

PPPI content (vol%)	σ_{tM} (MPa)	ε_{tB} (%)	E_t (MPa)
0	56.3 ± 8.2	4.48 ± 1.79	2160 ± 112
5	43.6 ± 4.6	2.54 ± 0.30	2344 ± 146
10	31.2 ± 5.8	1.63 ± 0.40	2556 ± 146

In Figure 90, the strength and strain of the material are plotted against the PPPI content. A nearly linear decrease of strength and strain with the addition of PPPI can be observed. A high standard deviation occurs for the unfilled epoxy samples.

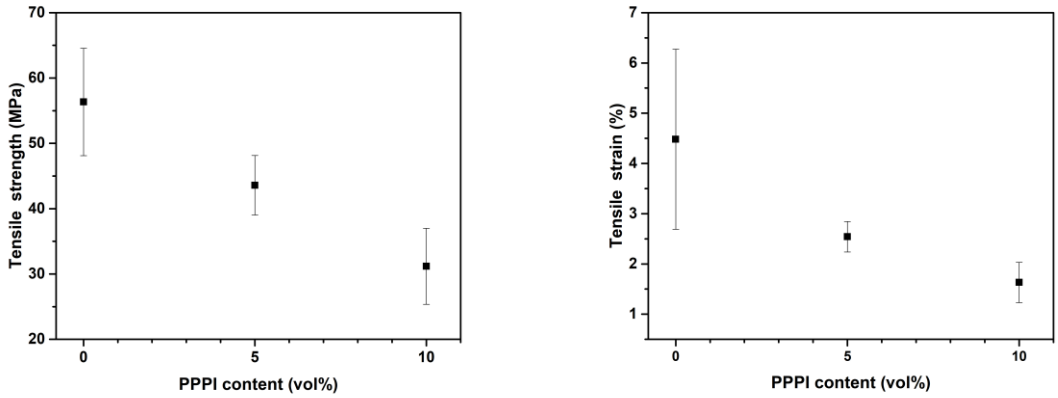

Figure 90: Tensile strength and strain versus PPPI content of unmodified, unfilled and composite epoxy samples, Epoxy_unmod

The Young's modulus of the epoxy samples is shown in Figure 91, in comparison with different models for the prediction of the modulus in composite materials. The measured values are in good accordance with the models, especially with the Halpin-Tsai equation (from Chapter 2.7).

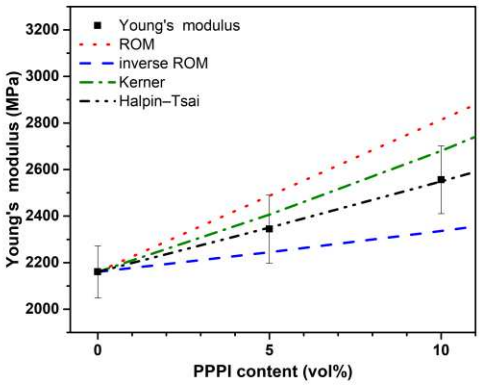

Figure 91: Young's modulus versus PPPI content of unmodified, unfilled and composite epoxy samples and common model predictions

5.4.8 Fracture surfaces – tensile tests

Figure 92 shows an image on a tensile test fracture service, its observation leads to a similar result as in the bending test. The point of failure is clearly visible on the left side of the sample, from which the initial crack is propagating. From this point striations or ramps propagate throughout the material, confirming the clear brittle behaviour of the epoxy matrix.

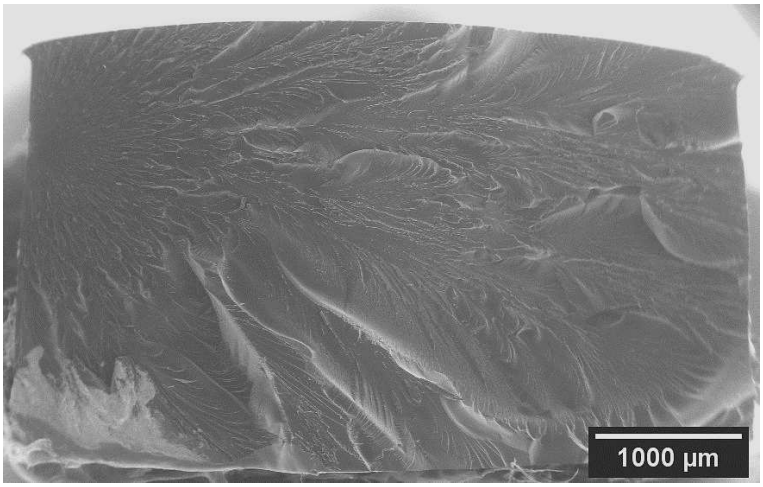

Figure 92: Fracture surface of tensile test of unmodified, unfilled epoxy, Epoxy_0_unmod sample (overview)

In Figure 93, a higher magnification of a 5 vol% PPPI sample is shown. The steps and ramps on the fracture surface are clearly visible, indicating a brittle behaviour. Also, secondary crack formation is observable in the form of breaking parabolas.

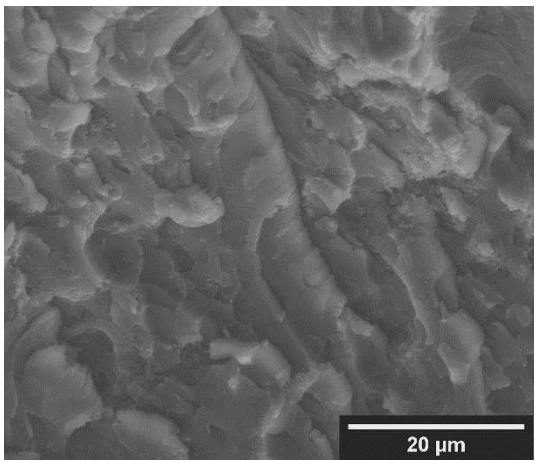

Figure 93: Fracture surface of tensile test of unmodified, epoxy-based composite, Epoxy_5_unmod sample

5.4.9 Dynamic mechanical analysis

In Figure 94 (left), the of the storage modulus of epoxy-based samples is plotted against temperature. The storage modulus at room temperature is increased by the addition of PPPI. A strong effect of the particle content on the thermomechanical properties can be observed. The transition between the glass like to rubbery region shifts to lower temperatures. A pronounced decrease in storage modulus occurs in the 15 vol% PPPI sample. The decrease of storage modulus is more pronounced for the 15 vol% PPPI composite, as for samples with lower PPPI content.

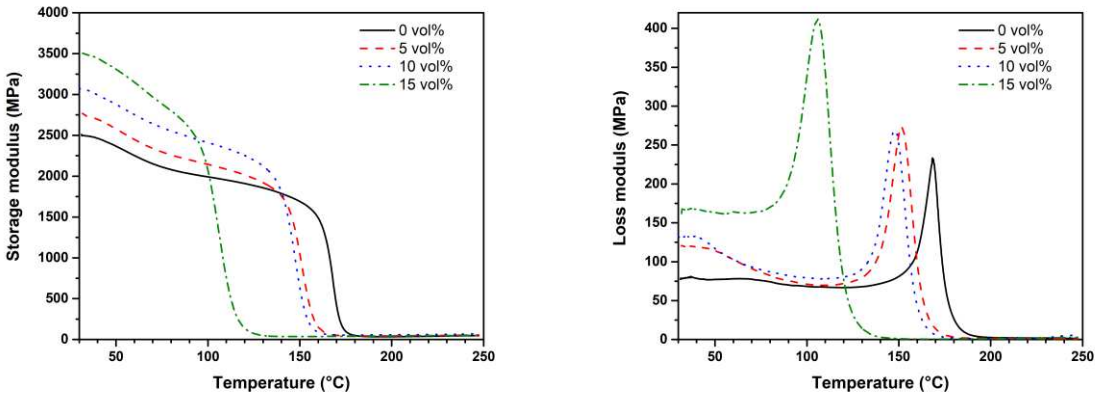

Figure 94: Storage modulus (left) and loss modulus (right) versus Temperature of unmodified, unfilled and composite epoxy samples, Epoxy_unmod

The values of storage modulus, glass-transition temperature and plateau modulus are listed in Table 27. The transition between glass-like and rubbery state can be indicated by the tangent delta of the phase angle between storage and loss modulus. The peak of tan delta, illustrated in Figure 95 (left), corresponds to the glass-transition temperature (T_g) of the material. A nearly linear decrease in T_g with higher filler content is observed in Figure 95 (right), starting at a T_g of 174 °C in the unfilled epoxy, T_g decreases to 159 °C with 5 vol% and to 156 °C with 10 vol% PPPI. An even stronger decrease to 117 °C can be observed in the 15 vol% sample.
The peak height decreases significantly in contrast to the neat epoxy sample. Therefore, the dampening of the material decreases. A broadening of the peak width can be detected in the composite samples as well. This is most pronounced in the 15 %vol PPPI composite, which can be related to inhomogeneities. [55, 61, 79]

The loss modulus shown in Figure 94 (right) depicts the glass-transition temperature in a similar way as the tan delta peaks in Figure 95 (left). The dampening is also correlated with the peak

height of the loss modulus curves. In this case, a higher dampening is indicated by a lower peak height of the loss modulus.

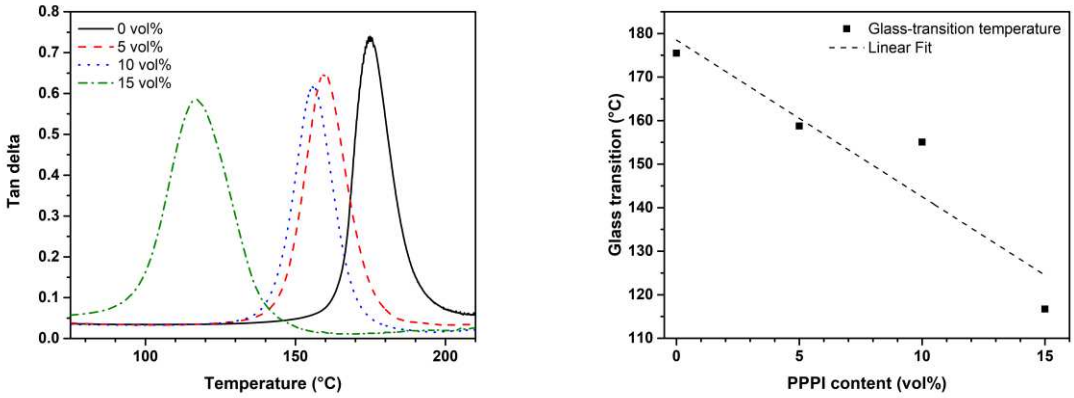

Figure 95: Tan delta versus Temperature (left) and Glass-transition temperature versus PPPI content (right) of unmodified, unfilled and composite epoxy samples, Epoxy_unmod

The storage modulus at 30 °C is plotted against the PPPI content in Figure 96. Common models were used to estimate the trend in storage modulus. The indentation modulus of the PPPI was used for modelling. In this case, ROM and Kerner equation predict the course of the modulus very accurately in this concentration range of filler, while the Halpin-Tsai model (from Chapter 2.7) underestimates the modulus.

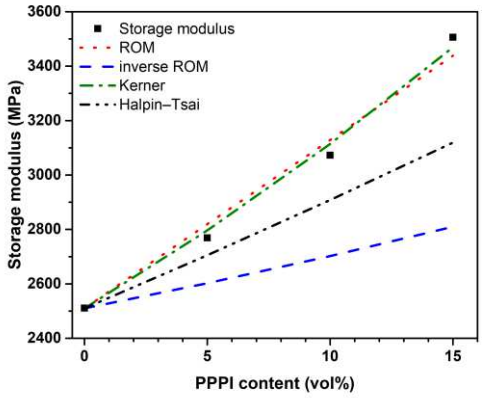

Figure 96: Storage modulus versus PPPI content of unmodified, unfilled and composite epoxy samples and common model predictions, Epoxy_unmod

The plateau modulus above the glass-transition temperature is shown in Figure 97. Using the plateau modulus, the cross-link density (V_e) of epoxy systems can be calculated, according to Equation (11).

Table 27: Storage modulus, plateau modulus and glass-transition temperature of unmodified, unfilled and composite epoxy samples

PPPI content (vol%)	E_s (MPa) at 30 °C	T_g (°C)	E_p (MPa) at T_g + 30 °C	V_e (mol/m³)
0	2510	175	34.9	2930
5	2768	159	42.9	3720
10	3072	155	56.0	4890
15	3506	117	36.2	3450

$$V_e = \frac{E_r}{3RT_r} \quad (11)$$

In equation (11) adapted from Nakka *et al.* [26], the crosslink density V_e is calculated with the storage modulus E_r at $T_r = T_g + 30\ °C$ and R as universal gas constant. Table 27 lists the values needed for the calculation of Equation (11).
The plateau modulus and the cross-link density increase in the composite material. The 5 and 10 vol% PPPI samples show a consistent trend in plateau modulus, as it can be observed in Figure 97. Contrary to this trend, the modulus of the 15 vol% sample is lower than of the other composite samples, but is still higher than the modulus of the unfilled epoxy.

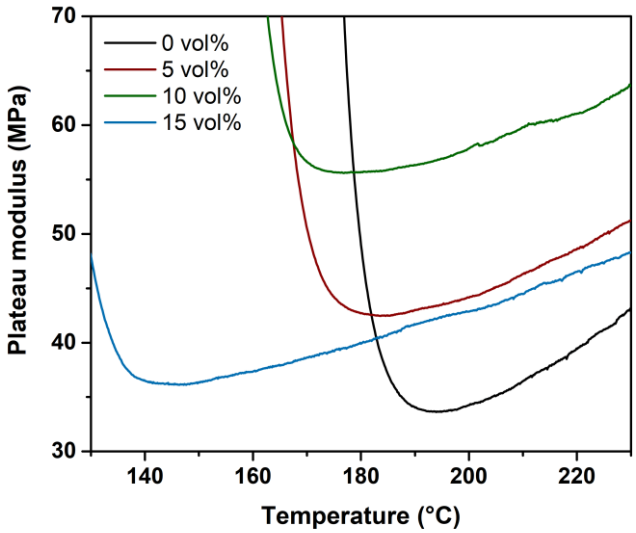

Figure 97: Plateau modulus versus Temperature of unmodified, unfilled and composite epoxy samples

5.4.10 Thermogravimetric analysis

To evaluate the degradation of the material with temperature, TGA was used, the results are listed in Table 28 and illustrated in Figure 98. An increase in degradation temperature can be observed from 313 °C in the neat epoxy to 364 °C in the 5 vol% filled composite. The degradation temperature does not increase significantly in the 10 and 15 vol% samples. In addition, the degradation of the PPPI can be noted at 630 °C. This is most pronounced in the 15 vol% PPPI sample.

Table 28: Degradation onset - temperature of unmodified, unfilled and composite epoxy samples

PPPI (vol%)	Onset of degradation (°C)
0	313
5	364
10	369
15	370

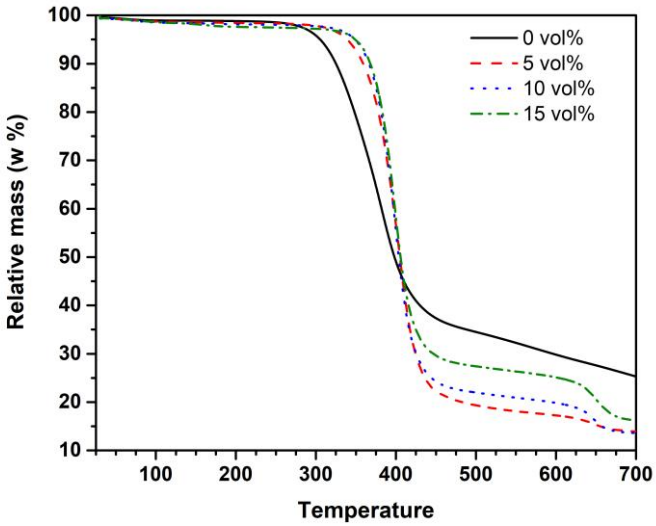

Figure 98: Thermogravimetric analysis of unmodified, unfilled and composite epoxy samples

6 Discussion

6.1 P84 NT – Composites – Direct forming

6.1.1 Density

6.1.1.1 Green Density

The difference in geometrical density between the two sample shapes most likely occurs due to a systematic measurement error. The cylindrical shapes could be measured more accurately with the caliper, and probably represent the actual density of the pressed material more precisely. As the surfaces of the bars weren't flat, the density determined via the geometrical method was underestimated consequently.
As shown in Figure 20, the relative density of the 10 vol% PPPI composite samples is 4.8 % lower than the reference P84 NT sample. This indicates a lower compaction of the sample caused by the PPPI particles in the composite sample.
The producer of P84 NT powder (Evonik) specifies a green density for the direct forming method of at least 1.3 g/cm^3 at applied pressures between 250 and 300 MPa. This value could not be achieved with cold isostatic pressing within the same pressure range. The low green density of the P84 NT samples causes the incomplete sintering of the unfilled and composite P84 NT samples.

6.1.1.2 Density after sintering

The higher density in the rectangular bar shaped samples underpins the assumption of a measuring error in the green density of these samples. All of the sintered samples show a similar, albeit low relative density. Therefore, sintering failed in the unfilled P84 NT as well as in the composite samples. Most of the tested samples were sintered as suggested by the powder producing company. To evaluate if the sintering was unfinished after the sintering time of one hour, the sintering time was expanded to three hours. As there was no increase in density, as shown in Figure 22, the influence of sintering time could be ruled out.
For all samples the relative density is around 90 % and therefore, the consolidation with the direct forming approach was not successful with these parameters.

6.1.2 Overall conclusion of P84 NT - Direct forming

The microstructural analysis via SEM confirmed an incomplete sintering. The sintering parameters for the P84 NT as suggested by the producer did not lead to successfully sintered parts. As mentioned before, the reason for the failed sintering is the low green density. Another cause of the failed sintering could be an insufficiently high temperature or the sintering under air, even though both accorded with the producer's recommendations.

For further investigations on this production route towards polyimide/polyimide composites, different pressing techniques like die pressing should be tested, in order to improve green densification. Also, a change of sintering parameters should be tested in this case, like sintering under inert gas or even under pressure.

6.2 P84 NT – Composites – Hot compression moulding

6.2.1 Density

The decrease in relative density is most likely caused by a hindering of material flow due to the rigid PPPI particles, as they do not soften at processing temperatures.

The decrease in relative density is only 0.8 % and is therefore hardly noticeable. In the case of the fine powdered P84 NT (1-10 µm), the decrease of relative density is less pronounced than for the other coarse-grained P84powders (425, 325, 200 mesh).
As high relative densities could be achieved for P84 NT/PPPI composites, the compaction via hot compression moulding was successful.

6.2.2 Microstructural analysis

The step-like fracture surface which appears in the neat P84 NT sample (Figure 99) can either be linked to a tearing of incomplete sintered P84 NT particles or a brittle fracture mechanism of the P84 NT. Interestingly, the fracture surfaces of the unfilled and composite samples look similar, which is most likely due to a failure mechanism dominated by the matrix, rather than the particles. This is also suggested by the results from the bending tests, in which the unfilled P84 NT and composite samples both break at a low rate of deformation.
The "voids" visible in the unfilled and composite material could be explained by a plastic deformation of the P84 NT matrix. When compared with ductile fracture behaviour in literature, these "voids", observed in Figure 99 (left), resemble the structures produced by plastic deformation.[4]

The "voids" could also be a sign of thermal degradation in the same way as observed in the P84 samples in Figure 99 (right). In this case, the "voids" would originate from gaseous decomposition products formed at excessive temperatures during hot compression moulding. Even though the hot compression moulding process for P84 NT powder is recommended at a temperature of 350 °C the origin of the voids through thermal degradation seems to be plausible.

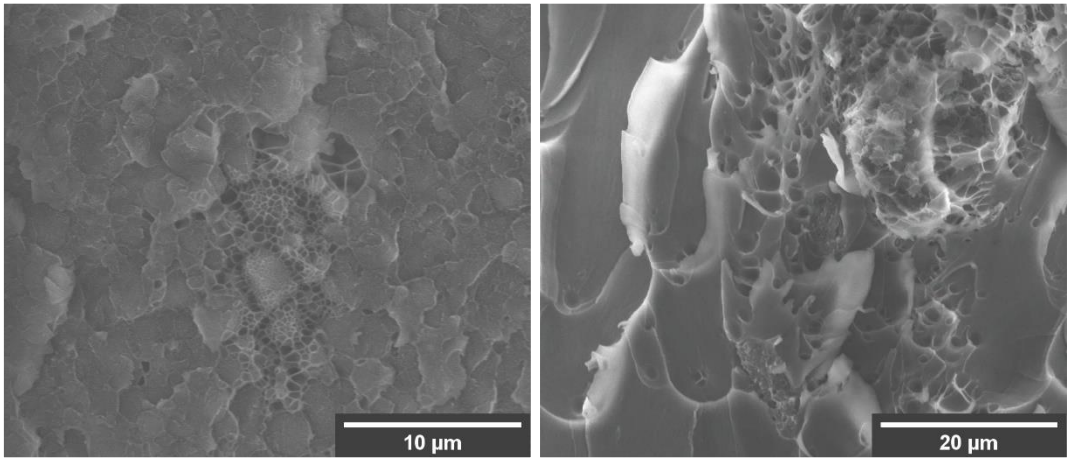

Figure 99: Fracture surfaces of P84 NT, hot compression moulding P84NT_HCM_0_IPA_35 (left) and unfilled P84 samples heated at 300 °C for 3 h under air, P84_0_425_35 (right)

6.2.3 Three-point bending test

The unfilled P84 NT samples exhibit strength and strain values far lower than the datasheet values supplied by the producer. Also, the lack of plastic deformation in the stress and strain curves is atypical for the unfilled P84 NT material.[45] This lack in plastic behaviour and poor mechanical properties imply damage or errors during the production of the samples.
The reason for the unlikely results in mechanical properties of the material could be linked to the "voids" or "steps" observed on the fracture surfaces (Figure 99 (left)).
Nevertheless, the flexural modulus of the composite material has improved, especially in the 10 vol% PPPI sample, in accordance with the ROM prediction.

6.2.4 Overall conclusion of P84 NT – Hot compression moulding

As for the direct forming procedure, the hot compression moulding procedure of P84 NT was most likely performed under insufficient conditions, though the used parameters were based on producers' recommendations. A plausible reason for the poor mechanical behaviour of the material is a degradation, caused by too much thermal stress during the hot compression moulding procedure indicated by the observed voids in microstructure.

6.3 P84 – Composites

6.3.1 Hot compression moulding - Preliminary tests

6.3.1.1 Influence of P84 particles size

The flexural strength and strain are significantly increased with finer P84 powder, as shown in Figure 34. This is most likely linked to a better material flow during hot compression moulding, caused by the higher surface area of finer P84 powder.

6.3.1.2 Influence of mixing techniques

Comparing differently mixed 10 vol% PPPI samples, only a slight change in density without striking differences in microstructure have been detected. As no change of mechanical properties of the resulting samples could be noticed, no significant influence of the tested mixing procedures was found.

6.3.1.3 Influence of moulding pressure

Comparing the samples pressed with 35 and 70 MPa, a reduction of flexural strength and strain was found with 70 MPa (Figure 34). Microstructural analysis of the unfilled or composite material pressed with 70 MPa couldn't provide a reason for this reduction.

6.3.1.4 Overall conclusion on P84 preliminary tests

The clear improvements of mechanical properties with the finest P84 powder (425 mesh), led to the use of this mesh grade for all following experiments.
No significant influence in mixing technique was found with the tested procedures. As it was assumed that the wet ball milling approach should yield the best homogeneity in the composites, this mixing technique was used for further investigations.
As the unfilled and composite P84 samples pressed using 70 MPa exhibited decreased mechanical properties, only a moulding pressure of 35 MPa was applied in further investigations.

6.3.2 Hot compression moulding - Unmodified Samples

6.3.2.1 Vickers hardness and nanoindentation

Comparing the hardness of the composites and the unfilled P84 samples, no improvement could be found in the unmodified composite samples, neither using the Vickers nor nanoindentation testing method.
While the nanoindentation hardness of the P84 matrix is 563 MPa, the hardness of the PPPI particles is 15 % higher, with a value of 648 MPa. This small increase most likely causes the lack of hardening of the P84 composites, as depicted in Figure 45.

6.3.2.2 Three-point bending tests

The decreasing strength and strain until break of the P84 composite material could be contributed to different reasons. The first and most plausible effect on the decrease in strength and strain is a lack of adhesion. This effect will be further discussed in the amine-modifications in chapter 6.3.3.

Another contribution towards a lowering of strength and stain is the formation of pores within the composite material, as plotted in Figure 100 (left). The 10 vol% PPPI composite follows this decreasing trend. The 5 vol% PPPI composite however shows no decrease in relative density, but a decrease of strength and strain.

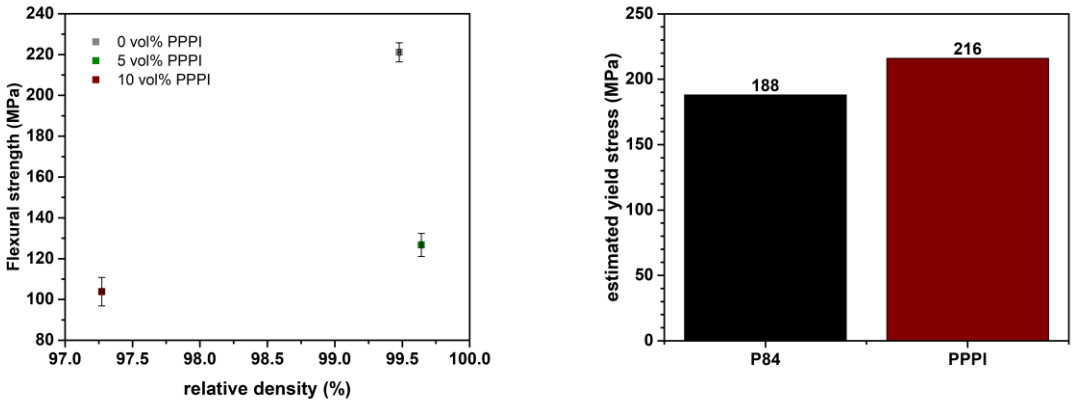

Figure 100: Flexural strength versus relative density of unmodified, unfilled and composite P84 samples, P84_425_IPA_35_unmod (left) and estimated yield stress of P84 matrix and PPPI particles (right)

The third possible answer for the decrease in strength and strain of the P84 composites could be a failure of the PPPI particles within the P84 matrix. To evaluate this theory, the hardness of the PPPI particles, measured with nanoindentation, was determined. For an estimation of the yield stress of a material, the hardness can be used in the equation $H_i \sim 3 \cdot \sigma_{tM}$.[34, 80]
Following this equation, the yield stress of the PPPI particles would be 216 MPa and the yield stress of the P84 matrix 188 MPa, as shown in Figure 100 (right). The high brittleness of the PPPI overweighs its higher yield stress (compared to the P84 matrix) and therefore, leads to the low strength and strain until break of the composite material. [20]

Even though it could not be shown in this work, the influence of particle size on strength of particle composite materials is often described in the literature.[34, 36] In these works, a particle size over 1 µm leads to a decrease in strength and strain until break of the composite materials. A common explanation for this is that larger particles act as stress centres at which critical failure of the material occurs. Consequently, the size of the PPPI particles, which is in between 1 and 10 µm is the most plausible explanation for the observed mechanical behaviour in the P84/PPPI composites.
A further reason for the decrease in strength and strain could be the microstructure of the composite material. As shown in Figure 41, the "enclosing" of P84 particles with PPPI particles could also led to the debonding of these PPPI surrounded P84 "clusters".

Despite the decrease in strength and strain, an increase in flexural modulus of the composite material was measured. This increase is due to the higher modulus of the PPPI particles, which has been confirmed via nanoindentation. The indentation modulus was used for an estimation of the composite modulus with increasing PPPI content. In Figure 101, the flexural modulus of P84 composites up to a content of 10 vol % PPPI is compared to its estimated development with increasing PPPI content. These model calculations show the possible boundaries of modulus increase with the addition of PPPI in the P84 composite material, giving a prediction for future investigation towards P84/PPPI composites or polyimide/PPPI composites in general.

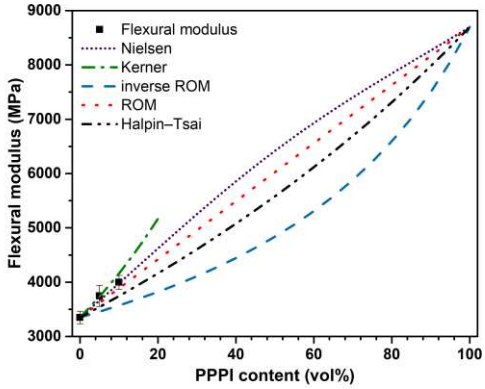

Figure 101: Flexural modulus versus PPPI content of unmodified, unfilled and composite P84 samples, P84_425_IPA_35_unmod and common model predictions

The reason for the improved modulus in contrast to the decreased strength and strain is that the flexural modulus only reflects the behaviour within the elastic deformation of the material. In this region, only low shear forces between the phases appear, and therefore, the particle-matrix interaction is not as important as in plastic deformation.

6.3.2.3 Dynamic mechanical analysis

The storage modulus measured in dynamic mechanical analysis is comparable to the flexural modulus measured in three-point bending tests. As shown in Figure 102, the flexural modulus is lower than the storage modulus in the P84 reference and composite samples. The difference in absolute values is due to a different sample geometry and different forces used in DMA and flexural tests.

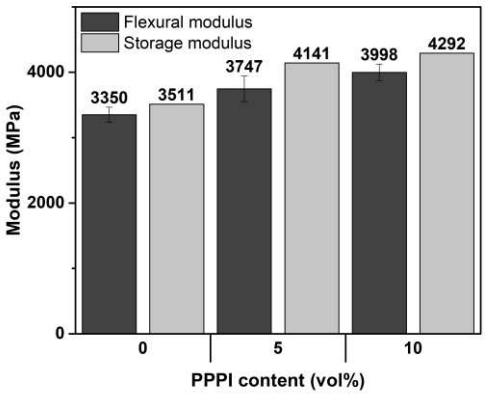

Figure 102: Comparison of flexural and storage modulus of unmodified, unfilled and composite P84 samples, P84_425_IPA_35_unmod

6.3.2.4 Thermogravimetric analysis and thermal degradation

The degradation temperature of P84 and composite samples is shown in Figure 103. The ROM model was calculated using the degradation temperature of PPPI and P84. The degradation temperature of PPPI was taken from previous works, with a value of 630 °C.[17, 74] The ROM model estimates the possible improvement of the degradation temperature for the composite material. In this case, the ROM model is simply used as a weighted average, to estimate the highest possible improvement of degradation temperature with the addition of PPPI in the P84 composite material. The measured unmodified composite samples show a similar increase as predicted by the weighted average. Therefore, the measured values of the composite samples most likely reflect the maximum possible improvement.

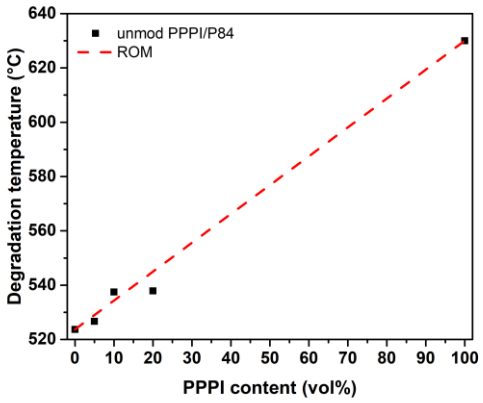

Figure 103: Degradation temperature of unmodified, unfilled and composite P84 samples and PPPI, P84_425_IPA_35_unmod and model predictions

6.3.2.5 Overall conclusion on P84 unmodified samples

A decrease of strength and strain until break of the composite material, compared to the P84 reference was found. No significant improvements in hardness or thermostability could be measured. Compared to the P84 reference material, the composite samples only show improvement in modulus. These results indicate that the PPPI particles can only improve the modulus of the P84 matrix and are not beneficial to the other properties of the composite studied in this work.

6.3.3 Hot compression moulding – Amine-modified Samples

To investigate possible improvements of the interfacial adhesion between the P84 and PPPI, composites were modified using different diamines. Here, the aminolysis reaction described in Chapter 2.8 most likely takes place on the surface of the PPPI and P84 particles. Covalent bonds between the PPPI and P84 would ideally be formed with this reaction, but an improvement on van der Waals interaction or hydrogen bonds would be plausible.

In order to determine the influence of the amine-modification on the composite material and interactions between the amine and polyimides, three different types of diamines were used. The principal focus was to understand the influence of the diamine chain length and flexibility. For this purpose, the following diamines were used: DACH with its short chains and low flexibility, HMDA as a diamine with medium chain length and flexibility, and the Jeffamines due to their long flexible chain between the amine groups.

6.3.3.1 Density and Microstructure

The decrease in density of the amine-modified samples with 2 or 5 % HMDA or Jeffamine, compared to the unmodified composite samples, is most likely caused by the formation of gaseous products during hot compression moulding. The amount of amine does not react completely with the polyimides (P84 or PPPI) and evaporates or decomposes instead. The produced gases then get trapped within the material, especially in the edge areas of the composite material, as shown in Figure 62.

6.3.3.2 Vickers hardness and Nanoindentation

Comparing the amine-modified and unmodified composites samples, no change in hardness was measured, neither using the Vickers nor the nanoindentation testing method.
The interfacial adhesion only seems to have a low influence on the hardness of the composite material. The occurring porosity has no influence on the measured hardness, as the pores are

relatively large and concentrated on the edge of the samples. The hardness was solely measured on test specimens which had been derived from the centre of the composite and reference samples, respectively.

6.3.3.3 Three-point bending tests

In case of the 1 % HMDA or DACH modifications with stirring in water under reflux (P84_10_425_Syn_35), a decrease in strength and strain was measured. These results are probably contributed to a degradation of both polyimides in the amine-modified composite samples, as described in the literature. [81]
The developed theory that long, flexible chains should lead to better phase interaction could only be confirmed partially with the comparison of the flexural strength of DACH and HMDA modified samples, as shown in Figure 104 (left). Here, the increase of strength and strain until break with the addition of 1 % HMDA in the dry or wet ball milling procedure is an indication of an enhanced phase interaction between PPPI and P84. Compared to the unmodified reference sample, modifications with DACH and Jeffamines didn't show an impact on the mechanical properties of the materials.

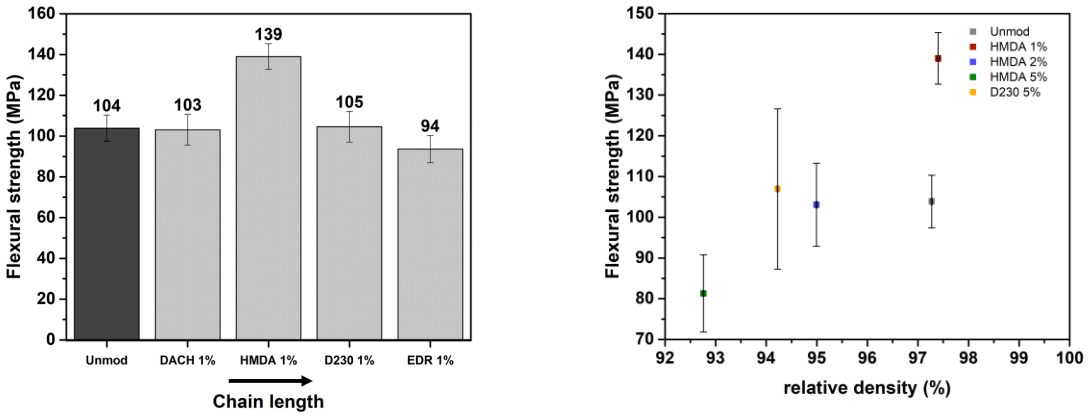

Figure 104: Influence of amine chain length on flexural strength (left) and flexural strength versus relative density of modified P84 composite samples (10 vol% PPPI), P84_10_425_IPA_35

To demonstrate a possible influence of relative density on flexural strength, the strength of selected amine-modified samples is plotted against their relative density in Figure 104 (right). With the addition of 2 and 5 % HMDA, and 5 % D230 Jeffamine, the flexural strength and the relative density is decreased compared to the 1 % HMDA modified composite sample Considering this correlation, the reason for the decrease in strength could be the decrease in relative density.

6.3.3.4 Overall conclusions on P84 modified samples

An increase of strength and strain until break of the 1 % HMDA modified composite sample compared to the unmodified composite sample was found. No significant improvements in hardness and thermostability could be measured. The 1 % HMDA modified composite samples show an improvement in the storage modulus compared to the unmodified composite sample. These results indicate that the amine-modification with HMDA leads to an improvement of mechanical properties of the P84/PPPI composite material.

6.4 Epoxy – Composites

6.4.1 Vickers Hardness and Nanoindentation

The hardness of the composites epoxy-based samples follows a linear increasing trend with the PPPI content, using both the Vickers and the nanoindentation testing method.
Compared to the nanoindentation hardness of the epoxy matrix (265 MPa), the hardness of the PPPI particles is 40 % higher, with a value of 648 MPa. The significantly higher hardness of the PPPI led to the hardening occurred in the epoxy-based composites, as depicted in Figure 78.

This hardening effect of the PPPI particles in the epoxy matrix gives an indication for particle-matrix interaction between the PPPI and epoxy. It can be assumed that the particle-matrix interaction is caused by the aminolysis reaction, taking place on the surface of the PPPI in the presence of the amine hardener of the epoxy system, and resulting in a beneficial load shearing mechanism within the composite.

6.4.2 Three-point bending tests

With the addition of PPPI particles to the epoxy matrix, the mechanical properties vary from those of the pure epoxy; while the strain until break decreases, the strength remains the same.

The reason for the decrease in flexural strain until break could be a debonding of the PPPI particles from the epoxy matrix. Another reason for this decrease could be the brittleness of the PPPI particles. Considering the studied fracture surfaces of the epoxy composites, a fracture mechanism caused by the debonding of particles from the matrix appears more plausible.
Compared to the unfilled epoxy, the flexural strength in the composites remains the same. Due to a higher yield stress of the PPPI particles, the fracture of the composite most likely occurs through debonding or exclusively in the epoxy matrix. This would imply, that the debonding requires the same stress as the fracture of the epoxy.

The hardness of the material is related to its yield stress. In case of the assumption that hardness is related with the yield stress in the ratio of $H_i \sim 3 \cdot \sigma_{tM}$, the yield stress of the epoxy matrix would be 88 MPa, and 216 MPa for the PPPI, as shown in Figure 105 (left).[34, 80]

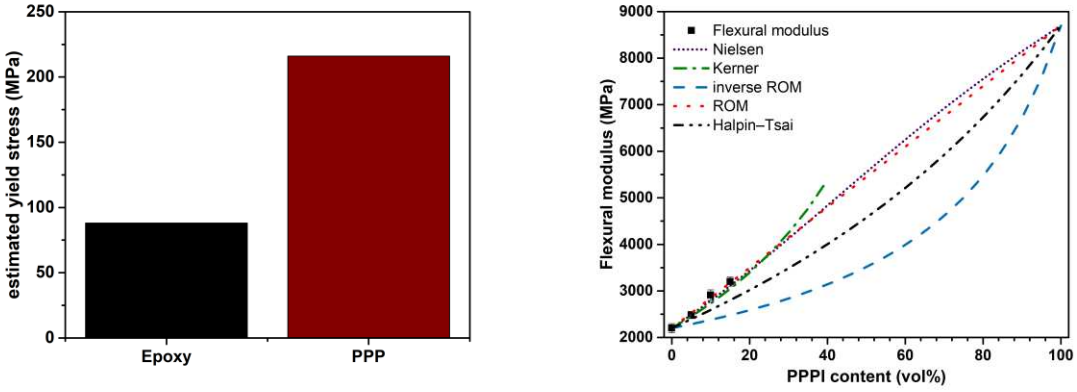

Figure 105: Estimated yield stress of epoxy matrix and PPPI particles(left) and flexural modulus versus PPPI content of unmodified, unfilled and composite epoxy samples, Epoxy_unmod and common model predictions(right)

The strength of a particle composite is largely influenced by the particle size. According to literature, a consistent flexural strength with the addition of rigid particles is unusual.[36] On the other hand, a consistent strength with the addition of thermoplastics into epoxy material has been reported in the literature. [5]

Despite the decrease in strain, an increase in flexural modulus of the composite material was measured. This increase is due to the higher modulus of the PPPI particles, which has been confirmed via nanoindentation. The indentation modulus was used for an estimation of the composite modulus with increasing PPPI content. In Figure 105, the flexural modulus of epoxy composites is compared to its estimating development with increasing PPPI content. These model calculations show the possible boundaries of modulus increase with the addition of PPPI in the P84 composite material, giving a prediction for future investigation towards P84/PPPI composites or polyimide/PPPI composites in general.

To study the effect of the aminolysis reaction between the amines of the epoxy curing agent and the PPPI particles, tests were conducted with an increased hardener content within the epoxy system. The 5 % increased hardener content does not change the mechanical properties significantly. However, the thermomechanical behaviour was not tested for these samples.

6.4.3 Tensile tests

Tensile tests displayed a clear difference between the epoxy matrix material and the composites. The tensile strain of the composite material decreases with the addition of PPPI. This follows the same trend as observed in the flexural tests. The decrease in tensile strain is complemented by a similar decrease in tensile strength. This decrease in tensile strength is contrary to the findings in the flexural tests, were flexural strength remains the same with PPPI addition, as shown in Figure 106.

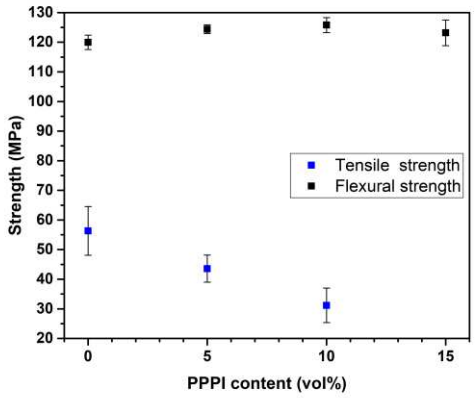

Figure 106: Comparison of flexural and tensile strength of unmodified, unfilled and composite epoxy samples, Epoxy_unmod

The most likely explanation for this is the unsuitability of tensile tests for brittle materials, as described in Chapter 6.5.4. The fracture surfaces show a similar fracture type as in flexural tests. The prominent origin of failure observed in Figure 92 proves the brittle failure mechanism.

6.4.4 Dynamic mechanical analysis

The results from thermomechanical testing showed a decrease of glass-transition temperature and an increase of cross-link density in the epoxy composite samples, with increasing PPPI content. This correlation is shown in Figure 107 (left). The sample with 15 vol% PPPI (Epoxy_15_unmod) does not follow the same trend as the other composite samples, with much lower glass-transition temperature and cross-link density. This drastic decrease of both values, in comparison with the other composite samples, is most likely due to an increased heterogeneity in the Epoxy_15_unmod sample.

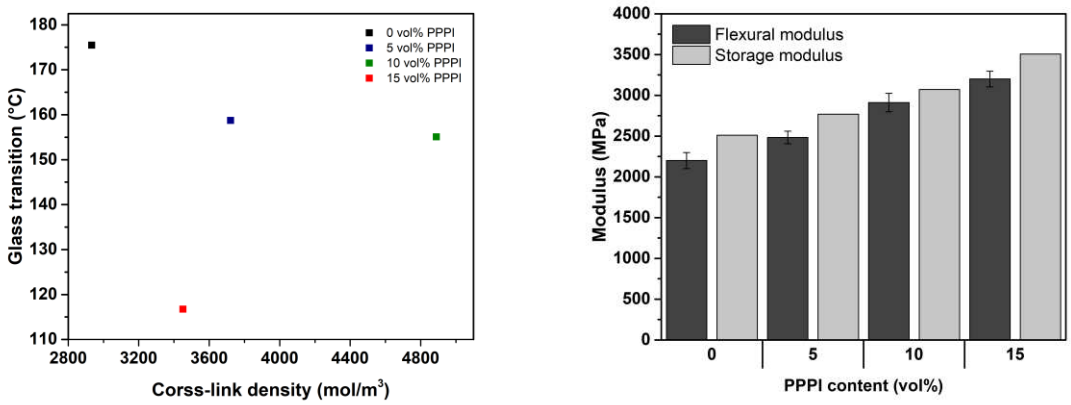

Figure 107: Glass-transition temperature versus cross-link density (left) and comparison of flexural and storage modulus (right) of unmodified, unfilled and composite epoxy samples, Epoxy_unmod

For micro fillers, an increase in T_g and cross-link density is generally reported.[82-84] A decrease in T_g is known for nanocomposites.[85, 86] In this case, the reduction of T_g is correlated with an increase in free volume or phase separation. In the literature, a higher cross-link density is commonly related with an increase in glass-transition temperature. [25-27, 87]
The most plausible hypothesis would be that the decrease in glass-transition temperature is correlated with the aminolysis reaction between PPPI and the amine hardener. If the amine hardener is consumed by the reaction with the PPPI, insufficient amount of hardener remains for a complete cross linking of the epoxy matrix. Considering this, the cross-link density should decrease and as a result, as well as the glass-transition temperature. However, the calculated cross-link density rises with the addition of PPPI.
Consequently, the reduction of glass-transition temperature can be explained by two different theories.
The first presumption relies on a higher cross-link density of the epoxy matrix in the composite material. This increase in cross-link density could be caused by the presence of small PPPI particles (< 0.1 µm). The decrease in glass-transition temperature on the other hand could be a result of increased free volume between the PPPI particles and the epoxy matrix.
The second theory bases on the increase in plateau modulus caused by the higher modulus of the PPPI particles. As a result, the calculated cross-link density of the composite increases due to the higher plateau modulus of the PPPI, but the actual cross-link density of the epoxy matrix is still reduced due to a shortage of amine hardener. Both theories could be investigated with additional methods for determining the cross-link density.

The storage modulus measured in dynamic mechanical analysis is comparable to the flexural modulus measured in three-point bending tests. As shown in Figure 107 (right), the flexural modulus is lower than the storage modulus in the epoxy reference and composite samples. The variation of absolute values is due to a different sample geometry and different forces used in DMA and flexural tests.

6.4.5 Thermogravimetric analysis

The increase in degradation onset-temperature in the composite material can be explained by the higher thermal resistance of PPPI. The ROM model was calculated using of the degradation temperature of PPPI and P84. The degradation temperature of PPPI was taken from previous works, with a value of 630 °C.[17, 74] In this case, the ROM model is simply used as a weighted average, to estimate the highest possible improvement of degradation temperature with the addition of PPPI in the epoxy composite material.
Compared to the unfilled epoxy sample, the measured degradation temperature of the composites

increases with a higher rate as predicted by the weighted average, as it can be seen in Figure 108. In the literature, the appearance of an increased thermal degradation temperature is commonly explained by a barrier effect of the filler particles, due to inhibited diffusion of decomposition products into the gas phase. [88, 89]

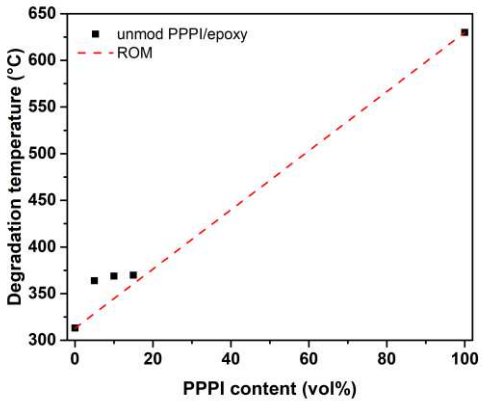

Figure 108: Degradation temperature of unmodified, unfilled and composite epoxy samples and PPPI, Epoxy_unmod and model prediction

6.4.6 Overall conclusions on epoxy samples

A decrease of flexural strain until break and an unchanged flexural strength of the composite material compared with the epoxy reference was found. In tensile testing, the tensile strength and strain until break decreased with the addition of PPPI. Significant improvements in modulus, hardness and thermostability could be measured after the addition of PPPI to the epoxy matrix. These results indicate that the PPPI particles can improve several properties of the epoxy matrix.

6.5 General observations for material testing of PPPI composites

6.5.1 Nanoindentation

Nanoindentation is the only existing technique to directly measure the mechanical properties of the PPPI particles. Due to the sample preparation, the hardness and indentation modulus of the particles could only be determined with a high standard deviation. As long as this technique delivers the only reasonable measurement of the PPPI particles, these values were used for all theories and models concerning the composite materials.
The measured indentation modulus of the PPPI, the two matrix materials, and the composites fit well with the calculated rule of mixture. Furthermore, the Young's modulus found in the literature (12200 MPa [20]) is in the same order of magnitude as the measured indentation modulus (8700 ± 1060 MPa). According to these previous two statements, the determined indentation modulus appears more plausible.
The measured hardness of PPPI appears plausible as well, as the measured hardness of the matrix materials and composites fit well with the calculated rule of mixture.

6.5.2 Hardness tests

The "macro" Vickers hardness results in lower values than measured by nanoindentation. As the measured hardness is influenced by the load applied on the indenter, these two values cannot be directly compared to each other.
As large indentation imprints were made with the force of 9.81 N, a large area of the sample was tested. Here, small pores and outbroken material could influence the results.

6.5.3 Three-point bending tests

As the specimens produced by hot compression moulding were too small for the initially suggested setup, the three-point bending tests were conducted with a different setup as proposed in standard. EN ISO 178: Support span L: 64.0 mm; Test specimens: 80.0 mm length, 10.0 mm width, 4.0 mm thickness.[76]
As described in the experimental procedure, the used setup had a support span of 25.4 mm. The standard suggests a relation between this length (L) and the thickness (h) of the test specimens of $L = 16 \cdot h$. This ratio results in a test specimen thickness of 1.6 mm.
An influence of specimen thickness on the flexural strain until break, was observed. Due to a sliding of the test specimen on the support, the determined strain of thinner test specimens was higher. In the composite materials, this effect was not noticed due to the low strain rates present in both composites.

In Figure 109, two stress/strain curves of the P84 and epoxy matrices are depicted. In both cases a stick/slip phenomenon is observable. This phenomenon is characterised by the "zig-zag" pattern of the plastic deformation zone. This material behaviour is typical for an unstable crack propagation as described in Chapter 2.2.2.
It could also be contributed to a slipping of the test specimens on the sample supports, caused by the small sample size, especially observed for thin samples. Interestingly, this behaviour does not occur with all tested samples of similar geometry.
A second behaviour noticed in nearly all samples is a sort of transient response or damping at the beginning of the stress/strain curve in the elastic zone. This might lead to an underestimation of the flexural modulus in the tested samples, as the flexural modulus was determined at a strain rate between 0.05 and 0.25 %, as specified in the standard.

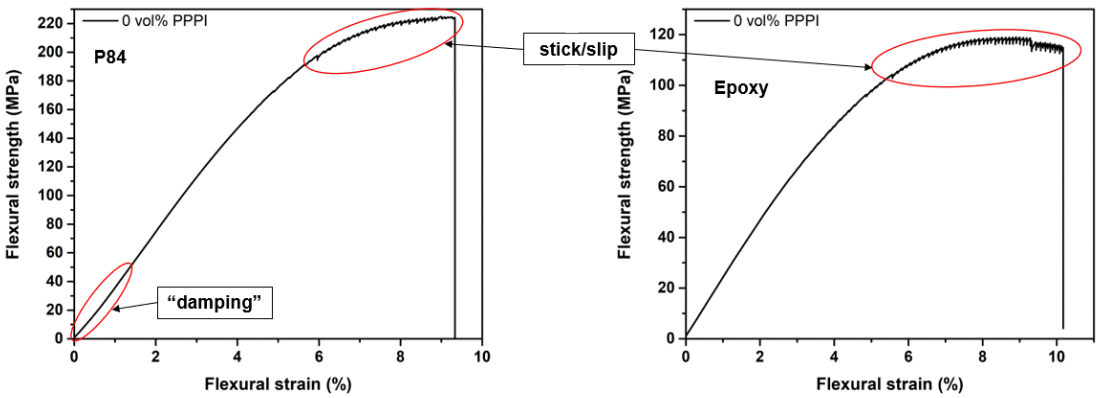

Figure 109: Example stress/strain curves – stick/slip behaviour and transient response bending tests, unmodified, unfilled P84 and epoxy samples, P84_0_425_35_5 (left) and Epoxy_0_unmod_9

All bending test specimens were grinded and polished until no scratches remained on the surface of the sample, as suggested in the standard. The observed breaking-out of PPPI particles in both composite materials could have a weakening effect on the material. Especially for brittle materials, surface defects can have a drastic effect on static material testing. Therefore, the broken-out PPPI particles could also contribute to the brittle failure and a lack of strength and strain until break was observed in flexural testing.
This problem could not be solved with any polishing procedure tested. During sample preparation, it could be observed that the breaking-out only occurs during the final polishing steps. Different polishing suspensions were tested, but no procedure was found to hinder the breaking-out of the particles, as described in detail in Chapter 6.5.6.

6.5.4 Tensile tests

The difference between the trend of flexural strength and tensile strength in the epoxy-based composites, shown in Figure 106, is most likely due to tensile testing itself.
The stiffer and more brittle a material gets, the more it is prone to failure due to surface defects. More important, brittle materials fail easily when torsion or shear forces are applied. Shear forces appear when the tensile test specimen is not parallel to the direction of force applied. Consequently, if the test specimen is not clamped exactly into the test rig, the ultimate tensile strength of the material cannot be reached and the material fractures too early. In a conventional tensile testing setup, the test specimen cannot be arranged perfectly parallel to the force direction. For this reason, tensile testing is not optimal for materials with a brittle mechanical behaviour.

Considering this, bending tests or even compressive strength tests are more suitable for the study of materials used in this work. This is especially true for both composite materials, which exhibit a relatively brittle behaviour.

6.5.5 Dynamic mechanical analysis

The force, strain rates, and frequency in dynamic testing have an influence on the measured moduli. To validate these measurements, sweep tests with varying frequency have to be considered for detailed analysis of the dynamic response of the materials. For example, the flattened tan delta peak-slopes observed in Figure 70 are caused by high force rates.

Because DMA testing is a time-consuming process with slow heating ramps, each sample variation could only be tested once. Consequently, no standard deviations of the measured values are given.

6.5.6 Microstructure – plastographic preparations

The plastographic preparations were accompanied by complications. The main reason was the breaking of the PPPI particles from different matrix materials. The breaking-out occurred during polishing of the samples, and is most likely a result of PPPI's brittle nature. This breaking-out was not observed in the grinding steps with SiC grinding paper or with diamond grinding plates. The use of fine SiC grinding paper did not lead to in a polished surface, with scratches remaining on the samples.
Therefore, the use of polishing pastes and polishing cloths was inevitable. Different polishing pastes were tested, consisting of diamonds, Al_2O_3, and SiO_2. Diamond pastes and lubricants based on ethanol (lubricant blue) yielded the best results.
Overall, the use of low force and low polishing speeds produced the best results in surface quality. Low forces and polishing speeds resulted in long polishing times, as described in the experimental section.

6.5.7 Microstructure – SEM fracture surfaces – Fracture mechanisms

For an understanding of the general fracture behaviour of the P84 matrix materials and the composite samples, the fracture surfaces of the three-point bending tests were analysed.
As the force rate, and therefore, the crack propagation in polymer materials is of great importance, the formation of these fracture surfaces has to be kept in mind. As polymers exhibit different fracture surface morphologies with different fracture speed, the rate of applied force has to be considered. For example, static force tests like flexural testing can lead to different fracture behaviour than dynamic force tests. In case of the materials studied in this work, the force rate does not affect the fracture mechanism drastically, due to the brittle nature of all used materials.

Furthermore, temperature does not seem to have a drastic impact on fracture behaviour. Fracture surfaces produced with liquid nitrogen cooling show the same morphology as observed in three-point bending tests at room temperature.

6.5.8 Thermogravimetric analysis

The influence of heating rate, gas atmosphere, and sample size are well known in TGA testing. Considering this, the degradation onsets could differ, especially when different heating rates are applied. The use of synthetic air, instead of nitrogen would change the degradation onset-temperature significantly.
As the particle size of a TGA sample has an influence on the onset degradation temperature, particle size of the samples was kept as constant as possible. Therefore, a sample preparation with cryo-milling and sifting was done. Cryo-milling could lead to degradation by mechanical stress and sifting of the powdered samples can lead to contaminations.

7 Summary and Conclusions

In this work, three different matrix materials for the production of PPPI based composites were tested. Two similar P84 polyimide variations were used in powder-based consolidation processes for the production of composites. A DGEBA/amine-based epoxy resin was used in a moulding procedure.
P84 NT is an incompletely imidized variation of the P84 polyimide, which was mainly used for the investigation of a direct forming process. The pressing and sintering experiments with this potential matrix material resulted in samples of low relative density in case of both unfilled matrix and PPPI composites. The problems in this production route are primarily caused by a low green density and an insufficient consolidation with the used sintering program at 350 °C and air atmosphere. The same P84 NT powder was tested for a possible application in hot compression moulding. This consolidation process resulted in samples of high relative density for both matrix material and PPPI composites. Low flexural strength and strain values of the consolidated samples indicate a need of adjusting the parameters during hot compression moulding. Most likely, a thermal degradation of the matrix material takes place at high temperatures.

A completely imidized variation of P84 was tested intensively as matrix material for PPPI composites. In this case, a direct forming approach was not successful, due to the high degree of imidization of P84. The 425 mesh P84 powder and a moulding pressure of 35 MPa led to the best results during hot compression moulding.
Dry or wet (isopropanol) ball milling procedures, proved to be a straightforward, up-scalable, and successful method for the incorporation of PPPI into the P84 matrix. The incorporation of PPPI within the P84 matrix resulted in slight decreases in relative density. Microstructural investigations showed a uniform but anisotropic microstructure with elongated P84 grains and PPPI particles clustering around the P84 grains. Although an anisotropy of the microstructure in the composite material was found, no directional dependency of mechanical properties could be measured. The strength and strain of the material was decreased by the incorporation of PPPI into the P84 matrix. The modulus of the composite material could yet be increased with the addition of PPPI.
Due to this strength and strain decrease, an amine-modification of the two polyimide phases was investigated using different diamines. The use of hexamethylenediamine resulted in higher strength and strain rates than in the unmodified composites, but still in a decrease compared to the unfilled P84 matrix material. No significant changes in hardness, thermal stability, and glass-transition temperature were observed with the addition of PPPI into the P84-based composite. Also, the use of different diamines did not change these properties in the composites.
In summary, the use of P84 as matrix material for the production of PPPI composites has to be reconsidered critically. The only advantage of the P84/PPPI composite in comparison with the P84 reference material is the increase in modulus. The other factor to consider, however, is the severe decrease in strength and strain until break of the composite material with the addition of PPPI. The main reason for the observed material behaviour is probably a lack of interfacial adhesion between particles and matrix. There is evidence which suggests that PPPI exhibits a slightly higher strength, higher modulus, but much higher brittleness than the P84. The intrinsic material behaviour of the PPPI particles could also be the cause for the for the decrease in strength and strain of the composite material.

A hot curing DGEBA/amine epoxy system was used as third matrix material in a simple moulding procedure, with dispersion of the PPPI particles in solution. In this case, the flexural strength of the material remained constant with the addition of PPPI, but with a decreasing trend in flexural strain until break. The modulus of the epoxy matrix could be improved due to the rigid nature of PPPI. Furthermore, an increase in hardness was measured within the composite material. This

leads to the assumption of a high interfacial adhesion, most likely due to an aminolysis reaction occurring between the PPPI and the amine hardener of the epoxy matrix. In tensile testing the consistent strength observed in flexural tests could not be confirmed. One drawback observed for the composite material is the reduction of glass-transition temperature with the addition of PPPI. Otherwise, an increase in thermal stability in the composite samples was observed.

Summarising, the combination of an amine-based epoxy system and the PPPI particles shows applicable synergies. The use of the high modulus, high strength PPPI particles in the low modulus epoxy matrix leads to a good balance between mechanical properties. The only drawbacks are the higher brittleness, caused by the PPPI, and a decrease of glass-transition temperature, the later could be handled with the optimisation of the epoxy system.

8 Outlook

In case of the P84 NT material, the parameters for the direct forming and hot compression moulding process have to be investigated in detail for the productions of suitable finished parts. A similar outcome in terms of mechanical and thermal behaviour as for the P84 composites is plausible.
The use of P84 as matrix material was not shown to be beneficial in this work. A further investigation on interfacial adhesion between the phases would be necessary in this case. Nevertheless, P84 and PPPI do not seem to show a good interaction in the hot compressed composite samples. Therefore, the use of different matrix materials and different production routes could be of more interest. For example, the use of a more ductile matrix polyimide would probably result in a better synergy with the rigid PPPI particles. In general, the production of composites without using of a liquid phases seems to yield materials with low interactions between phases. Therefore, a compounding procedure using a melted or dissolved matrix phase could be more promising.

The epoxy system proved to be a promising candidate for the use in PPPI-based composites. Different epoxy and hardener systems for this application should be investigated in the future. In case of the used epoxy/hardener system, the production procedure of test specimens can be improved or reconsidered in upcoming works. The used dispersion times may be limited to a necessary minimum, and also the use of masterbatches (epoxy resin + PPPI) should be considered. Efforts to reach a higher PPPI particle loading in these composites would require a more detailed investigation of rheological properties with different epoxy systems in the presence of PPPI. Due to the interaction between the amine hardener and PPPI, detailed investigations of amine-PPPI interactions are necessary. Especially the undetermined reason for the change in glass-transition temperature has to be investigated in the future.

In general, the reduction of the PPPI particle size would be beneficial for the use in composite materials. Also, a tailoring of the polyimide particle properties would be an interesting way to achieve desired mechanical composite properties. Especially a reduction of brittleness within the particles would be an eligible goal for the use in structural applications.

In terms of additional testing for the composites investigated in this work, the study of fracture toughness would be appealing for a better understanding of fracture mechanisms within the composite material. Here, the influence of the PPPI on the fracture mechanism should be investigated with a notched beam test. Alternatively, the use of impact tests (Charpy, Izod) would result in dynamic mechanical properties, in order to investigate fracture behaviour of such composites. The composite behaviour under compression, would also be interesting for further investigation of composite properties. Furthermore, investigations with scratch, creep and tribology testing should be considered for the study of these composite materials.
Considering the results of this work, static mechanical testing should be done by three-point bending tests rather than tensile testing. Ideally, standardised test specimens should be used in this case. With this standardised rectangular geometry, the test specimens would be suited for three-point bending, notched beam and Charpy tests at the same time. Therefore, the efficiency of the productions of test specimens could be improved.

References

[1] Hull D, Clyne TW. General introduction. In: Hull D, Clyne TW, editors. An Introduction to Composite Materials. 2 ed. Cambridge: Cambridge University Press; 1996. p. 1-8.
[2] Meador MA. Recent advances in the development of processable high-temperature polymers. 1998;28(1):599-630.
[3] Rosato DV, Rosato DV. Chapter 1 - Introduction. In: Rosato DV, Rosato DV, editors. Reinforced Plastics Handbook (Third Edition). Amsterdam: Elsevier Science; 2005. p. 1-23.
[4] Michler GH. Atlas of Polymer Structures: Morphology, Deformation and Fracture Structures: Carl Hanser Verlag GmbH & Company KG; 2016.
[5] Paul DR, Bucknall CB. Polymer Blends: Formulation and Performance, Performance: Wiley; 2000.
[6] Elias PDH-G. Makromoleküle, Band 3 Industrielle Polymere und Synthesen. Makromoleküle, Band 3 Industrielle Polymere und Synthesen: WILEY-VCH; 2001. p. 426 ff.
[7] Abbasi H, Antunes M, Velasco J. Polyimides from: Handbook of Thermoplastics CRC Press. Handbook of Thermoplastics, Second Edition2015. p. 491 ff.
[8] Mittal V. High Performance Polymers and Engineering Plastics: Wiley-Scrivener; 2011.
[9] Saeed MB, Zhan M-S. Adhesive strength of nano-size particles filled thermoplastic polyimides. Part-I: Multi-walled carbon nano-tubes (MWNT)–polyimide composite films. International Journal of Adhesion and Adhesives. 2007;27(4):306-18.
[10] Saeed MB, Zhan M-S. Adhesive strength of nano-size particles filled thermoplastic polyimides. Part-II: Aluminum nitride (AlN) nano-powder–polyimide composite films. International Journal of Adhesion and Adhesives. 2007;27(4):319-29.
[11] Su C, Xue F, Li T, Xin Y, Wang M. Study on the Tribological Properties of Carbon Fabric/Polyimide Composites Filled with SiC Nanoparticles. Journal of Macromolecular Science, Part B. 2016;55(6):627-41.
[12] Vespel S Line Design Handbook. du Pont de Nemours and Company.
[13] Liaw D-J, Wang K-L, Huang Y-C, Lee K-R, Lai J-Y, Ha C-S. Advanced polyimide materials: Syntheses, physical properties and applications. Progress in Polymer Science. 2012;37(7):907-74.
[14] Tashiro K. Molecular theory of mechanical properties of crystalline polymers. 1993;18(3):377-435.
[15] Wakabayashi K, Uchida T, Yamazaki S, Kimura K. Micro-flowers of poly(p-phenylene pyromelliteimide) crystals. Polymer. 2011;52(3):837-43.
[16] Nagata Y, Ohnishi Y, Kajiyama T. Highly Crystalline Polyimide Particles. Polymer Journal. 1996;28(11):980-5.
[17] Baumgartner B, Bojdys MJ, Unterlass MM. Geomimetics for green polymer synthesis: highly ordered polyimides via hydrothermal techniques. 2014;5(12):3771.
[18] Taublaender MJ, Reiter M, Unterlass MM. Exerting Additive-Assisted Morphological Control during Hydrothermal Polymerization. Macromolecular Chemistry and Physics. 2018;219(3):1700397.
[19] Ree M, Kim K, Woo SH, Chang H. Structure, chain orientation, and properties in thin films of aromatic polyimides with various chain rigidities. Journal of Applied Physics. 1997;81(2):698-708.
[20] Kim SI, Shin TJ, Pyo SM, Moon JM, Ree M. Structure and properties of rodlike poly(p-phenylene pyromellitimide)s containing short side groups. Polymer. 1999;40(6):1603-10.
[21] Thomas S, Sinturel C, Thomas R. Micro- and Nanostructured Epoxy/Rubber Blends2014.
[22] Pham HQ, Marks MJ. Ullmann's Encyclopedia of Industrial Chemistry. Ullmann's Encyclopedia of Industrial Chemistry: Wiley-VCH; 2005.
[23] Halary JL, Laupretre F, Monnerie L. Polymer Materials: Macroscopic Properties and Molecular Interpretations. Wiley; 2011. p. 53 f.
[24] Cukierman S, Halary J-L, Monnerie L. Dynamic mechanical response of model epoxy networks in the glassy state. Polymer Engineering and Science. 1991;31(20):1476-82.

[25] Shan L, Verghese KNE, Robertson CG, Reifsnider KL. Effect of network structure of epoxy DGEBA-poly(oxypropylene)diamines on tensile behavior. 1999;37(19):2815-9.
[26] Nakka JS, Jansen KMB, Ernst LJ, Jager WF. Effect of the epoxy resin chemistry on the viscoelasticity of its cured product. 2008;108(3):1414-20.
[27] Gerard JF, Galy J, Pascault JP, Cukierman S, Halary JL. Viscoelastic response of model epoxy networks in the glass transition region. Polymer Engineering and Science. 1991;31(8):615-21.
[28] Meeks AC. Fracture and mechanical properties of epoxy resins and rubber-modified epoxy resins. 1974;15(10):675-81.
[29] Kinloch AJ. Fracture Behaviour of Polymers: Springer Netherlands; 2013.
[30] Deformationsmechanismen – Lexikon der Kunststoffprüfung. 2018.
[31] Brucharten – Lexikon der Kunststoffprüfung. https://wiki.polymerservice-merseburg.de/index.php/Brucharten2018.
[32] Rampen, Schollen und Stufen – Lexikon der Kunststoffprüfung. https://wiki.polymerservice-merseburg.de/index.php/Rampen,_Schollen_und_Stufen2019.
[33] Bruchparabeln – Lexikon der Kunststoffprüfung. https://wiki.polymerservice-merseburg.de/index.php/Bruchparabeln2019.
[34] German RM. Particulate Composites: Fundamentals and Applications: Springer International Publishing; 2016.
[35] Wypych G. Handbook of Fillers: Rapra; 1999.
[36] Fu S-Y, Feng X-Q, Lauke B, Mai Y-W. Effects of particle size, particle/matrix interface adhesion and particle loading on mechanical properties of particulate–polymer composites. Composites Part B: Engineering. 2008;39(6):933-61.
[37] Hodgkin JH, Simon GP, Varley RJ. Thermoplastic toughening of epoxy resins: a critical review. Polymers for Advanced Technologies. 1998;9(1):3-10.
[38] Pearson RA, Yee AF. Toughening mechanisms in thermoplastic-modified epoxies: 1. Modification using poly(phenylene oxide). Polymer. 1993;34(17):3658-70.
[39] Kim GM, Michler GH, Rösch J, Mülhaupt R. Micromechanical deformation processes in toughened PP/PA/SEBS-g-MA blends prepared by reactive processing. Acta Polymerica. 1998;49(2-3):88-95.
[40] Qu L, Lin Y, Hill DE, Zhou B, Wang W, Sun X, et al. Polyimide-Functionalized Carbon Nanotubes: Synthesis and Dispersion in Nanocomposite Films. Macromolecules. 2004;37(16):6055-60.
[41] Zhang Y, Shen J, Li Q, Xu Z, Yeung KWK, Yi C, et al. Development and characterization of co-polyimide/attapulgite nanocomposites with highly enhanced thermal and mechanical properties. Polymer Composites. 2014;35(1):86-96.
[42] Zhang Q, Li D, Lai D, Ou B. Hexadecyltrimethylammonium bromide-modified sericite mica-based polyimide composites: A comparison between In situ polymerization and solution intercalation processes. Macromolecular Research. 2015;23(9):802-8.
[43] Lan T, Kaviratna PD, Pinnavaia TJ. On the Nature of Polyimide-Clay Hybrid Composites. 1994;6(5):573-5.
[44] P84 Polyimide - Polyimides-Moulding Powder - Technical brochure Lenzing: HP Polymer GmbH; 1997.
[45] Polyimide P84 NT - Technical brochure. Schörfling am Attersee: Evonik Industries.
[46] Zhang X-R, Pei X-Q, Wang Q-H. Friction and wear studies of polyimide composites filled with short carbon fibers and graphite and micro SiO2. Materials & Design. 2009;30(10):4414-20.
[47] Min C, Shen C, Zeng M, Nie P, Song H-J, Li S. Influence of graphene oxide as filler on tribological behaviors of polyimide/graphene oxide nanocomposites under seawater lubrication. Monatshefte für Chemie - Chemical Monthly. 2016;148(7):1301-9.
[48] Zhu L, You L, Shi Z, Song H, Li S. An investigation on the graphitic carbon nitride reinforced polyimide composite and evaluation of its tribological properties. Journal of Applied Polymer Science. 2017;134(41).

[49] Qin S, Cui M, Dai Z, Qiu S, Zhao H, Wang L, et al. Noncovalent Functionalized Graphene-Filled Polyimides with Improved Thermal, Mechanical, and Wear Resistance Properties. Tribology Letters. 2018;66(2):69.
[50] Wang H, Ding D, Liu Q, Chen Y, Zhang Q. Highly anisotropic thermally conductive polyimide composites via the alignment of boron nitride platelets. Composites Part B: Engineering. 2019;158:311-8.
[51] Samyn P, Schoukens G. The lubricity of graphite flake inclusions in sintered polyimides affected by chemical reactions at high temperatures. Carbon. 2008;46(7):1072-84.
[52] Chen J, Yang S, Tao Z, Hu A, Gao S, Fan L. Short Carbon Fiber-Reinforced PMR Polyimide Composites with Improved Thermo-oxidative and Hygrothermal Stabilities. 2006;18(3):265-82.
[53] Throne JL. Study of the compaction and sintering of two high-performance thermoplastic polyimides. Advances in Polymer Technology. 1989;9(4):281-91.
[54] Yokota R, Horiuchi R, Kochi M, Soma H, Mita I. High strength and high modulus aromatic polyimide/polyimide molecular composite films. Journal of Polymer Science Part C: Polymer Letters. 1988;26(5):215-23.
[55] Sajjad M, Feichtenschlager B, Pabisch S, Svehla J, Koch T, Seidler S, et al. Study of the effect of the concentration, size and surface chemistry of zirconia and silica nanoparticle fillers within an epoxy resin on the bulk properties of the resulting nanocomposites. Polymer International. 2012;61(2):274-85.
[56] Medina R, Haupert F, Schlarb AK. Improvement of tensile properties and toughness of an epoxy resin by nanozirconium-dioxide reinforcement. Journal of Materials Science. 2008;43(9):3245-52.
[57] Bazrgari D, Moztarzadeh F, Sabbagh-Alvani AA, Rasoulianboroujeni M, Tahriri M, Tayebi L. Mechanical properties and tribological performance of epoxy/Al2O3 nanocomposite. Ceramics International. 2018;44(1):1220-4.
[58] Bisht A, Kumar RM, Dasgupta K, Lahiri D. Spatial distribution of nanodiamond and its effect on mechanical behaviour of epoxy based composite using 2D modulus mapping. Mechanics of Materials. 2019;135:114-28.
[59] Amdouni N, Sautereau H, Gerard JF. Epoxy composites based on glass beads. II. Mechanical properties. 1992;46(10):1723-35.
[60] Capela C, Oliveira SE, Ferreira JAM. Fatigue behavior of short carbon fiber reinforced epoxy composites. Composites Part B: Engineering. 2019;164:191-7.
[61] Matykiewicz D, Barczewski M, Michałowski S. Basalt powder as an eco-friendly filler for epoxy composites: Thermal and thermo-mechanical properties assessment. Composites Part B: Engineering. 2019;164:272-9.
[62] Nohales A, Muñoz-Espí R, Félix P, Gómez CM. Sepiolite-reinforced epoxy nanocomposites: Thermal, mechanical, and morphological behavior. Journal of Applied Polymer Science. 2011;119(1):539-47.
[63] Zabihi O, Ahmadi M, Nikafshar S, Chandrakumar Preyeswary K, Naebe M. A technical review on epoxy-clay nanocomposites: Structure, properties, and their applications in fiber reinforced composites. Composites Part B: Engineering. 2018;135:1-24.
[64] Ratna D, Banthia AK. Rubber toughened epoxy. Macromolecular Research. 2004;12(1):11-21.
[65] Sahu M, Raichur AM. Toughening of high performance tetrafunctional epoxy with poly(allyl amine) grafted graphene oxide. Composites Part B: Engineering. 2019;168:15-24.
[66] Cho JB, Hwang JW, Cho K, An JH, Park CE. Effects of morphology on toughening of tetrafunctional epoxy resins with poly(ether imide). 1993;34(23):4832-6.
[67] Bucknall CB, Gilbert AH. Toughening tetrafunctional epoxy resins using polyetherimide. Polymer. 1989;30(2):213-7.
[68] Chen Y, Sui L, Fang H, Ding C, Li Z, Jiang S, et al. Superior mechanical enhancement of epoxy composites reinforced by polyimide nanofibers via a vacuum-assisted hot-pressing. Composites Science and Technology. 2019;174:20-6.

[69] Hull D, Clyne TW. Strength of composites. In: Hull D, Clyne TW, editors. An Introduction to Composite Materials. 2 ed. Cambridge: Cambridge University Press; 1996. p. 158-207.
[70] Ahmed S, Jones FR. A review of particulate reinforcement theories for polymer composites. Journal of Materials Science. 1990;25(12):4933-42.
[71] Halpin JC, Kardos JL. The Halpin-Tsai equations: A review. Polymer Engineering and Science. 1976;16(5):344-52.
[72] Kerner EH. The Elastic and Thermo-elastic Properties of Composite Media. Proceedings of the Physical Society Section B. 1956;69(8):808-13.
[73] Nielsen LE. Generalized Equation for the Elastic Moduli of Composite Materials. Journal of Applied Physics. 1970;41(11):4626-7.
[74] Taublaender MJ. Personal Communication. 2019.
[75] Advanced Materials Araldite® LY 1564 / Hardener XB 3473 - Technical brochure. Basel: Huntsman Advanced Materials GmbH; 2012.
[76] DIN EN ISO 178 Kunststoffe – Bestimmung der Biegeeigenschaften. Berlin: DIN Deutsches Institut für Normung e. V; 2017. p. 65.
[77] DIN EN ISO 527 Kunststoffe – Bestimmung der Zugeigenschaften. Berlin: DIN Deutsches Institut für Normung e. V.; 2018. p. 67.
[78] Dynamisch-Mechanische Analyse (DMA) – Grundlagen – Lexikon der Kunststoffprüfung. https://wiki.polymerservice-merseburg.de/index.php/Dynamisch-Mechanische_Analyse_(DMA)_%E2%80%93_Grundlagen2018.
[79] Saba N, Jawaid M, Alothman OY, Paridah MT. A review on dynamic mechanical properties of natural fibre reinforced polymer composites. Construction and Building Materials. 2016;106:149-59.
[80] Koch T, Seidler S. Correlations Between Indentation Hardness and Yield Stress in Thermoplastic Polymers. Strain. 2009;45(1):26-33.
[81] Deiasi R, Russell J. Aqueous degradation of polyimides. Journal of Applied Polymer Science. 1971;15(12):2965-74.
[82] Yung KC, Zhu BL, Yue TM, Xie CS. Effect of the filler size and content on the thermomechanical properties of particulate aluminum nitride filled epoxy composites. Journal of Applied Polymer Science. 2010;116(1):225-36.
[83] Bleach NC, Nazhat SN, Tanner KE, Kellomäki M, Törmälä P. Effect of filler content on mechanical and dynamic mechanical properties of particulate biphasic calcium phosphate—polylactide composites. Biomaterials. 2002;23(7):1579-85.
[84] Goyanes SN, König PG, Marconi JD. Dynamic mechanical analysis of particulate-filled epoxy resin. 2003;88(4):883-92.
[85] Becker O, Varley R, Simon G. Morphology, thermal relaxations and mechanical properties of layered silicate nanocomposites based upon high-functionality epoxy resins. 2002;43(16):4365-73.
[86] Mathur V, Sharma K. Evaluation of Morphological Effect on Thermal and Mechanical Performance of PS/PMMA/CdS Nanocomposite Systems. Advances in Nanoparticles. 2013;02(03):205-16.
[87] D'Escamard G, Rosa CD, Auriemma F. Predicting the glass transition temperature as function of crosslink density and polymer interactions in rubber compounds. AIP Conference Proceedings. 2016;1736(1):020176.
[88] Gao Z, Zhao L. Effect of nano-fillers on the thermal conductivity of epoxy composites with micro-Al2O3 particles. Materials & Design (1980-2015). 2015;66:176-82.
[89] Eksik O, Bartolucci SF, Gupta T, Fard H, Borca-Tasciuc T, Koratkar N. A novel approach to enhance the thermal conductivity of epoxy nanocomposites using graphene core–shell additives. Carbon. 2016;101:239-44.